The Reactivity of Au^{III} Difluorides

Lachlan Barwise

A thesis submitted in total fulfilment of the requirement for the Master of Science by Research

Department of Chemistry and Physics
College of Science, Health and Engineering
La Trobe Institute for Molecular Science
La Trobe University
Melbourne, Victoria, Australia
November 2020

Abstract

The current understanding of the chemistry associated with transition metals has brought us a wide scope of reactivity and the ability to undertake seemingly infeasible reactions with ease. Yet, the $Au^{I/III}$ redox couple, while isoelectronic to the highly active $Pd^{0/II}$ catalysts, is historically considered catalytically dead. A recent method from our lab has presented the synthesis of tricationic Au^{III} complexes which can be efficiently fluorinated with the use of nucleophilic fluoride sources. This work follows on from those recent discoveries and experiments with these surprisingly economically affordable and yet rare class of $[(L)_2Au(F)_2]^+$ as a potential step in observing and developing a Au based catalytic system in C-F bond formation. Due to the cationic nature of the Au complexes, fluorination can be achieved by KF and the modification driven solely by the thermodynamical favourability of Si-F bond formation using TMS compounds.

A series of $Au(L)_2$ complexes were synthesised and oxidised with XeF_2 and attempts at exchanging CF_3 moieties for the metal's fluorides produced a mix of products. Substitution of the CF_3 from the TMS-delivery for NHCs and N-ligands were seen to exchange with the metal's fluoride with great efficiency. Though throughout all experimentation attempts at mono-substitution were incredibly unfavoured as the *trans* effects between the ligand and F^- would exacerbate decomposition.

An alternative pathway using electrochemistry rather than stoichiometric I^{III} was approached for achieving the high oxidation state and appears fruitful. Holding a Au^I specimen under a constant oxidative potential in the presence of excess ligand saw a notable change in response by cyclic voltammetry. This pathway provides a possible method for the cheap oxidation of Au^I species while eliminating the need for the more toxic regents such as XeF_2.

These Au fluorides have shown to be very effective in Si-N and $Si\text{-}C_{(carbene)}$ activation and the TMS-F driving force is enough alone to complete the ligand metathesis at the Au centre when lesser *trans* effectors are ligated. No reductive elimination was observed throughout this work, but this new methods for oxidation and fluoride-ligand exchange at the metal centre, opens new doors in coordination chemistry and methods in developing novel complexes that may aid in catalytic design around $Au^{I/III}$.

Statement of Authorship and Ethics

Except where reference is made in the text of the thesis, this thesis contains no material published elsewhere or extracted in whole or in part from a thesis accepted for the award of any other degree or diploma. No other person's work is used without acknowledgment in the main text of the thesis. This thesis has not been submitted for award of any degree or diploma in any other tertiary institution.

Computational data analysed within section 2.5 was calculated from within our group by a person other than the author and approved by the authors peer to independently analyse the data for use within this thesis.

Signature ___[redacted]__ Date 14-November-2020

Acknowledgments

"I was dreaming when I wrote this, forgive me if it goes astray"

- Prince (1958-2016) '1999', 1982

This work was supported by an Australian Government Research Training Program Scholarship.

I would like to thank my supervisor A/Prof Jason Dutton for the support, guidance, and training over the last two years. My teammates Mohammad, Lachlan[I], Tiffany, Sathsara, Nilan, and Sevan for all the help in and out of the lab, and a special thanks to Claudia for the computational data analysed here in. As well as my peers Michael and Joel for the support and encouragement over this course.

To my family, Kerrie Mason, Gary James, Evan Barwise, Anne Cooke, and Rhys Barwise, as well as my late father Neil (Dad, I bet you would never have seen this one coming ey) for the years of support.

Maeve and the late Dr. Patrick Wolfe, for convincing me to return to the world of education and not letting me drop out of university…. And somehow convincing me that writing a 18,000-word document full of my deranged William S. Burroughs-style ramblings was a "good idea". This thesis really should be titled "Cities of the Gold Night", and because of that I feel I must offer some words of advice to any reader who attempts to get through this and that is *do not let your children grow up reading the writing of Burroughs....*

Geordie Dalzell and Lindsey Meldrum, for feeding me through all the poverty.

Angus Arnold, Angus Leslie, Nick Batty, Brendon Eslick, Jake Glas, while you all kept me decently liquored up through-out the years of student poverty, if I had a dollar for every time you told me to "just do the degree" I would have had no need to have done the degree in the first place.

Amy, for the excessive amount of coffee over the last 5 years.

SARS-CoV-2 for taking away nearly half a years' worth of research in my Masters by Research and sending me back into that isolative and depressive state I fought so hard to escape from years ago.

Sean Baxter, every time we found the time to sit down and have a drink over the past few years you'd constantly say "finish your studies, then we'll make music", the Melbourne music scene will never be the same without you buddy and my heart goes out to Annalee and Oskar Koernig. Finally, for Dani Ongarello, I have no idea what to say, you gave me hope and happiness, and helped me keep my head above water over the past few years, and now I will never get to hear your voice again…

And I now regret stopping the count, 15 maybe?

Table of Contents

List of Abbreviations

The following is a list of abbreviations used throughout this thesis.

4-DMAP	**4-(dimethylamino)pyridine**
DCM	**Dichloromethane**
DIPP	**2,6-diisopropylphenyl**
DMBI	**1,3-dimethylbenzoimidazolium**
CV	**Cyclic Voltammogram**
ESI	**Electron Spray Ionisation**
MeCN	**Acetonitrile**
MeIM	**Methylimidazole**
MS	**Mass Spectrum**
NHC	**n-Heterocyclic Carbene**
NMR	**Nuclear Magnetic Resonance**
OAc	**Acetate**
O^{t}Bu	**tert-Butoxide**
Ph	**Phenyl**
Py	**Pyridine**
TBA	**Tetrabutylammonium**
terpy	**(2,2`:6`,2``)-terpyridine**
THF	**Tetrahydrofuran**
THT	**Tetrahydrothiophene**
TMS	**Trimethylsilane**

1 Introduction

While stable high oxidation state gold complexes are becoming increasingly more abundant, they remain underexplored in the realm of catalytic activity. Other transition metals often play an important role in the synthesis of organic compounds that would be otherwise impractical to synthesise, though the catalytic activity of the $Au^{I/III}$ redox couple has not found extensive use. Through this work a synthetic understanding in the synthesis and manipulation of $Au^{I/III}$ and L_2AuF_2 complexes will be explored on the route towards developing catalytic activity of the $Au^{I/III}$ redox couple. To understand the place of Au amongst its catalytically active neighbours a brief introduction to the similarities of the highly reactive isoelectronic late transition metals will be discussed along with some recent work on high oxidation state Au complexes stabilised by fluorides.

1.1 Transition Metals and Catalysts

The use of Au catalysts is limited compared to the other late transition metals, with a large body of research residing in the group 10 metals such as palladium and platinum[1-3], both well known for their catalytic roles in often stereoselective C-C bonds formation, and halogenation.[1, 2] In group 10, organometallic copper has been extensively applied as a catalyst (dubbed "Gilman reagents", figure 1) for a variety of bond forming reactions. Due to the extensive energy required for achieving higher oxidation states (which in this case the Cu ion is only stabilised at Cu^{III} by the presence of lithium, rather than the use of more electronegative and/or backbonding ligands like many high oxidation Pd and Pt ions) it is aided by forming lower energy complexes which are succeeded by the coupling event, an idea that could be shared to Au.[4] As when travelling further down the groups achieving these higher oxidation states becomes increasingly more difficult and for Au, results in it being generally considered to be chemically inert to traditional oxidation, despite the isoelectronic state to the $Pd^{0/II}$ couple.[5, 6]

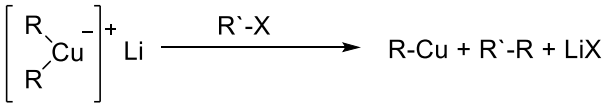

Figure 1. Generalised reaction between Gilman reagents and alkylhalides

The facile nature of oxidation state transitions in late transition metals has brought group 10 catalysts an extensive amount of use, particularly with the $Pd^{0/II}$ redox couple which can undertake a variety of catalytic behaviour in the presence of haloalkanes or aryl-boronic acids, with alkane/enes/ynes highlighted by figure 2.

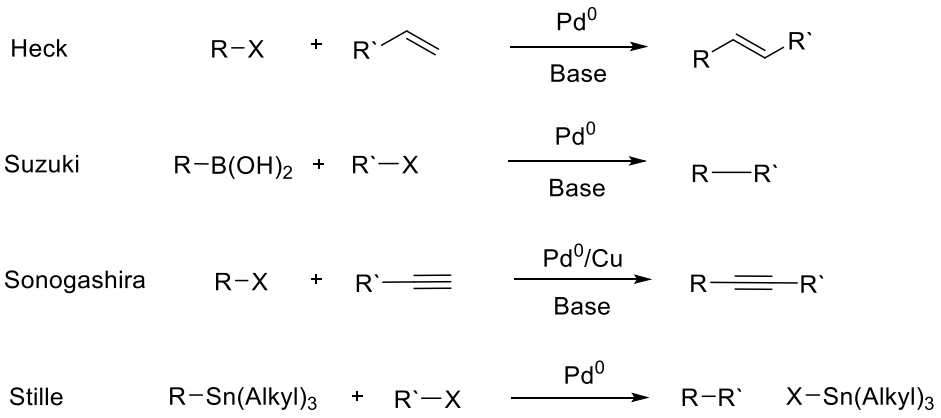

Figure 2. Generalised schemes of various catalytic actions by $Pd^{0/II}$

Within these reactions, a renewable cycle takes place where the $Pd^{0/II}$ complex undergoes a series of oxidations and reductions, conformational changes, and rearrangements. The Heck coupling reaction is shown below (Figure 3) illustrating these steps where the cycle is initiated with the oxidative addition of an aryl bromide over the metal centre, bringing it to the tetracoordinated square planar Pd^{II}.

The addition of an alkene creates a complex with the Pd^{II}, causing an insertion event and creation of a σ bond between the aryl ring and the alkenyl group. A β-hydride elimination reforms the C-C double bond and freeing the hydrocarbon from the metal centre. Then the cycle can be renewed due to the regeneration of the catalyst by simultaneous $Pd^{II/0}$ reduction and elimination of HBr.

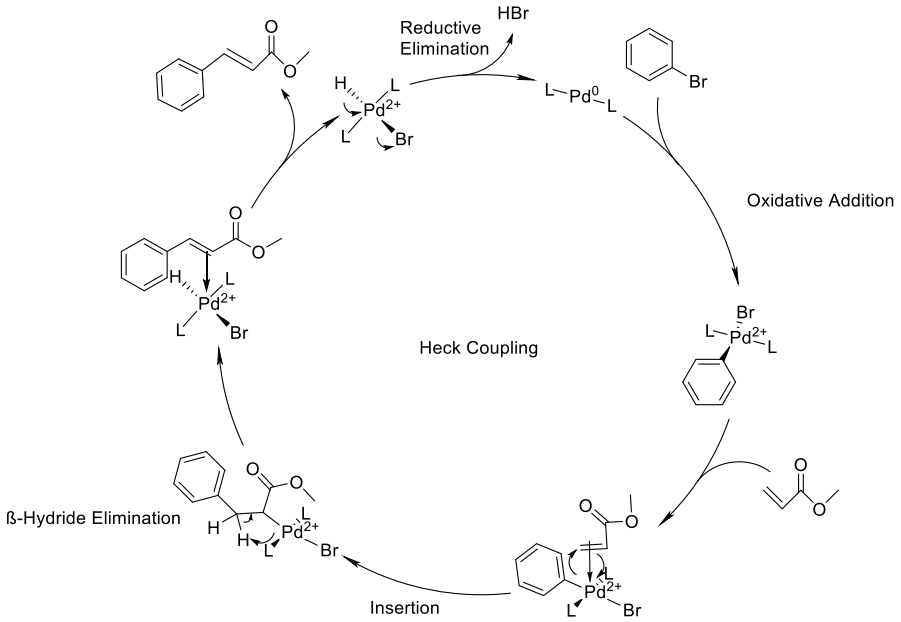

Figure 3. Heck coupling catalytic cycle by $Pd^{0/II}$

Despite a large amount of reactivity observed with $Pd^{0/II}$, the isoelectronic $Au^{I/III}$ counterpart is historically considered catalytically dead, largely due to the increased potential for oxidation of Au^{I} to Au^{III}.(+1.41 V vs H_2, $Pd^{0/II}$ +0.915 V vs H_2), this oxidation tends to require the use of strong and dangerous oxidants such as XeF_2 or hypervalent iodide to reach the Au^{III} state.[7, 8] Despite these limitations a new interest in devising an efficient Au catalyst has grown in recent decades, with reports showing $Au^{I/III}$ complexes demonstrating crude but fundamental steps of catalytic activity.[7, 9-12]

1.2 Gold

Gold has been known and extensively used for thousands of years and was even a heavily sought-after element to the alchemists for a variety of reasons from immortality to riches. Aside from this, it has found a common place in modern times as being prized for jewellery, coinage, and more recently in electronics. The inertness of Au and its resistance to corrosion has made it ideal for many of these roles. Yet despite being so similar to its group 10 neighbour, the $Pd^{0/II}$ redox couple, with the same electronic structure (s^0d^{10}/s^0d^8) and linear and square planar coordination geometries, its organometallic chemistry has only recently flourished.

1.3 Chemistry of Gold

1.3.1 Oxidative Addition

Examples of oxidative addition of Au unwittingly date back to the days of alchemists. While they were some of the first to note that gold does not dissolve in any substance but a mixture of HCl and HNO_3, little to their knowledge this was an oxidative process producing $HAuCl_4$.

Though being experimented on and with for thousands of years, it wasn't until the late 1940's when a variety of unstable Au^{I} and Au^{III} phosphine complexes were characterised and reported.[13, 14] Many of these species were short-lived and would spontaneously eliminate small alkanes (through reductive elimination processes). Two and half decades of pondering led Kochi and Tamaki to propose a novel mechanism suggesting this to be redox activity for the coupling between alkyl halides and alkylgold phosphines (Figure 4).

Kochi and Tamaki assumed the initial oxidation precedes a fast alkyl transfer, then thermally induced reduction at Au takes place with formation of a coupled alkane[11], the authors noted that the liberation of the heavier ethyl groups was to be expected over methyl groups. Komiya and Shibue proposed the increasing electron donation from the alkyl group to the metal centre as the length of the alkyl chain increases to aid in the coupling effect.[15]

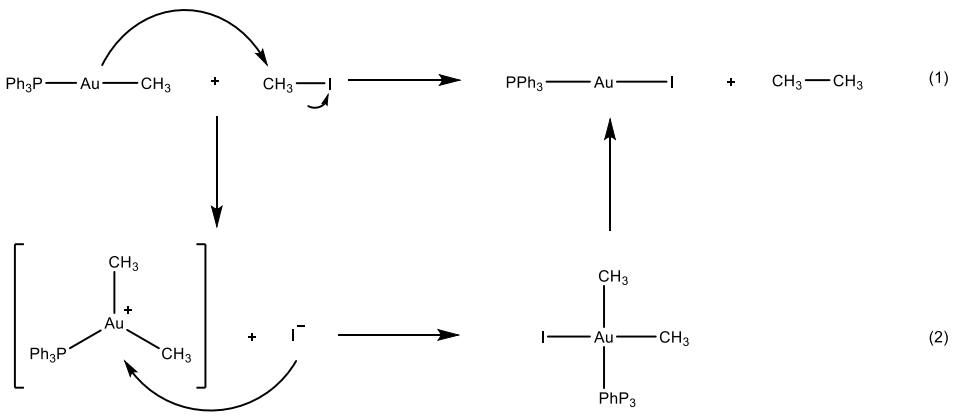

Figure 4. A suggested mechanism for the formation of an alkane through Au(I/III) coupling, where pathway 1 shows the general C-C coupling scheme, while pathway 2 demonstrates a proposed transition state and mechanism of the rapid alkyl transfer

While a simple and crude reaction towards C-C bond formation, as it is driven solely through instability at the Au^{III} state and this early notion showed the catalytic possibilities of Au complexes. Yet, it remained relatively unexplored for quite some time until recent work by

Bourissou *et. al* showed an analogous ability of $Au^{I/III}$ in intramolecular oxidative addition to that of group 10 metals. They observed the activation of Si-Si and Sn-Sn bonds along with migratory insertion when Au^{I} could be supported in proximity by either di- or mono-phosphine substituents (Figure 5(1)).[16] While they reported no detectable intermediate, modification of the molecular bridging between the Ph_2P and Si groups to increase the distance between Au and the M-M bond allowed them to not just isolate a highly stable cyclometaled Au^{I} complex, but to highlight the direct role the $Au^{I/III}$ couple played in the M-M activation and insertion (Figure 5(2)).[6, 17] Not only does this ability to control the catalytic activity of the $Au^{I/III}$ redox cycle by modification of the scaffold demonstrates the potential for catalyst design around this redox couple, but also that Au^{III} complexes were seen to be capable of activating a variety of bonds.

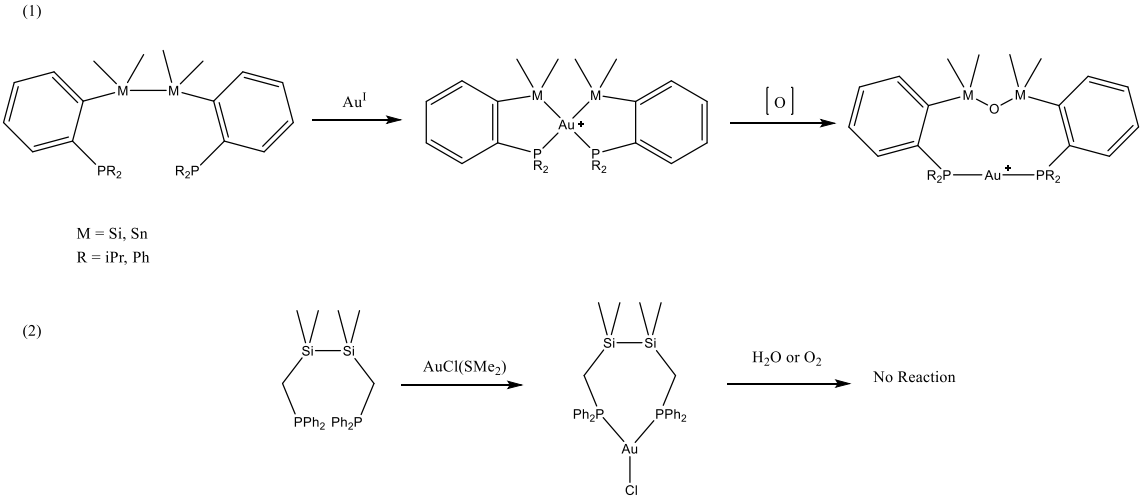

Figure 5. Pathway 1 shows the formation of the intramolecular cyclometallation and oxidative addition observed in σ-SiSi, SiSn, SnSn bridged compounds, while 2 shows the isolation of a non-oxygen-reactive specimen from modification of the Si-phosphine bridge.

Within years of this preliminary research, Bourissou *et. al* saw more C-X activation with the oxidative addition of aryl halides on to Au^{I} complexes. Their work demonstrated brominated aromatic phosphides and bis(diphenylphosphane)alkenes could successfully form previously unknown cyclometaled square planar Au^{III} complexes (Figure 6; figure 7) in *cis*-isomers similar to Pd^{II} complexes.[18]

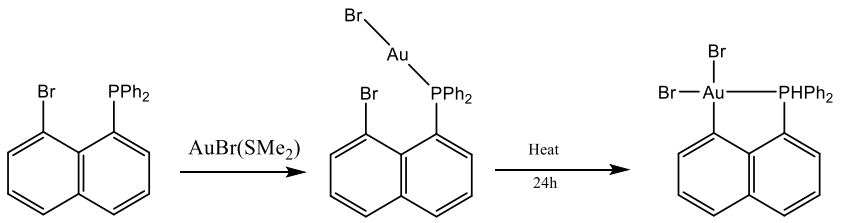

Figure 6. Intramolecular cyclometallation of bromo-napthalene phosphide

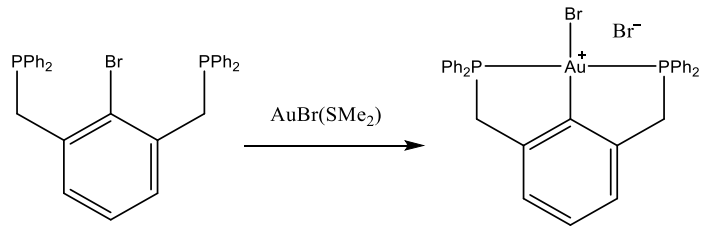

Figure 7. Formation of cyclometalated pincer complexes synthesised and proposed by Bourissou

1.3.2 Reductive Eliminations

For these purposes we are only going to be discussing oxidative addition and reductive elimination as they are effectively the beginning and end of catalytic cycles. Though due to the instability of Au^{III} complexes and therefore instability towards reductive elimination, it is appropriate to consider some history of attempts at controlling Au complexes towards this process.

Reductive elimination for Au^{III} complexes has been studied and observed since the 1970s.[19] It was suggested aryl-halides could be formed with the use of decomposing tetracoordinate dibromo-Au^{III}-phosphine complexes. A few years later Kochi came to a similar conclusion after the observation of a similar process of elimination and evolution of alkyl groups from various methylated tetracoordinate Au^{III}-phosphine complexes under heat.[20] Their team deduced the reductive elimination is controlled by the rate of dissociation of the loosely coordinating phosphine ligand to form a tricoordinate Au complex. Work by Tobias and Kuch on cationic variants of R-Au^{III}-R` complexes led to the same mechanistic conclusion.[21,22]

While research on NHC-Au^{I} iodides showed hindrance of the rate of methyl iodide production when additions of small amounts of I^- were made, similar to the results observed in the earlier days of Au chemistry that would suggest a tricoordinate decomposition pathway (Figure 4; pathway 2).[11] Only, this time the researchers noted a saturation point could be reached that

could increase the decomposition rate of the Au^{III} complexes. Suggesting to them that while the favoured decomposition pathway follows a tricoordinate structure, under saturated conditions it can undergo elimination via a pentacoordinate transition state, both mechanistic pathways fit the behaviour involved with the catalytic activity of other square planar metal complexes like Pt and Pd.[23,24]

While these observations and advancements had shown no recyclability and the only catalytic activity was through an uncontrolled decomposition pathway the research began leaning more towards stabilisation of Au^{III} using fluorides. Fluorides ligands have been used to stabilise metal ions in high oxidation states and efforts to produce more stable Au^{III} complexes brought Mankad and Toste to replace the commonly used I_2 oxidant with XeF_2, reporting the first *cis*-difluoro alkyl-Au^{III} complex.[10]

The fluorides stronger ionic interaction between the Au ion not only stabilised the cationic complexes bringing a longer shelf life than other known Au^{III} species. It showed a very early and rare example of C-F reductive elimination and β-hydride elimination with $Au^{I/III}$.[7]

Mankad and Toste's incorporation of fluorides into these complexes were not limited to those two reactions, they noted that Au alkyl difluorides could couple with aryl-boronic acids for C-C bond formation (Figure 8).

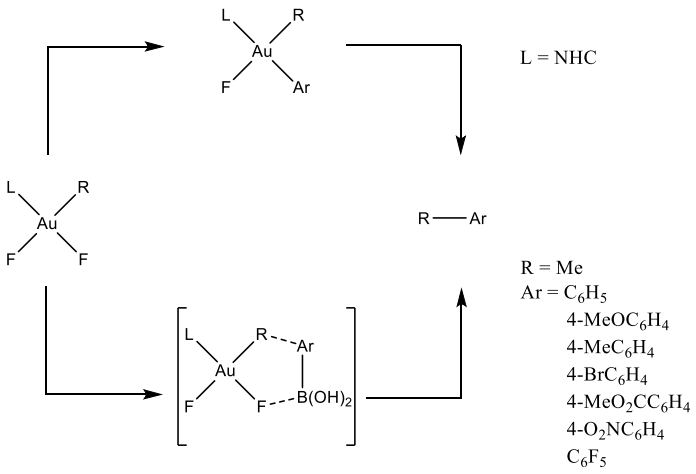

Figure 8. The proposed mechanism involved for C-C coupling with arylboronic acids

This behaviour not observed in the previously mentioned iodide analogue[10] is largely due to the extended lifetime of the alkyl-Au^{III}-fluoride and the *cis*-orientation allowing for a concerted $C(Sp_3)$-$C(Sp_2)$ coupling to take place by a pathway involving electrostatic complexing.[7] These observations were similar to work performed by Nevado, where they saw the direct

transmetalation of B-C bonds onto the Au centre allowing for the reductive elimination of a C-C bond between two aryl substituents. Within their work they also noted distortion of the square planar geometries when substituting Cl^- for F^-, assumed to be caused by the susceptibility of the F^- to the *trans* effect, resulting in elongation of the Au-F bond and allowing for the further reactivity observed from the Cl equivalents. This was fitting to the proposed intermediates of unique activity suggested by Mankad and Toste and this use of fluorides saw a renewed interest in the potential catalytic processes of $Au^{I/III}$.[25, 26]

1.4 $Au^{I/III}$ Fluorides

The use of fluoride to stabilise gold at high oxidation states has introduced the world of chemistry to an exciting new realm of previously unknown complexes and reactivity. Since Mankad and Toste reported the first isolated Au^I fluoride through the conversion of Au^I chloride in 2005 (Figure 9), in the years since, the isolation of Au^{III} difluorides has scarcely been achieved. To date, only 8 unique Au^I and 16 Au^{III} complexes bearing a Au-F bond have been analysed by x-ray crystallography, and the amount of research in the field is comparatively limited and open for exploration.[25, 27]

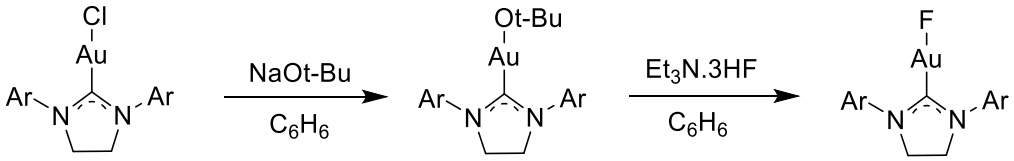

Figure 9. Mankad and Toste's synthetic scheme of the first isolated Au-F

After Toste's team showed the first example of a trans-difluoro alkylgold^{III} complex, and the reporting of $AuF_2(CF_3)_2$ and various derivates of the Au trifluoromethines our team reported the formation of Au^{III} complexes supported solely by neutral ligands.[8, 10, 28] Our team reported the cationic Au^{III} difluorides exhibiting the shortest known bond length, these cationic complexes were unique in that they were susceptible to nucleophilic fluorides, making the synthesis of Au^{III}-F_2 achievable by the much more economical and safer KF (Figure 10).

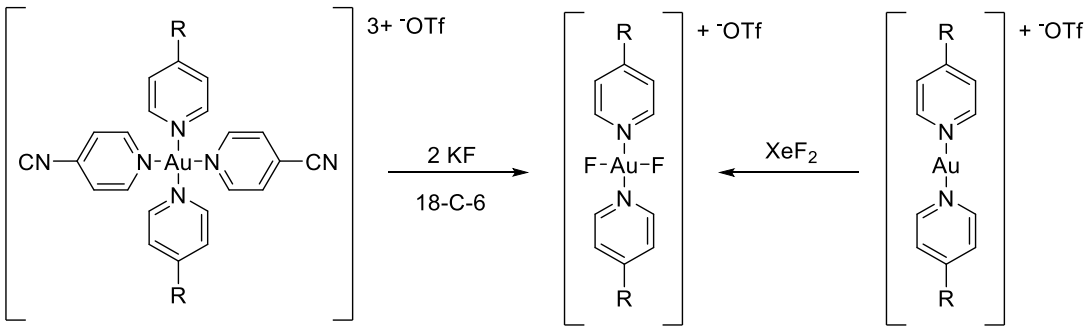

Figure 10. Albayer, Corbo and Dutton's synthetic schemes for [$L_2Au^{III}F_2$]OTf

This method was able to produce a Au^{III}-F_2 complex with the shortest known Au-F bond at 1.90 Å (compared to the more commonly seen range of 2.0-2.2 Å), making it more stable and easier to handle than most known Au complexes reported.[8, 29]

To date, Au^{III} difluorides are still quite scarce and while many teams have presented crystallised complexes with varying ligand to date until recently all have been of the *cis* geometries and many have shown an array of catalytic activity,[16, 26, 30, 31] and only recently have the first *trans*-species been observed and only a handful have been reported to the CCDC.

This world of Au^{III}-F_2 is quite novel and the catalytic activity unexplored, and this advent of the nucleophilic fluoride ligation pathway our group has presented offers the question of if it is possible to use this method to create a C-F bond. As the lability of the F^- might usher a system that could fluorinate a substrate without the use of the more commonly used expensive and toxic reagents required for fluorination, reagents such as the electrophilic fluoride source XeF_2. And a method as simple as being driven by the favourability of Si-F bond formation and the high reduction potential of the $Au^{III/I}$ couple.

Approaching from this direction would be ideal as F^+ reagents, while effective fluorinating agents are more often derived from the reactive F_2. The use of electrophilic fluorine sources is not alien however and a group headed by Ritter in 2011 presented a method for the formation of a Pd^{IV} fluoride capable fluorination of a nucleophilic substrate by a S_N2 reaction. While the complex still undergoes a series of possible steps leading to oxidative addition through the formation of a $[Pd^{IV}]^+$ ^-F complex, the initial synthesis requires the use of harsh F_2 and our teams cationic complexes themselves avoid the necessity for the formation of $[Au^{III}]^+$ ^-F complex and are susceptible to less harsh fluorinating sources, and still leaving it remarkably reactive.[32]

1.5 C-F Bonds

The reason why we desire C-F bond formation is due to their currently held importance in the world of medicinal chemistry. The change from C-H to C-F in medicinal compounds is shown to increase the bioavailability and protein binding affinity of orally administered drugs, and is readily made use of for drugs such as Prozac and Crestor.[33] Yet, the conversion to the C-F bond itself is currently troublesome. Often performed with highly reactive, unselective, or expensive electrophilic fluoride sources like F_2 or Selectfluor, they tend to produce a variety of competitive side reactions from indiscriminate oxidations and fluorinations, or various solvent interactions.[34]

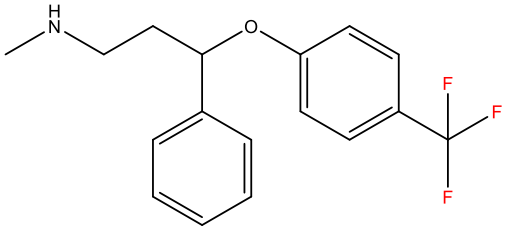

Prozac

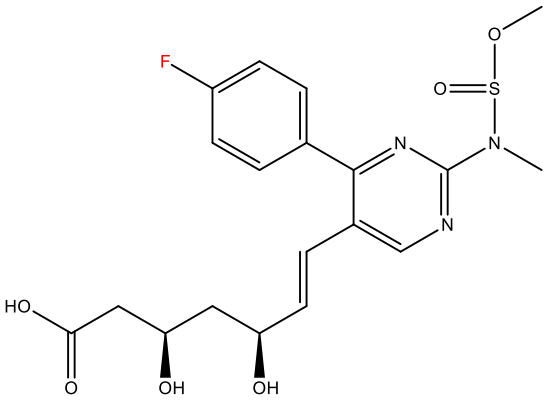

Crestor

Though C-F bonds are the strongest C-X bond and the thermodynamics heavily favours C-F bond formation with nucleophilic fluorides, nucleophilic fluorination has many issues of its own including indiscriminate fluorination. Transition metal mediated fluorination has been the more successful of these methods, but it still requires harsh reaction conditions and comes with many competitive side reactions.[34]

However, the cost-effective method for fluorination of L_4Au^{III} complexes presented by our team offers an opportunity to explore the undeveloped world of $Au^{I/III}$ chemistry and substrate fluorination seemed favourable due the ability of Au^{III} to auto-reduce.

1.6 Aim

This work aims to synthesise a Au^{III}-F_2 complex capable of C-F coupling via the I/III redox cycle using an efficient and cost-effective synthetic method and driven by Si-F bond formation, with the use of electrochemistry to replace the more traditional chemical oxidation.

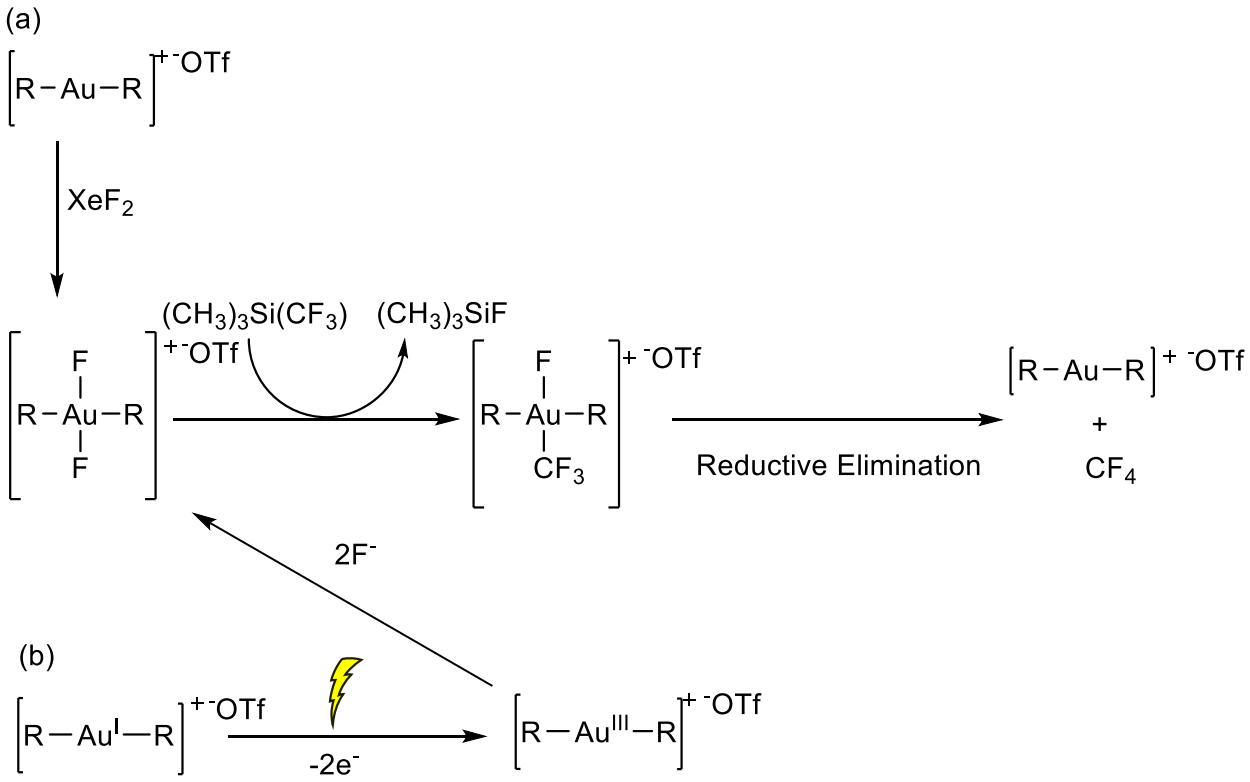

Scheme 1. Generalised reaction intentions of this work. Pathway (a) showing the traditional chemical oxidation with XeF_2, and pathway (b) showing the intended general electrochemical pathway.

2 Results and Discussion.

Recent work from our group has presented a method of producing *trans*-Au^{III}-F_2 by the use of KF to displace nitrogenous ligands, making it more economical and safer than the current methods of XeF_2 oxidation.[29] It presents a good route to explore in creating a C-F bond forming Au complex that could be produced by either XeF_2 or KF.

For this work, multiple approaches were taken towards the formation of a C-F bond forming system. Using neutral nitrogenous ligands and NHCs ligated to $LAu^{III}F_2$ complexes to support the metal centre, as well as modification to the TMS 'delivery system' to explore the possible complexes that could form via the favourable formation of Si-F bonds.

2.1 N-Ligand $Au^{I/III}$ Complex Synthesis

The exploration began by synthesising a series of Au^I complexes supported by N-ligands from gold powder. The initial steps used aqua regia to oxidise and isolate $HAuCl_4$ for reduction to the Au^I state as THT-AuCl (**T-B1**) with the addition of THT (64%) (Scheme 2).

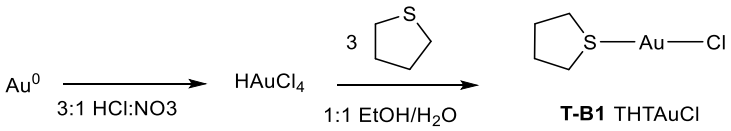

Scheme 2. Synthesis of THTAuCl

The THT-AuCl complex mirrors the commonly used Me_2S-AuCl complexes for Au redox investigations, the lability of the thioether moiety allows for the easy substitution of various N-ligands. From here using the known literature, complexes **T-B2** (70%) and **T-B3** (62%) were synthesised (Scheme 3, 4).[29]

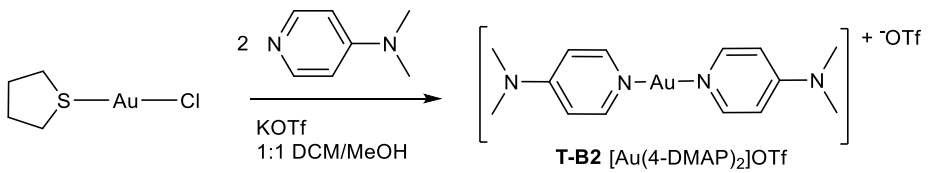

*Scheme 3. Synthesis of **T-B2** [Au(4-DMAP)$_2$]OTf*

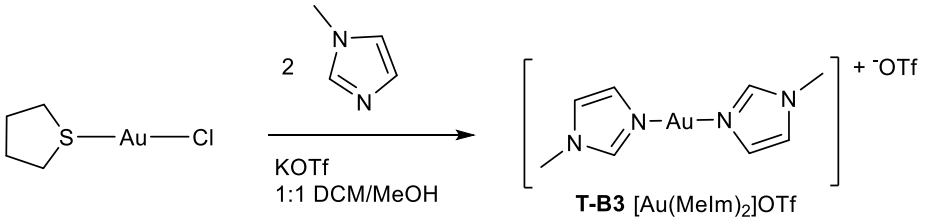

*Scheme 4. Synthesis of **T-B3** [Au(MeIM)$_2$]OTf*

The high stability, susceptibility towards oxidation by XeF_2, and alternative pathway of producing the Au difluorides using nucleophilic fluoride sources (e.g KF, figure 10), made them excellent candidates for this work.

Complex **T-B4** (41%) was also synthesised by an alternative pathway to the above, using the direct oxidation of Au powder presented in the literature (Scheme 5)[29].

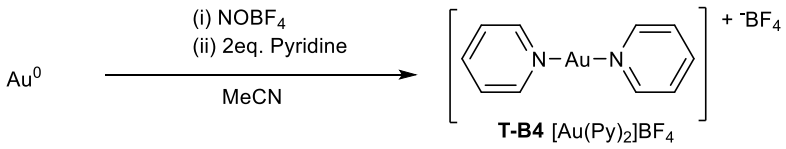

*Scheme 5. Synthesis of **T-B5** [Au(Py)$_2$]BF$_4$*

To make the investigatory process quicker the use of the oxidant XeF_2 to oxidise and deliver fluorides at the same time helped bypass the KF step by going from Au^{I} to Au^{III}-F_2 directly, yielding 70% and 67% when 4-DMAP and MeIM were the chosen ligands.

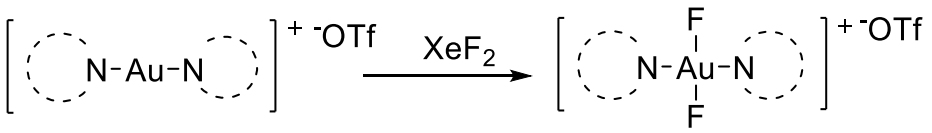

Scheme 6. Oxidation and fluorination of Au^{I} species by XeF$_2$

In the case of Py; the weaker base of the N-ligands chosen, the complex showed higher sensitivity to XeF_2, and the creation of a presumably weaker Au-F bond due to the observations of decomposition if not tended to within a few hours (and in many cases during work-up), only yielding 42%. The NMR of the three complexes was observed to match the known literature[29].

2.1.1 Trifluoromethylation

With the Si-F bond being the strongest single bond, taking advantage of this with the use of $TMSCF_3$ to substitute one or both of the fluorides at the metal centre for the CF_3 moiety posed as a good initial route to investigate the favourability of the Au-F/Au-X ligand exchange.

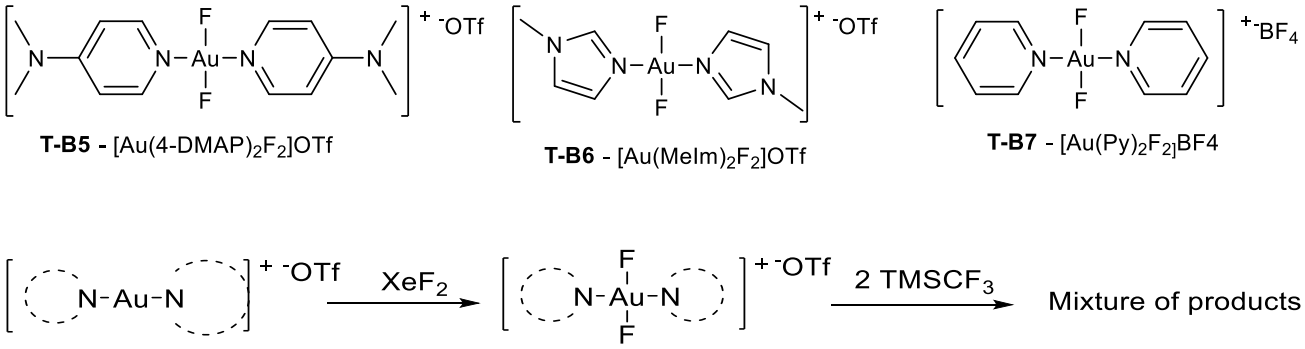

Scheme 7. Oxidation of $[Au(L)_2]OTf$ and subsequent trifluoromethylation

A multitude of attempts was undertaken with $TMSCF_3$ to synthesise the intended $[L_2Au(CF_3)_2]^+$ (compounds **T-B8**, **T-B9**, **T-B10**) as a precursor for C-F reduction (Scheme 7).

The initial experimentation made use of MeCN as the solvent with a 1:1 ratio between these N-ligand bound Au^{III} difluorides and $TMSCF_3$, the chemicals were reacted for timescales between 1 hour and 2 days. In all cases, ^{19}F NMR comparisons showed the loss of the upfield peaks (-249 ppm for **T-B5**) suggesting consumption of the starting material. A peak observed at -157 ppm (Figure 11) also indicates the generation of TMS-F from these $[L_2\text{-}Au\text{-}F_2]^+$ species[35], and a variety of peaks within the region observed for $Au\text{-}CF_3$ species ranging from -10 ppm to -40 ppm were seen (Figure 11)., such as $Au(CF_3)_2(Cl)_2$ at -33 ppm and $Au(CF_3)2(Br)_2$ at -13 ppm.[28]

Consolidating these results indicate ligand exchange had taken place, yet all attempts at the isolation of an individual species when reacted at this ratio was hindered by decomposition.

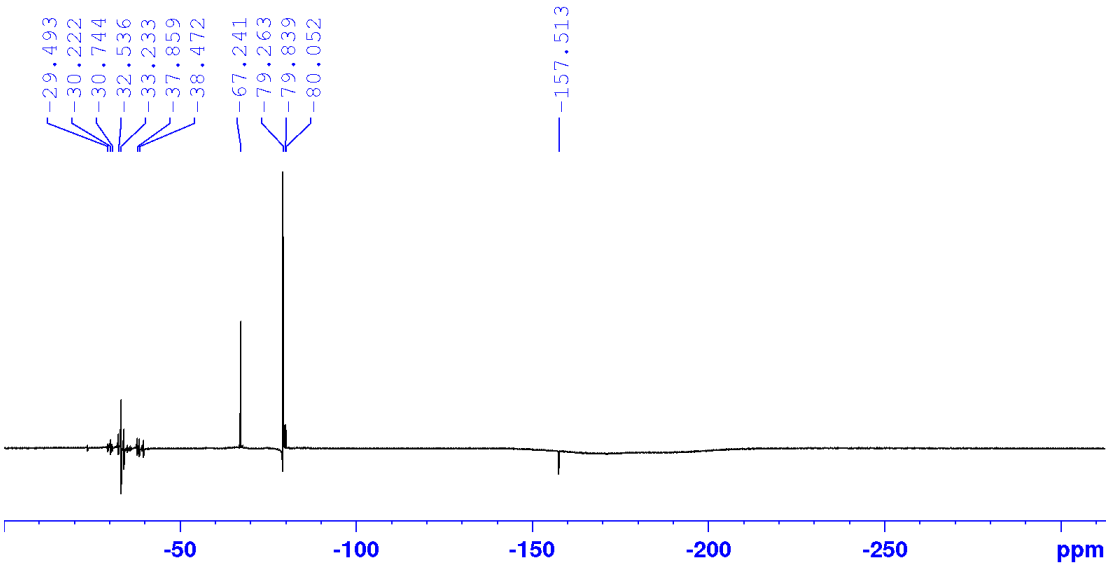

*Figure 11. In situ reaction ^{19}F NMR of **T-B5** and $TMSCF_3$ at 2 hours in CD_3CN, -79ppm is OTf, -157ppm is TMSF, -67ppm is $TMSCF_3$.*

Due to the coordinating nature of MeCN observed with Au species,[36] the solvent was changed to DCM and THF to eliminate the competitiveness of the MeCN ligated species suspected to cause the scattering observed in the in situ reaction spectra in CD_3CN (Figure 11).

Though noticeably less soluble in these solvents, the ratio of $TMSCF_3$ to $[L_2AuF_2]^+$ was increased to both 2:1 and 10:1, and the reaction was monitored by ^{19}F NMR for up to two weeks to see if the increased ratio of TMS reagent could synthesise **T-B8**, **T-B9**, and **T-B10**.

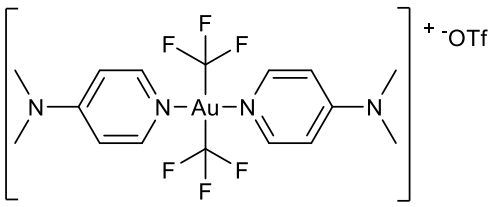

T-B8 - $[Au(4\text{-}DMAP)_2(CF_3)_2]OTf$

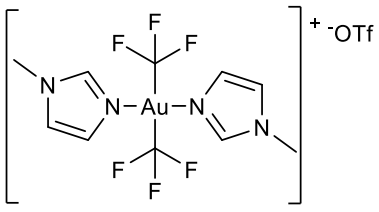

T-B9 - $[Au(MeIM)_2(CF_3)_2]OTf$

No reaction occurred in THF, likely due to the poor solubility of the starting gold complex, and the increased ratio of TMS reagent appeared to hinder the rate of decomposition of the Au species similar to the observations hinting at tricoordinate pathway mentioned earlier.[11]

DCM brought a cleaner reaction in terms of spectra, than what was seen with MeCN and the time constraints for the reaction to take place appeared to be less apparent. The reaction mixture was seen to be stable for multiple days showing that Au complexes are remarkably sensitive to the solvent, and there is a possibility that the reaction requires initiation by solvolysis with the

use of a mild Brønsted-Lowry acid or base, as it was observed the use of the less reactive THF failed to produce any reaction.

Addition of Et_2O to the DCM reaction mixture easily recovered a mixed product with only three fluoride environments in the Au-CF_3 region (Figure 12), yet each product appeared to have similar solubility in the available solvents and were unable to be isolated from one another.

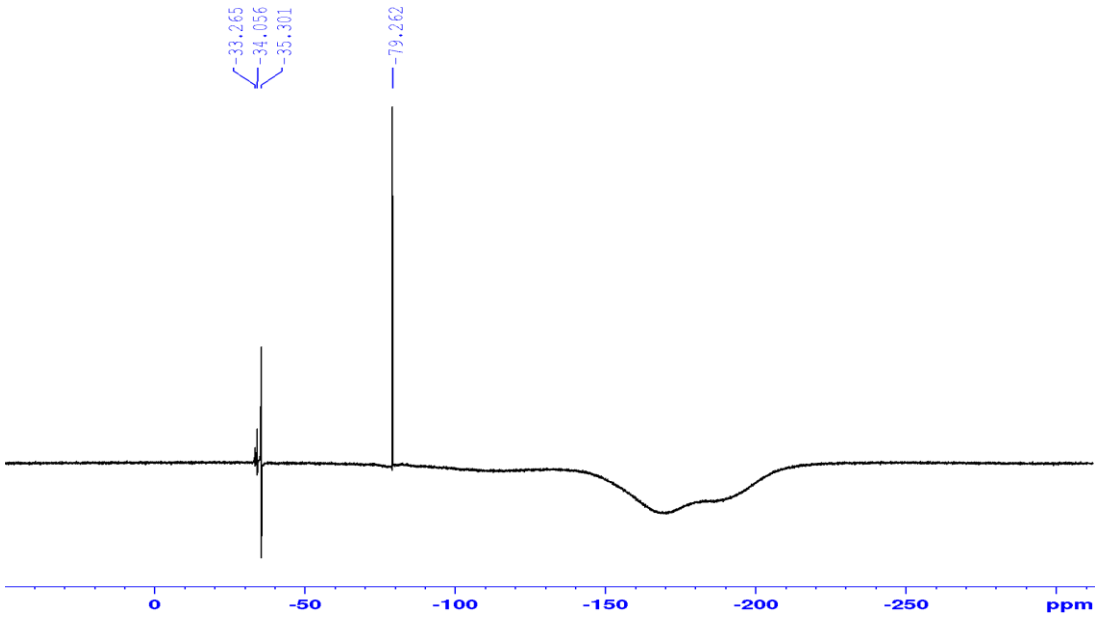

*Figure 12. ^{19}F NMR of the products isolated from reacting **T-B5** + $TMSCF_3$ in DCM*

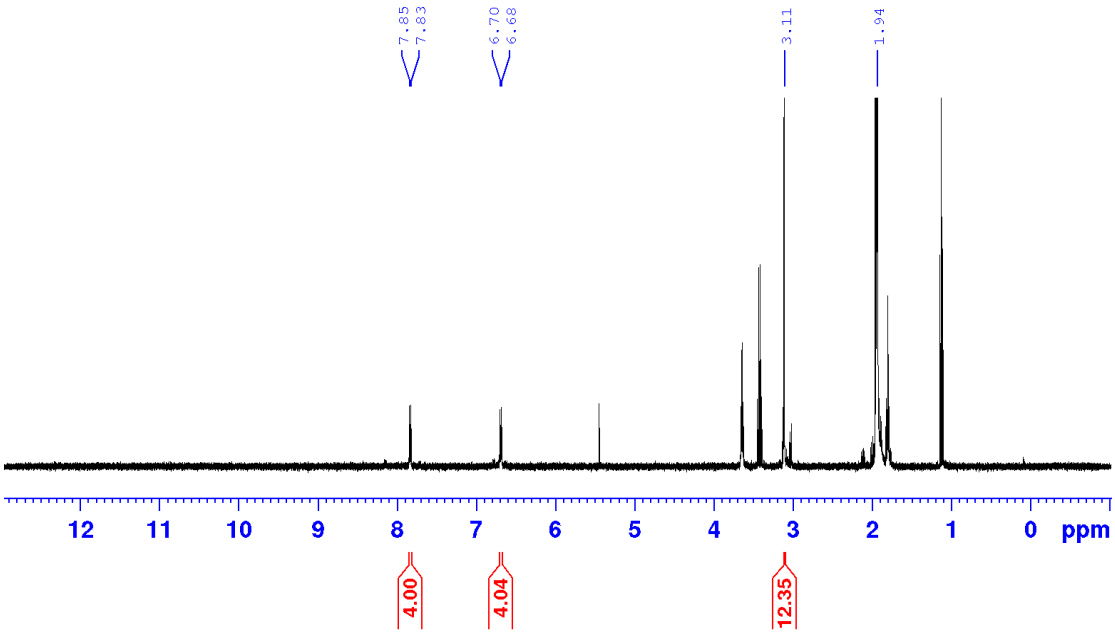

*Figure 13. ^{1}H NMR of the product isolated from reacting **T-B5** + $TMSCF_3$ in DCM*

Despite the appearance of a single 4-DMAP environment in figure 13 shifted slightly upfield from the starting material, the complimentary mass spectrum showed the expected product **T-B5** only within the background noise. Heating to reflux and cooling with a -78 °C bath was attempted to see if either potential product could be formed under kinetic or thermodynamic control, however these methods made no difference to the outcome of the reaction and the same three chemical shifts were observed after work up, while the ^{1}H NMR still showed a difference from the starting material, no isolatable product was able to be confirmed.

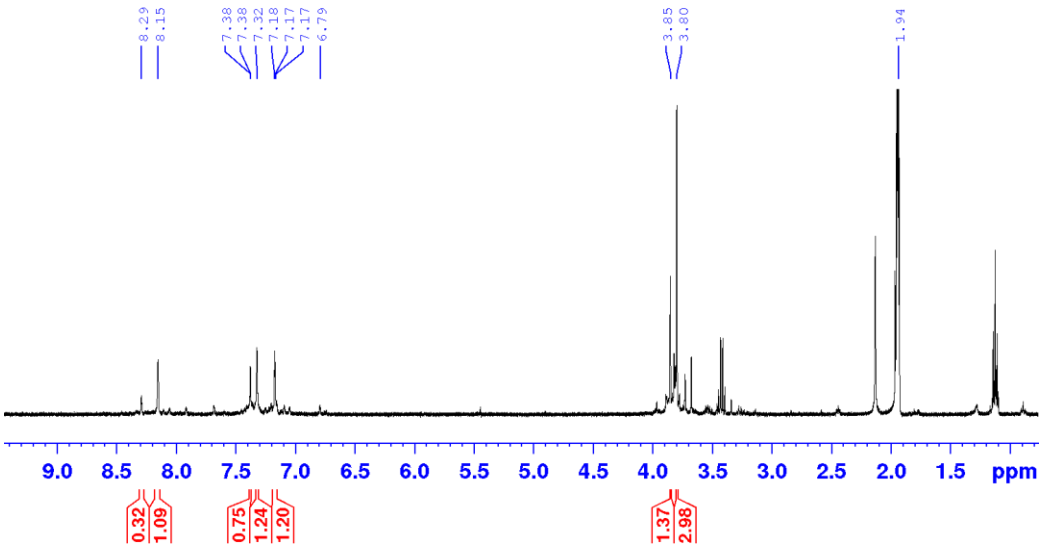

*Figure 14. ^{1}H NMR of the product isolated from reacting **T-B6** and $TMSCF_3$ in DCM*

Even at a 2:1 ratio of $TMSCF_3$ to **T-B7** it only exacerbated the decomposition of **T-B7**. However, for the reaction with **T-B6** and $TMSCF_3$ (Figure 14 and 15, above and below), a similar result was observed with multiple fluoride environments in the expected region (Figure 15). Only the ^{1}H NMR (Figure 14) gave a clearer image than what was seen in figure 12 of the multiple products, with 3 fairly distinct products formed around the methyl resonances at 3.80 and 3.85 ppm (the third, a more minor product and slightly downfield). A ratio of 1:2 was observed of the methyl chemical shifts (figure 14, 3.80/3.85 ppm), and the mass spectrum of this reaction mixture (Figure 16) saw more promise than the reaction between **T-B5** and $TMSCF_3$ by the observation of the disubstituted species appearing at 499 m/z(+), though no attempt at isolation was fruitful.

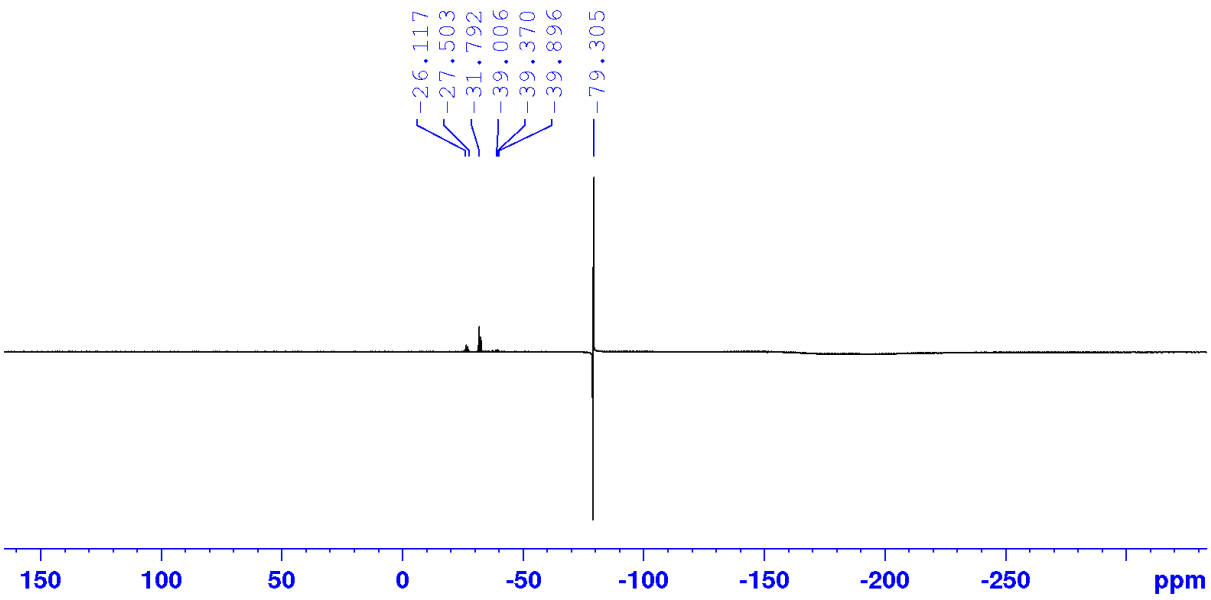

*Figure 15. ^{19}F NMR of the product isolated from reacting **T-B6** + $TMSCF_3$ in DCM*

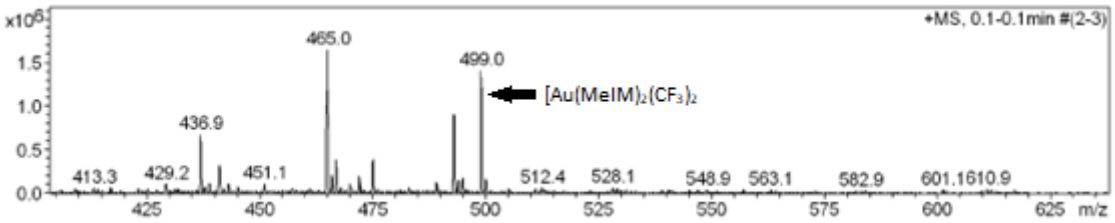

*Figure 16. ESI-MS of the product isolated from reacting **T-B6** and $TMSCF_3$ in DCM*

The peak appearing at 465 m/z(+) bears the typical isotope splitting pattern of chloride and the expected mass for [Au(MeIM)Cl(CF_3)], and could be partly responsible for the multiple products observed in figures 14 and 15. The observation of this possible complex shows the favourable halide substitution for lesser labile, or halides that are effected less by the *trans* effect, to be a remarkable hurdle as the presence of Cl^- presumably from DCM appears to displace the F^- after an extended sitting time. While the electronegativity of fluorine tends to help stabilise Au at its III oxidation state more so than other halides or ligands, there is a favourability of halide substitution towards heavier elements which makes this system highly susceptible to contamination and no mono-substituted (F-Au-CF_3) complexes were observed with these N-ligand complexes unless the favourable 'Cl for F' substitution took place. While this tendency is another limitation in preparing these Au complexes it suggests that a single fluoride moiety might only destabilise the complex.[37]

As mentioned above, the peaks witnessed after trifluoromethylation all fit the region for Au-CF_3 ^{19}F chemical shifts and in all cases, complete consumption of the starting material was observed. No Py-CF_3 or CF_4 eliminated products had been observed[38, 39] and the persistent product mixture proved difficult in isolation.

The results obtained throughout this stage of experimentation left the author unsure if $TMSCF_3$ was capable of efficiently delivering a CF_3 group to the Au metal centre despite the constant formation of TMS-F. While the system shows the thermodynamic driving force of Si-F formation is enough for our system to achieve Si-C activation, the formation of the Au-CF_3 appears to be unfavourable by this method.

2.1.2 Determination of ^{19}F $[Au^{III}(CF_3)_2]$ Peak.

To proceed further, reverse-engineering the desired di-substituted products of **T-B8** and **T-B10** in hopes of determining the possible stability and to determine the ^{19}F resonances of the disubstituted CF_3 products from the previous section, appeared as an appropriate pathway. From here it could then be compared with the mixtures from the previous reactions to help clarify the remaining questions about the product formation.

As recent work has demonstrated the simultaneous ligand delivery and oxidising ability of hypervalent iodine species with Au^I, synthesis of **T-B11** was chosen from literature to fulfil this desired product synthesis for determining ^{19}F NMR chemical shift and stability.[8, 37]

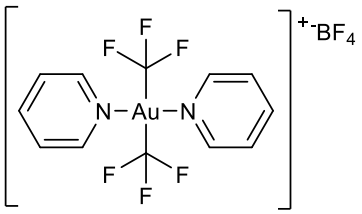

T-B10 - $[Au(Py)_2(CF_3)]BF_4$

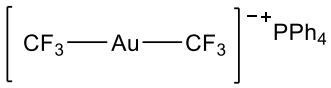

T-B11 - $[Au(CF_3)_2]PPh_4$

The synthesis of **T-B11** acquired from literature required mild modification, as the initial methods use of the lipophilic and weakly coordinating counterion PPh_4 prevented isolation by the suggested means with Et_2O.[40] Isolation of the product was only achieved by the addition of hexane to an unsaturated Et_2O solution to a point where the solvent mixture was non-polar enough to allow precipitation of the anionic Au complex as a lipophilic PPh_4 salt. The yields was 20% but showing values consistent with that of the initial procedure at -28 ppm in ^{19}F NMR and a mass to charge ratio of 334.9 m/z(-).[28, 41]

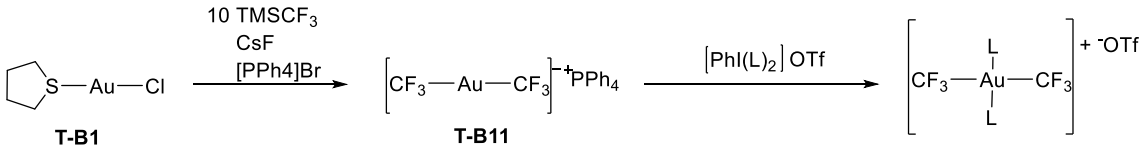

Scheme 8. Synthesis of $[Au(CF_3)_2]^-$ and oxidation to $[Au(L)_2(CF_3)_2]^+$

To achieve the Au^{III} state and deliver our initial supporting N-ligands, $[PhI(4\text{-}DMAP)_2]OTf$ and $[PhI(Py)_2]OTf$ were synthesised by known methods.[8] The two compounds were reacted with **T-B11** allowing us to observe chemical shifts of **T-B8** and **T-B10**.

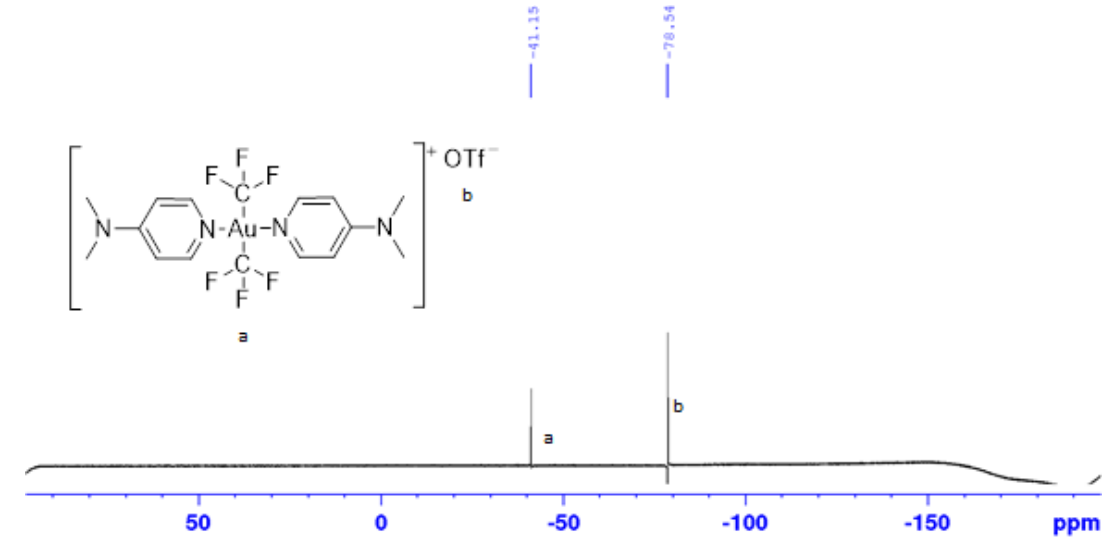

*Figure 17. ^{19}F NMR of the reaction between **T-B11** and $[PhI(4\text{-}DMAP)_2]OTf$*

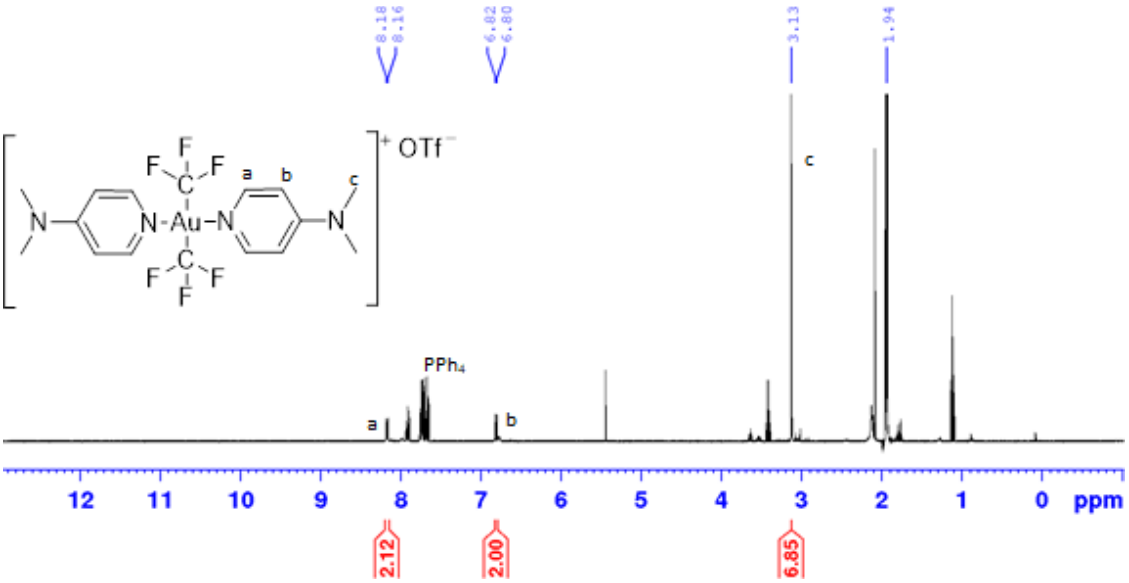

*Figure 18. ^{1}H NMR of the reaction between **T-B11** and $[PhI(4\text{-}DMAP)_2]OTf$*

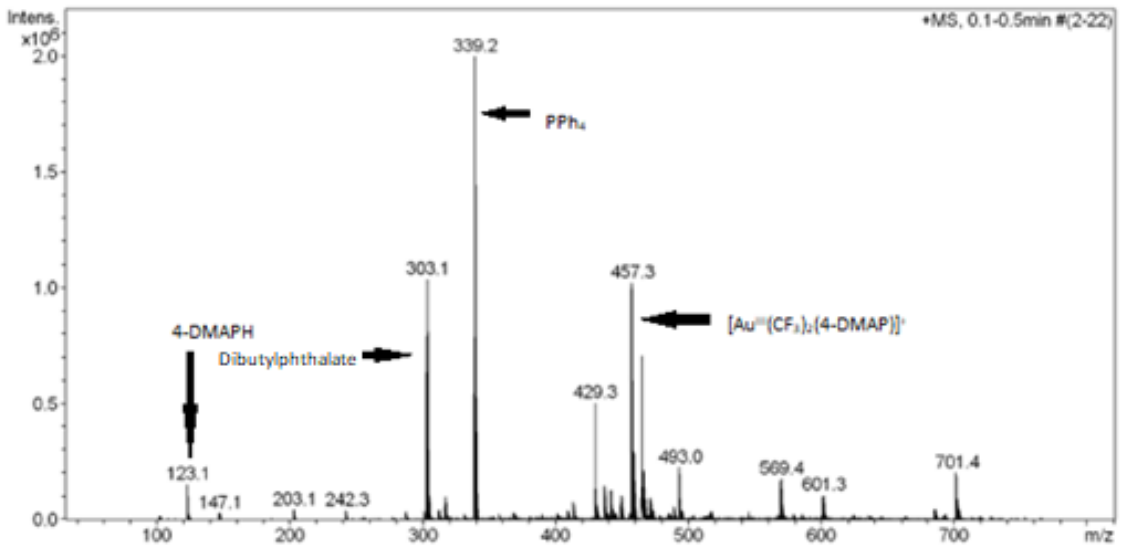

*Figure 19. ESI-MS of reaction between **T-B4** and [PhI(4-DMAP)$_2$]OTf*

The reaction of **T-B11** and iodo 4-DMAP oxidant produced a ^{19}F NMR peak at -41 ppm (Figure 17), in the area we expect to see it but different from the reactions with $[L_2AuF_2]^+$ and $TMSCF_3$. The ^{1}H NMR shows a single 4-DMAP environment shifted slightly upfield from both that of the Au^I starting material and ^{19}F environment of complex **T-B11**. A fragment of the complex; $[Au^{III}(CF_3)_2(4\text{-DMAP})]^+$, was observed by mass spectroscopy. Yet when **T-B11** was oxidised by $[PhI(Py)_2]OTf$, two environments were observed in ^{19}F NMR (Figure 20), with the main environment (-41 ppm) close to what was seen in figure 17. A second peak was observed flanking the other side of the region of interest at -31 ppm. Dibutylphtatlate can be seen in figure 19 and 21 at 303.1 m/z(+) presumed due to being present as a plasticiser in the Eppendorf tubes used for sample preparation.

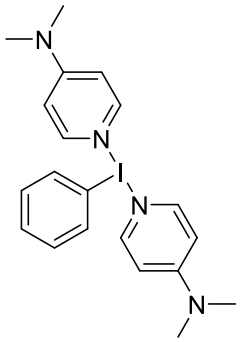

PhI(4-DMAP)$_2$

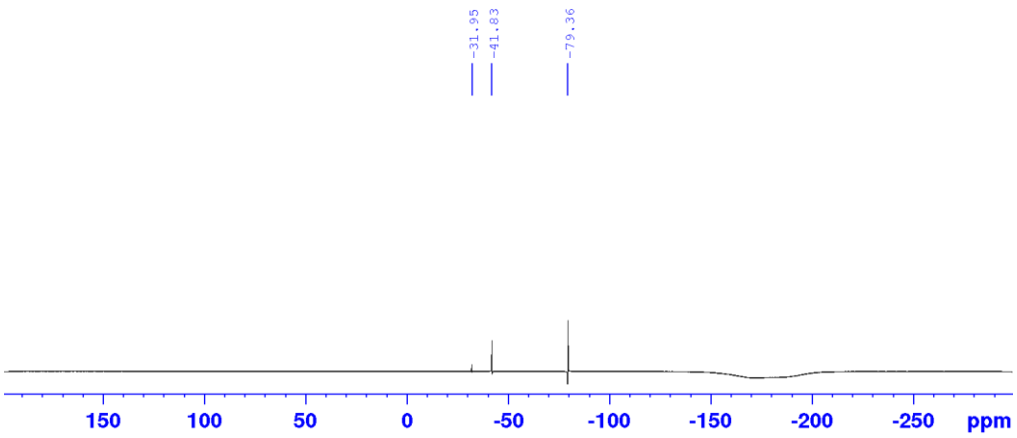

*Figure 20. ^{19}F NMR of reaction between **T-B11** and $[PhI(Py)_2]OTf$*

While both reaction sequences gave back unstable products which would decompose within a couple of hours at room temperature, the suspected **T-B10** product from these reactions was notably more unstable following the typical trend our group has observed with the lesser back-bonding pyridyl ligands leading towards reduced stability. Which could be indicative of why two environments were observed in figure 20, as the -31 ppm resonance could be a product of decomposition, without catalytic activity as it does not fit the reported resonances of CF_4 or C_2F_6.

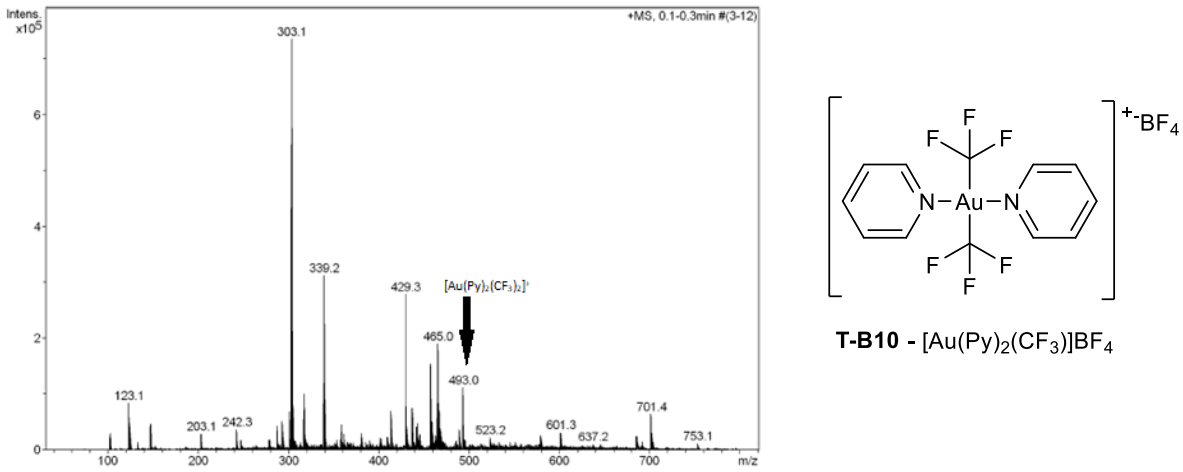

*Figure 21. ESI-MS of reaction between **T-11** and $[PhI(Py)_2]OTf$*

The above spectra (Figure 21) shows a possible observation of the product at 493 m/z(+), however, this peak was also observed in figure 19 which was recorded directly prior.

As the relative intensity between the 493 m/z peak and the 303.1 m/z peak appears to stay relatively similar across both spectra and the only stark difference between the first and second spectra is the loss of the 457.3 m/z peak. This suggests that the peak is not truly of **T-B10** but an impurity from the communal mass spectrometer used. Though it adds more validity to the

observation of **T-B8** peak at 457.3 m/z(+) in figure 19 due to the vastly less apparent strength of the signal in figure 21 at this mass to charge ratio.

While **T-B8** and **T-B10** appeared to be briefly stable they presented a ^{19}F chemical shift not previously witnessed in this work with the $TMSCF_3$ reactions. The appearance of these peaks (at -31 and -41 ppm), while within the expected region,[28] did not match any of the observed resonances in the initial complimentary TMS metathesis reactions. The appearance of the different peaks made the author suspect the L_2AuF_2 $TMSCF_3$ system might not be an appropriate path towards di-substitution let alone mono substitution, as no consistent observations were seen through the complimentary reaction pathways to produce the same target complexes and no isolatable product were obtained.

The dominant factor to consider in this system seems to lie in the *trans* effect and the ability of the substituent ligand to increase the rate of substitution at the *trans* fluoride in the square planar complexes[42]. The combination of the weak F and the strong CF_3 *trans* influences suggest a state where once a single CF_3 group is bound, it labilises the fluoride *trans* to it and with a lack of available $(CH_3)_3Si$ to bond too, the complex becomes unstable.

The persistent decomposition observed of these Au^{III}-F_2 complexes when in the presence of a half the stoichiometric amount of an organosilicon compound is further supported by this notion for the requirement for the moiety at the *trans* position (to F) to be of similar σ-donating and similar electronic p orbital character to the fluoride or else the increasing lability of the *trans*-F will result in instability.[23]

As suggested above the use of excessive amounts of $TMSCF_3$ that helped brought stability to the complex is like the observations between alkylgold phosphines and the addition of methyliodide. Though this would possibly suggest a tricoordinate pathway of formation, an excessive amount of $TMSCF_3$ should drive the reaction to completion as a single CF_3 moiety on the Au centre seems to drive the lability and reactivity of the *trans*-F, very favourably. Yet multiple products are still formed, suggestive of a pentacoordinate pathway involving metathesis, after the Au^{III}-F_2 complexes with the Si-X, which could give rise to the multiple states for CF_3 observed when compared to the tri-coordinate decomposition pathway.

In theory, minute adjustments to tune the supporting ligands may give more control over this and garner less indiscriminate reactions, however time constraints had limited the level of experimentation with modification of the Au complexes ‘backbone’ and how the modification

of the ligands effects the reactivity of the Au-F bond had to be performed *in-silico* as described in a later section.

2.2 Oxidation and Trifluoromethylation of NHC-Au Complexes.

As briefly introduced in chapter 1 NHCs have been traditionally used to stabilise Au-F species, and it seemed appropriate to follow suit in this research and make use of dimethylbenzimidazolium (DMBI) and diisopropylphenylimidazolium NHCs to support our system. For attempts to diminish the *trans* effects labilising of the fluorides, it gained the advantage of slight adjustments to the complexes stability by being able to modify the opposing bond.

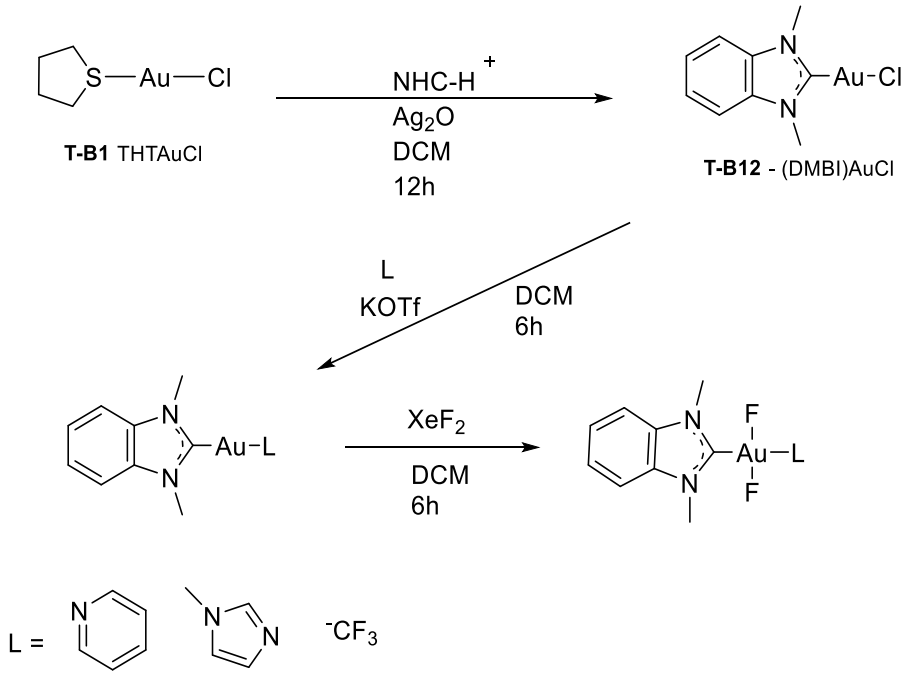

Scheme 9. Synthesis of NHC-Au-L

Starting from **T-B1**, Ag^{I} could be used to transmetalate the selected NHC onto the THT bearing Au^{I} compound, yielding **T-B12** (37%) and **T-B13** (62%).[43] The use of these complexes as mentioned above allowed us to adjust the electronic distribution of the system by incorporating a single unit of the previously used N-ligands so the Au complexes would no longer have symmetrical bonding interactions, a CF_3 moiety was also selected to directly observe a chemical shift for NHC-Au-CF_3 at both I and III oxidation states and give more clarity into the expected ^{19}F NMR regions of the CF_3 group.

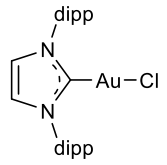

T-B13 - (DIPP-imidazolium)AuCl

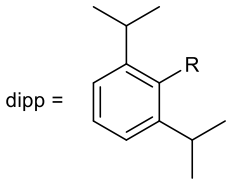

For complexes **T-B14** and **T-B16** the ligation of the nitrogenous ligands was achieved through this same method of transmetalation with Ag^{I}, the addition of hexane isolated beige powders identified as **T-B14** (52%) and **T-B16** (95%). In both cases, there was a marginal change in the chemical shift of the NHCs aryl protons from the chloride salt to the neutral ligand complexes. For the complexes containing DMBI NHC, the shift change was more notable with the addition of Py, which could be the reasoning for the instability during oxidation by XeF_2 when compared to the other two complexes. **T-B16** was remarkably more stable than **T-B14**, The mass spectrum for **T-B16** showed a very dominant peak at the target mass of 425.1 m/z(+) and was easily crystallised by vapour diffusion with Et_2O/DCM (Figure 22). The Au-N bond length was measured at 2.074 Å and 1.982 Å for the Au-$C_{(carbene)}$ bond. The slight decrease in Au-N bond length from the reported length of the Py variant is to be expected due to the increase in pKa from Py to MeIM. This increased basicity appears to decrease the back bonding of the Au centre towards the NHC resulting in a slightly longer bond when compared to the same Py var iant, and the MeIM ligand can be considered a stronger *trans* effecting ligand than Py.[44, 45]

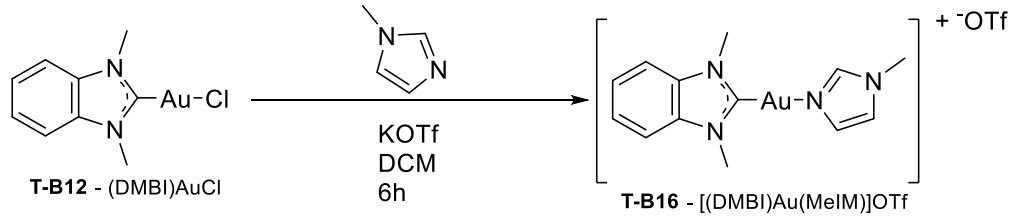

Scheme 10. Synthesis of NHC-Au-L

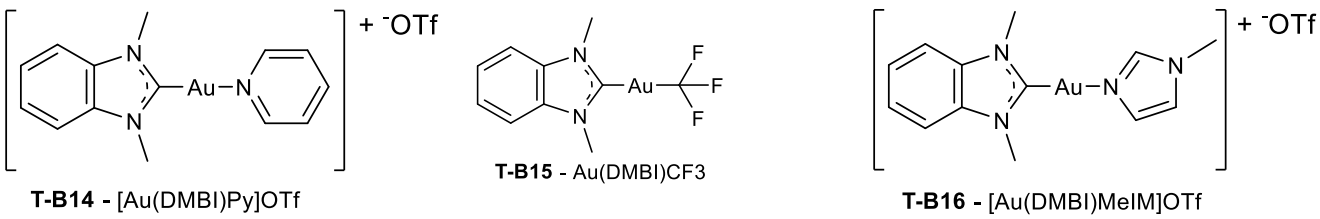

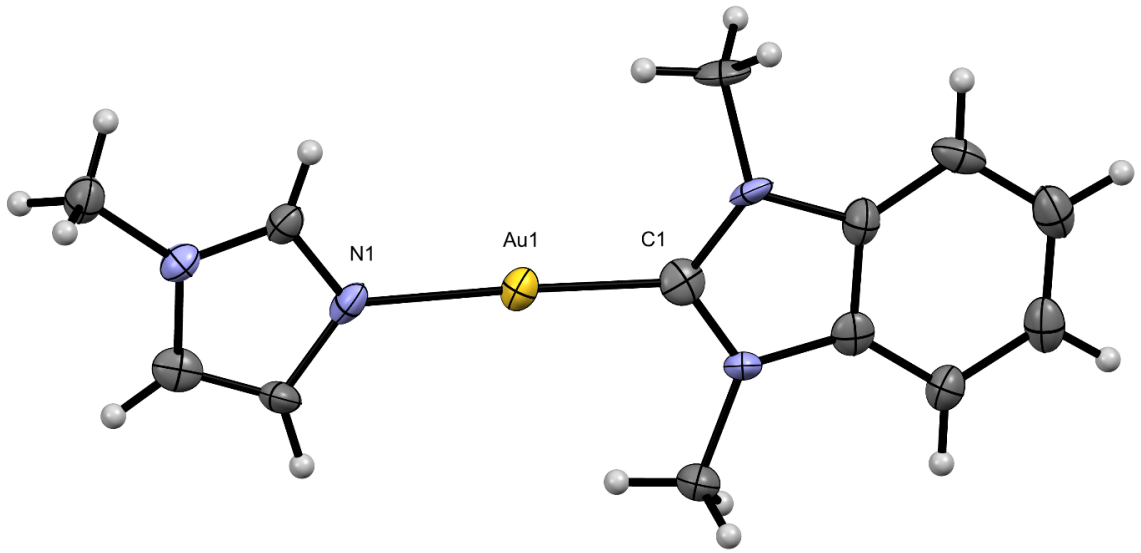

*Figure 22. Crystal structure of **T-B16**.*

To directly observe a chemical shift of the asymmetrical NHC-Au^{I}-CF_3, the synthesis of complex **T-B15** was pursued utilising the initial proposed driving force of the Au^{III}-F Si-X metathesis by activation of $TMSCF_3$ in the presence of a nucleophilic fluoride source to generate the opposing CF_3 ligand to the NHC, revealed a singular environment in ^{19}F NMR (Figure 23) that appears at a similar frequency as **T-B11** possibly suggesting a similar Au-C bond strength between the two complexes.

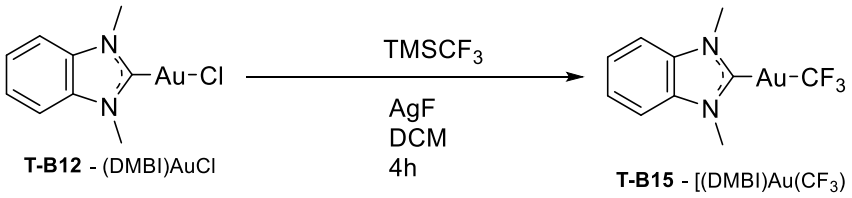

*Scheme 11. Synthesis of T-**B15***

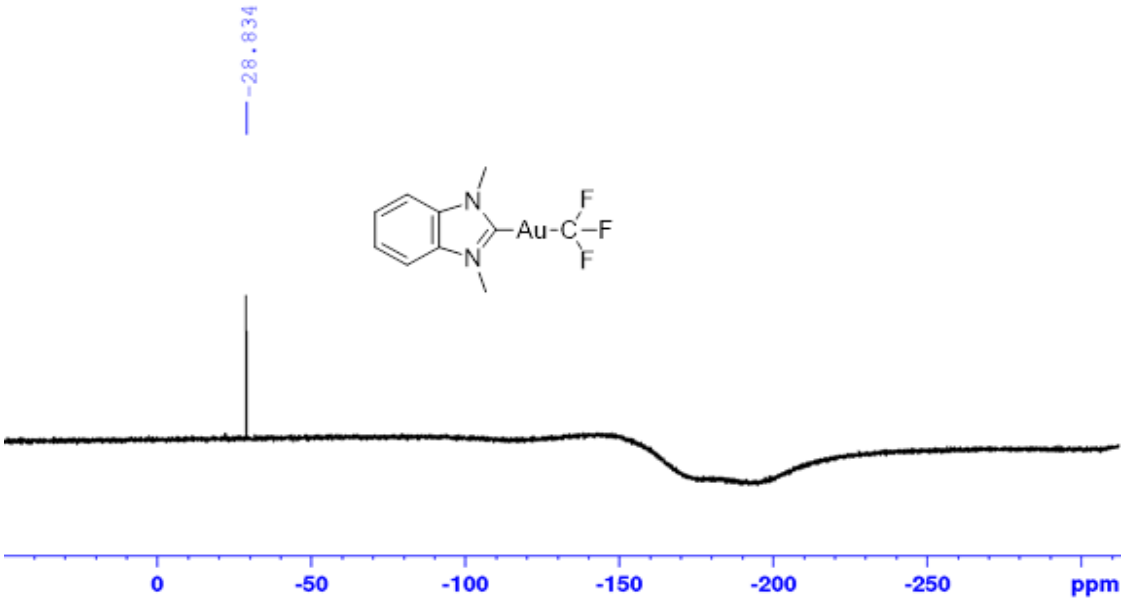

*Figure 23. ^{19}F NMR of **T-B15**, -28 ppm is CF_3, the large dip between -150 ppm and ~225 ppm is Teflon from the NMR spinner.*

With these three complexes, we followed the pathway undertaken in section 2.2 with oxidation by XeF_2 and attempts at TMS metathesis of the Au fluorides for CF_3 groups. Oxidation of **T-B15** to **T-B18** (Scheme 12) how much of a range the ^{19}F NMR CF_3 chemical shift around the Au^{I} and Au^{III} species spans with the appearance of two peaks shifted upfield by 5 and 10 ppm (Figure 24).

The appearance of two peaks within the Au-CF_3 ^{19}F NMR region (Figure 24) along with the sets of upfield peaks seen in figure 25 could be indicative of the formation of two different isomers. Though the complimentary ^{1}H NMR (Figure 26) only shows a single environment for the NHCs aromatic resonances shifted upfield from the starting material, and of the methyl groups suggestive of a singular compound.

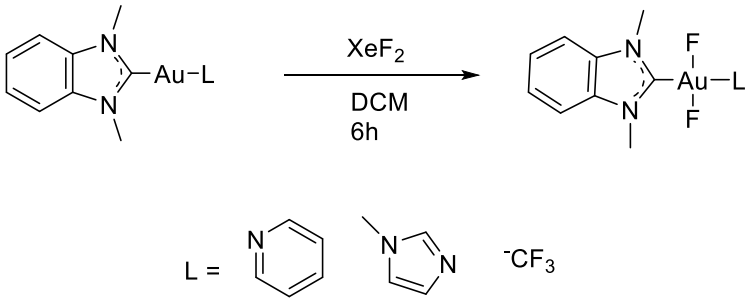

Scheme 12. Oxidation and fluorination of NHC-Au-L by XeF_2

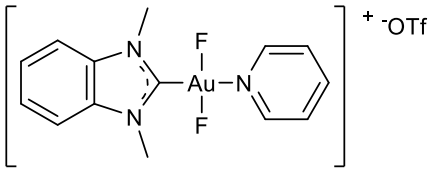

T-B17 - [Au(DMBI)PyF$_2$]OTf

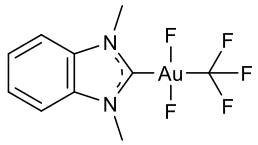

T-B18 - Au(DMBI)(CF$_3$)F$_2$)

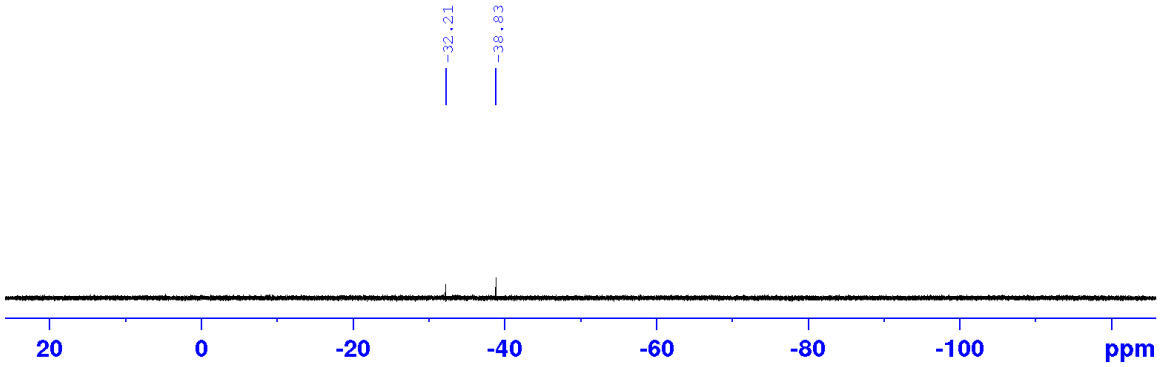

*Figure 24. ^{19}F NMR of **T-B18** first attempt, limited scan-width was not noticed for 24 hours due to server update delay*

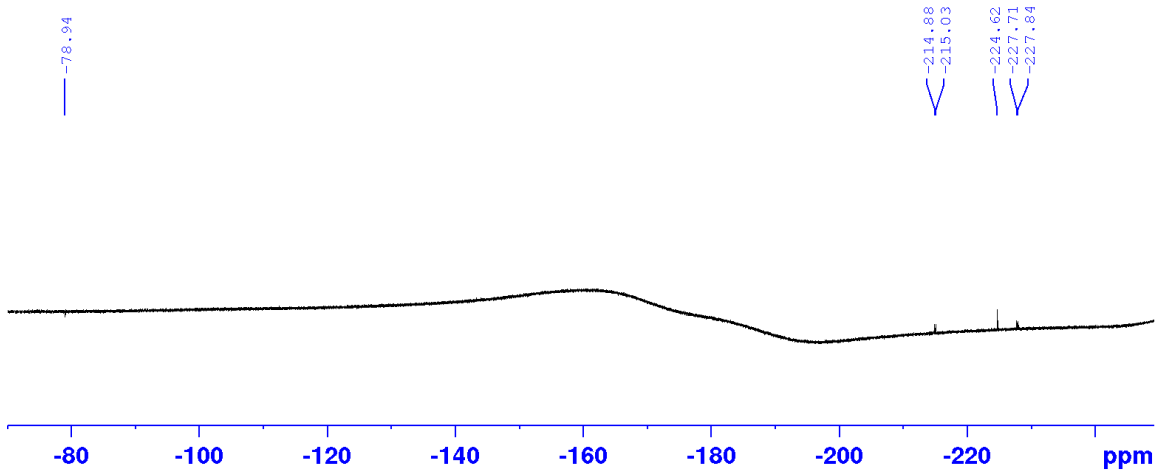

*Figure 25. ^{19}F NMR of **T-B18** second attempt, increased scan width but required resynthesis, the more downfield region (approaching 0) omitted due to poor resolution of that area compared to the size of the Teflon peak (~-150 ppm to ~-200 ppm).*

However, technical difficulties brought about a 24-hour delay for the NMR server update when performing the ^{19}F NMR analysis and resulted in the experiments to be broken up into multiple days and multiple syntheses. This begs to question the variance in the spectra and the validity of synthesising two different isomers, or just degradation products as the peaks at -32 ppm and -38 ppm were missing from figure 25 (but not shown above). In the secondary ^{19}F NMR (Figure

25) multiple peaks are seen at -215, -224, and -227 ppm which are very common areas in which Au^{III}-F species are observed, and suggestive of *cis* and *trans* isomers, or multiple products.

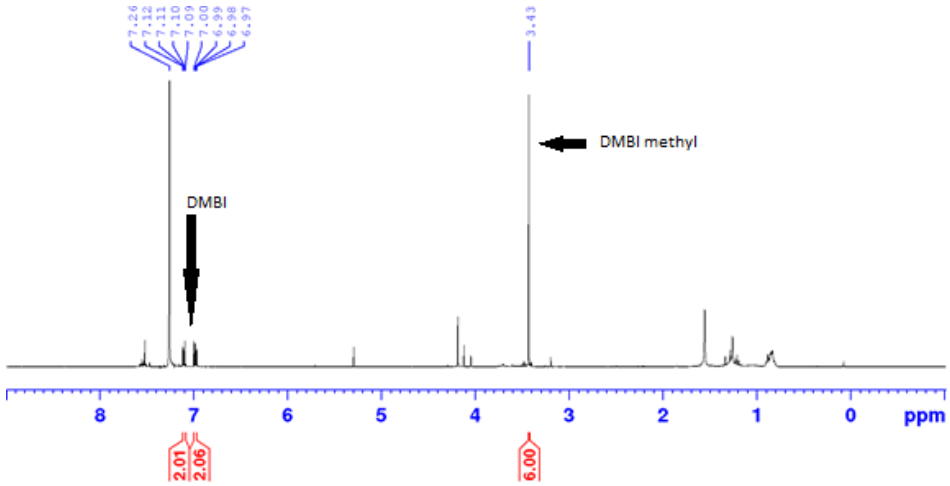

*Figure 26. ^{1}H NMR of **T-B18** in CDCl3*

As briefly noted in chapter 1, much of the early work with XeF_2 and Au fluorides have seen predominantly *cis* formations when small but bulky methyl groups are used as ligands,[7, 10] and is not out of reason in suspecting the formation of both *cis* and *trans* complexes due to the relative size comparisons of CH_3 to CF_3.

The synthesis of compound **T-B18** did serve a purpose in bringing a direct examinable peak (like **T-B9** by the PhI(4-DMAP) method) and further confirmation of the region of NHC-Au-CF_3 for both Au^I and Au^{III} species. For our purposes, the current modifications of this Au system limits itself to only elimination product of tetrafluoromethane, or possible trifluoromethylation through modification of the Au-F bond. While further investigation could be fruitful when conceptually coupled with the TMS compounds to be discussed later, and experimentation between the two could offer an interesting sacrificial system for trifluoromethylation. Issues with the complexes shelf-life prevented reaction of **T-B18** with the TMS series synthesised later and should be revisited for its potential for trifluoromethylation reactions for small compounds.

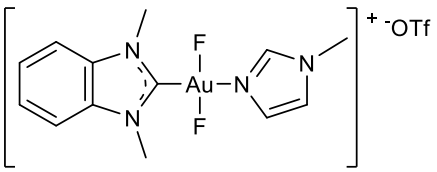

T-B19 - [Au(DMBI)MeIMF$_2$]OTf

Oxidation of **T-B16 (**to **T-B19**; scheme 12, figure 27**)** yielded a single fluoride environment in ^{19}F NMR at -305 ppm and mass spectrum peak at 463.1 m/z(+) (Figure 28). The comparatively electronically richer fluoride environment (to the prior synthesised species) suggests the fluorides to be the more labile of the complexes synthesised, with the Au-$C_{carbene}$ bond distance for the Au^{I} precursor already appearing slightly larger than others reported.[46, 47] Possibly suggestive as to why the exposure to vacuum exacerbated decomposition turning the sample purple (a colour of the monoatomic Au^{0} state), which prevented further experimentation. Presumed to be caused by dissociation of the weaker $C_{(carbene)}$-Au prior to release of F^{-}, a behaviour shared by the highly labile and weak bonding interaction between THT and Au.

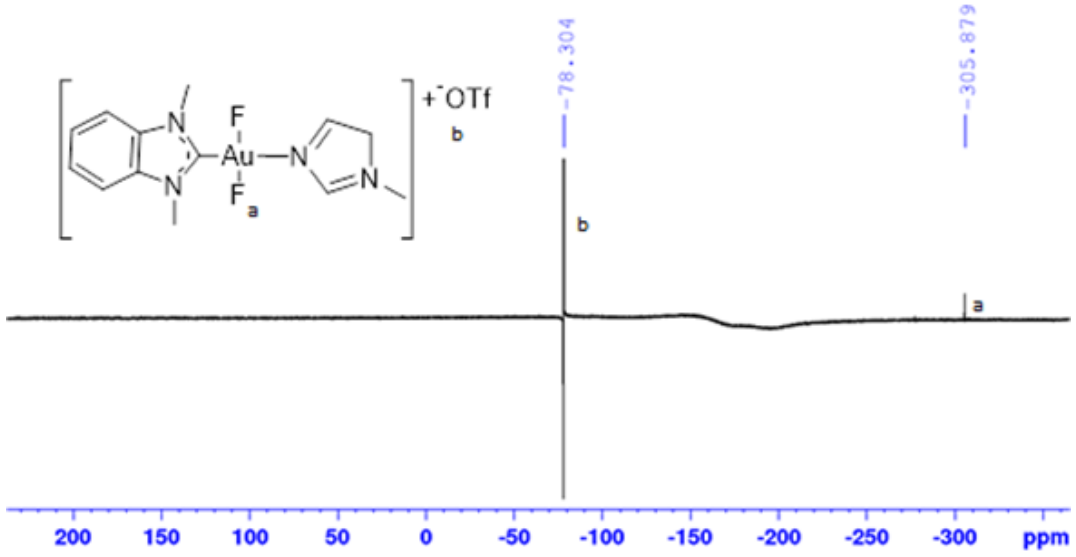

*Figure 27. ^{19}F NMR of **T-B19***

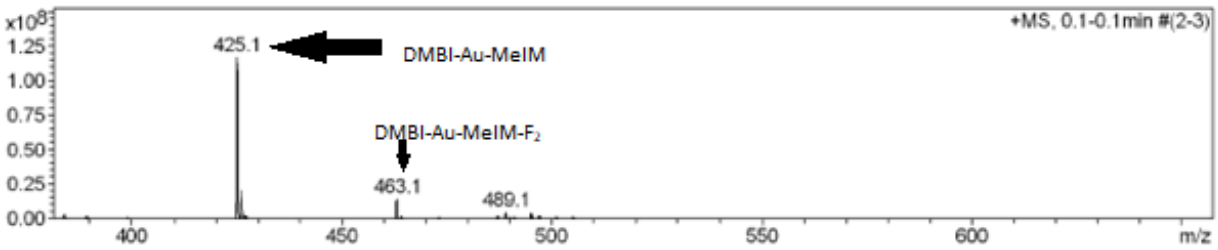

*Figure 28. ESI-MS of **T-B19***

With the only complex from this series to survive vacuum and oxidation, **T-B17** (Figure 29, synthesised by way of scheme 12), it was reacted with $TMSCF_3$. Again, the NMR spectra of the reaction showed complete consumption of the Au-F species with the loss of the upfield peak at -287 ppm from figure 29 to figure 30.

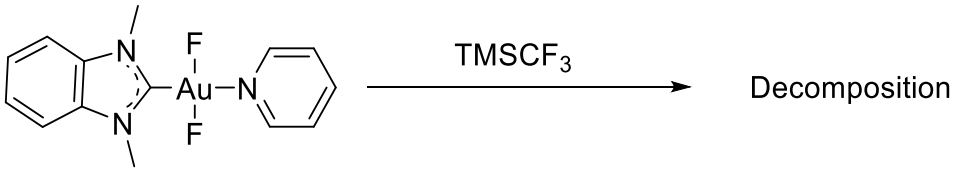

*Scheme 13. Trifluoromethylation reaction scheme of **T-B17***

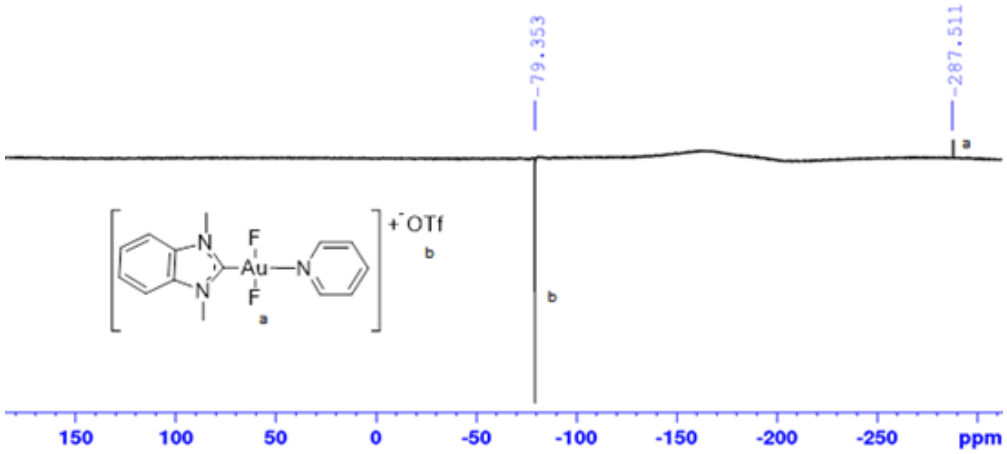

*Figure 29. ^{19}F NMR of **T-B17***

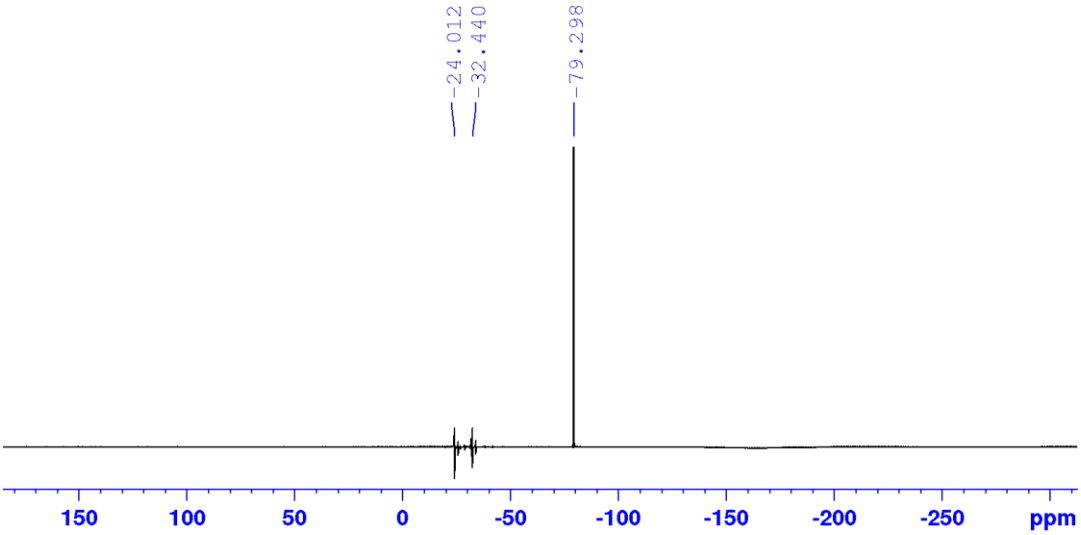

*Figure 30. ^{19}F NMR of reaction between **T-B17** and 2 equivalents of $TMSCF_3$*

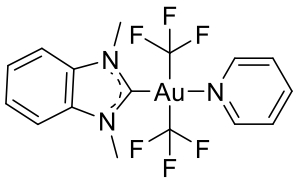

T-B20 - $Au(Py)(CF_3)_2$

The formation of the two new peaks above, appear in the expected Au-CF_3 region expected for compound **T-B20**, though the appearance of the peak at -24 ppm is further downfield from the Au^I-CF_3 seen in figure 23, and is indicative of a change in the CF_3 moieties chemical environment, yet the absence of any peak outside of this region indicates no C-F or R-CF_3 reductive elimination.[48] The difference between the peaks in

figure 30 is of a similar ppm to the difference between the two peaks in figure 24, as two major Au-CF_3 environments exist here, it could suggest the formation of two isomers.

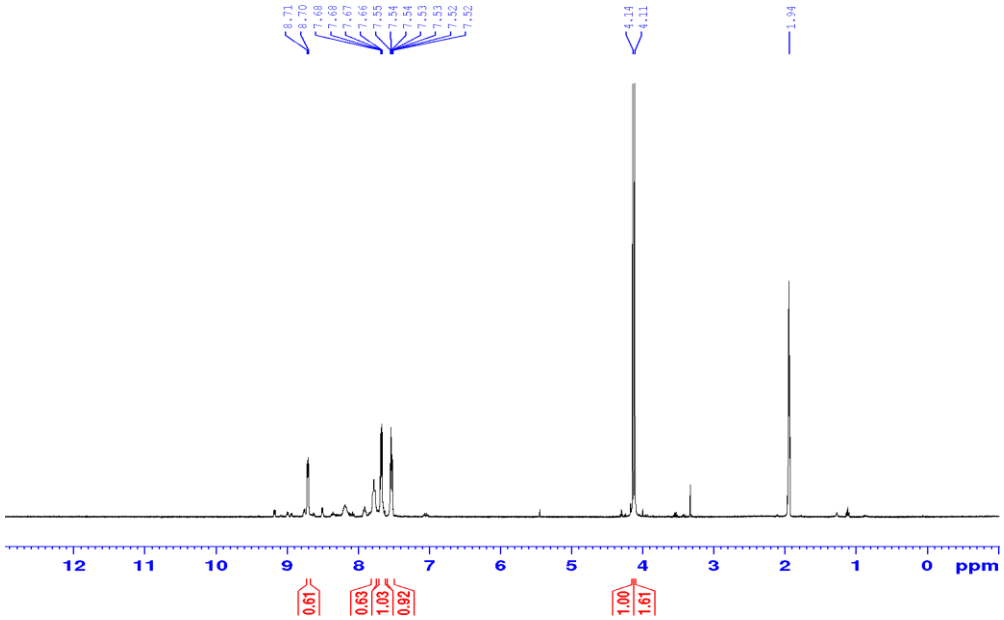

Figure 31. ^{1}H NMR of T-B17 when reacted with 2eq $TMSCF_3$.

The ^{1}H NMR above for the reaction further supports the formation of two compounds, a major and a minor product. Best observed by the splitting of the NHC-methyl peak at 4.14 and 4.11 ppm into two distinct peaks at a 2:3 ratio. The mixture was inseparable by the available equipment.

2.3 Modification of TMS-Ligand Delivery

As the reactions with the variety of Au difluorides with $TMSCF_3$ presented throughout this work, from N-ligand support to NHC bound complexes, persistently formed multiple and short-lived products it seemed appropriate to investigate the reality of whether TMS activation of Au-F from our complexes was feasible but clean consumption of Au-F and formation of TMS-F was promising.

In doing so known stable complexes were targeted for synthesis by making a series of modifications to TMSOTf to deliver other moieties and the required counterion simultaneously (Scheme 14).

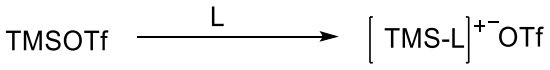

Scheme 14. Reaction scheme for TMS-L synthesis

Much of the world of $[L_2AuF_2]^+$ complexes, and in particular *trans* difluorides, is brand new and extensively unexplored. Making use of our teams' previous work to devise a series of TMS-L compounds that would be capable of recreating some of these known and reported complexes, but by the method generalised in scheme 14.[8]

A series of known compounds **T-B21**, **T-B22**, **T-B23**, & **T-B24** were targeted for their simple one-pot synthesis with the combination of the respective ligands (4-DMAP, Py, MeIM, and 4-CyPy) and TMSOTf (Scheme 14).[49-51]

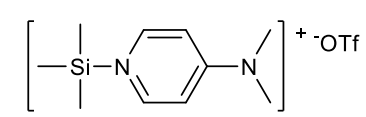

T-B21 - [Trimethylsilyl(4-DMAP)]OTf

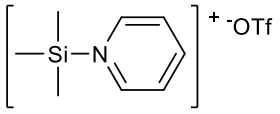

T-B22 - [Trimethylsilyl(Py)]OTf

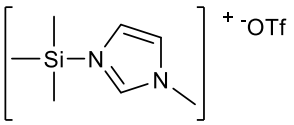

T-B23 - [Trimethylsilyl(MeIm)]OTf

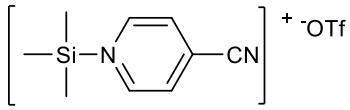

T-B24 - [Trimethylsilyl(CyPy)]OTf

After a brief reaction time all reactions to synthesise **T-B21** to **T-B24** produced a white solid and were recovered in a range of yields (~60% to 90%). While mild chemical shift differences were observed to the literature; notably with the TMS peak, this is attributed to the use of a different solvent.[49-51]

The decreased basicity of cyanopyridine resulted in compound **T-B24** appearing notably less stable than the others and would be seen to emit a smoky substance with any slight change of pressure or temperature, no NMR was taken out of fear of potential damage to equipment. Though **T-B21** through to **T-B23** appeared bench stable under a N_2 environment.

Multiple attempts were also made at synthesising $[TMSPPh_3]^+$, however using ^{31}P NMR only the starting material was observed. Heating to reflux or cooling the reaction in attempts to overcome a possibly energy barrier and determine whether the starting materials are more favoured at room temperature made no difference, and again only the starting material was observed. While this compound is known to exist, much like with cyanopyridine the starting point of TMSOTf appears to not be a strong enough Lewis acid to react with PPh_3.[52]

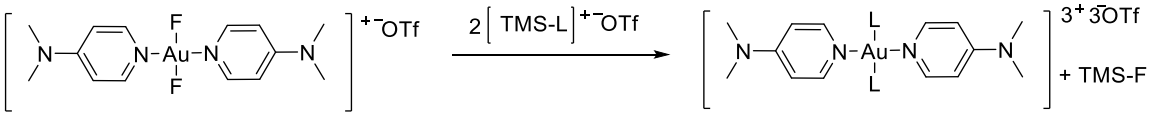

Scheme 15. Synthesis of known compounds by TMS-L delivery method.

Once the TMS-compounds mentioned above were synthesised (namely **T-B21** and **T-B22**), they were reacted with **T-B5** (Scheme 15). with a slight excess of the respective TMS-L to ensure complete conversion. In the case of preparing **T-B25** by TMS metathesis (~82%), 4 days of stirring formed a red solution and crude ^{1}H NMR showed a dominate solitary environment for the 4-DMAP aromatic protons.

Multiple peaks were still observed about the methyl group, yet due to the reduced amount of the TMS methyl protons (determined from the integration) and development of TMS-F methyl peaks at a lower ratio[53], these peaks observed are just the unreacted excess of **T-B21**.

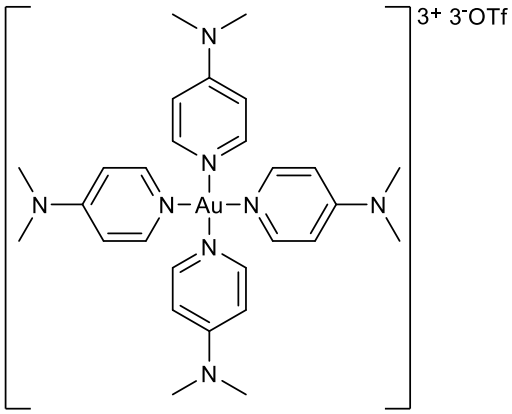

T-B25 - [Au(4-DMAP)$_4$]3OTf

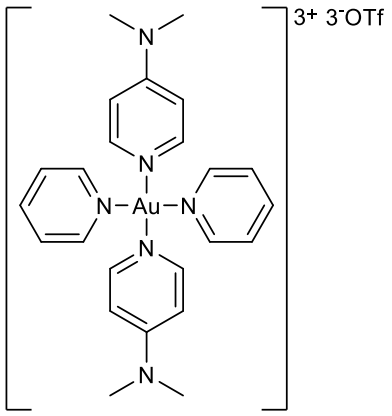

T-B26 - [Au(4-DMAP)$_2$(Py)$_2$]3OTf

The key features of the results (4-DMAP, Ar, and Me peak) were identical to complexes our team had already characterised,[8] showing the TMS-L delivery works efficiently and requiring minimal work-up, which encouraged the reaction between **T-B5** and **T-B22** (synthesis of **T-B26**; scheme 15) highlighting the potential application of the TMS-L delivery system.

The use of **T-B22** proceeded at a much faster rate than the prior reaction (producing **T-B26**), and the results just as consistent probably due to the decreased basicity of the Py moiety to the 4-DMAP resulting in a weaker N-Si bond, and more favourable formation of a Si-F bond.[8] This shows that Si-N activation and ligand exchange by the favourable formation of Si-F can

proceed efficiently and a clear proof of concept for the modification of Au-F bonds by TMS reagents.

As activation of Si-N has now been observed in our system, reattempts at mono-substitution using one equivalent of $[TMS\text{-}Py]^+$ were attempted but all cases led towards either no reaction and/or decomposition observed by the pooling of Au^0 at the bottom of the reaction vessel, further supporting the notion of the necessity for closer to equal *trans* effector as F^- to produce a viably stable compound.

2.4 TMS-NHC and L_2AuF_2 Reactivity.

To investigate whether TMS activation by these Au-F complexes were limited to Si-N compounds, the TMS-L delivery underwent further modification by moving back from Si-N to Si-C to test whether a carbon fronted compound could be delivered to the Au centre and if the issue of the F^- lability could be overcome by the compensating character of the NHC-Au bond.

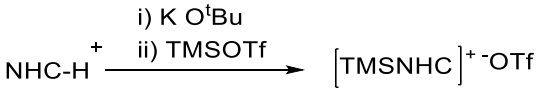

Scheme 16. Synthetic scheme of [TMS-NHC]OTf compounds

As the appropriate pathway to investigate whether the carbon delivery by Si-C activation is possible made use of NHCs due to their back bonding ability, as it's been suggested the Au-NHC bond tends to change its quality and binding modes based of the presence and occupation of p-orbitals and π bonds that are *trans* to it and from the work earlier it was seen that NHCs act as stable supports for Au^{III}-F complexes.

In the initial attempts (Scheme 16) with DMBI-NHC, chosen as similar compounds exist, when allowed to react with TMSOTf at -78 °C would return a viscous oil.[54] The ^1H NMR (Figure 32) showed the formation of multiple products. With the methyl environment spread out over multiple peaks, two sets of aromatic protons and a small singlet observed at 8.93 ppm, suggest not just protonation of the NHC but also possible $C_{(carbene)}$-$C_{(carbene)}$ bonding, as dimers of DMBI NHC are known to exist.[55] However, no comparable deuterated solvent was available to compare to the literature and is it did not fit the purpose of this experimentation, it was abandoned.

Only a marginal peak was seen in the TMS region and due to its relative size is assumed to be grease from the reaction vessel. While a white powder was recovered at 20% (to the mass of NHC used), no isolated TMS-DMBI-NHC could be observed by the method.

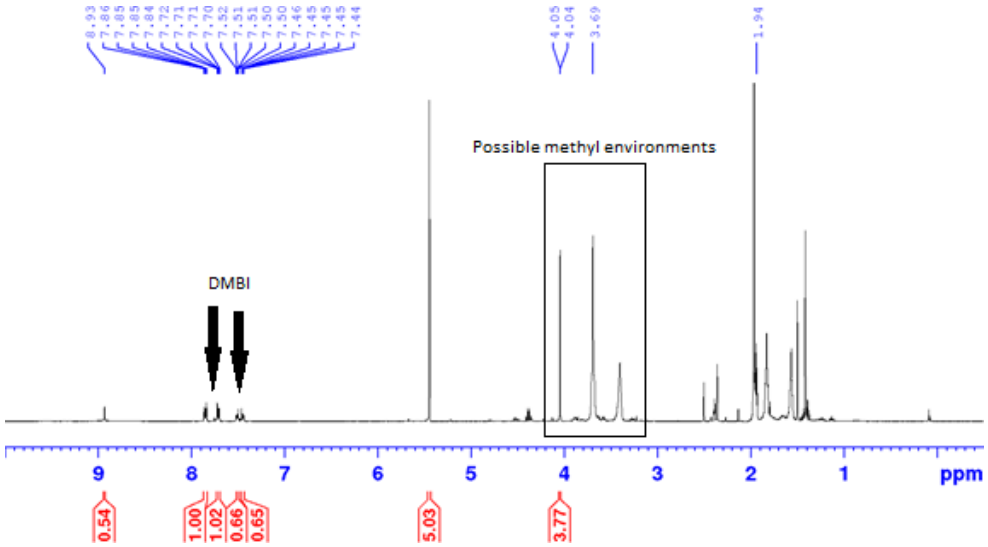

Figure 32. An attempt at formation of TMS-DMBI-NHC, peaks between 7 ppm and 8 ppm show two groups of DMBI-NHC, the boxed section shows possible different methyl environments.

A second attempt with DIPP-NHC was performed, as the bulkier diisopropylphenyl moieties would prevent the carbene carbon from reacting with another carbene carbon.

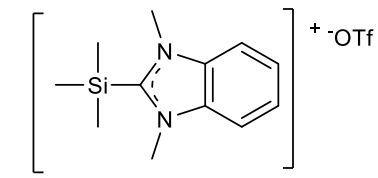

T-B27 - [Trimethylsilyl(DMBI)]OTf

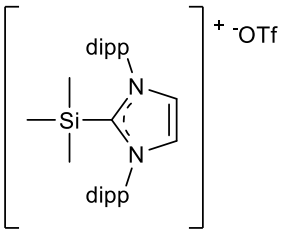

T-B28 - [Trimethylsilyl(dippIm)]OTf

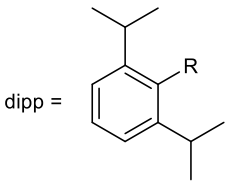

Straightforward synthesis of **T-B28** was achieved at a 95% yield, by deprotonation with O^{t}Bu and reacting the 'free' carbene with TMSOTf in Et_2O. The addition of the TMSOTf instantly resulted in the precipitation of a white solid **T-B28** identified by ^{1}H NMR to match the known literature.[56]

After the TMS-NHC was isolated it was used to test the efficiency of the metathesis ligand exchange by reacting with the initial $[Au(L)_2F_2]^+$ complexes (Scheme 17).

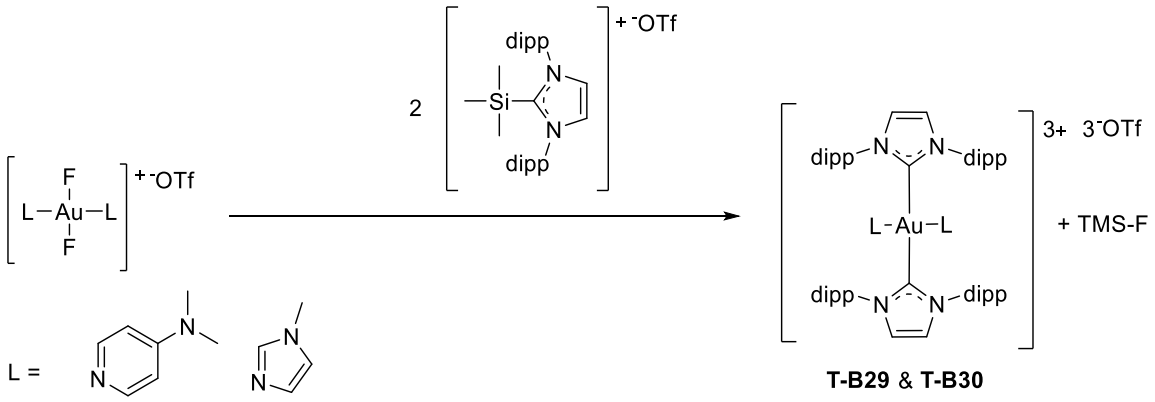

Scheme 17. Reaction scheme between TMS-NHC and N-Ligand $Au^{III}F_2$ complexes

The reaction between 2 equivalents of **T-B28** and **T-B5** proceeded efficiently synthesising **T-B29**. Multiple peaks were observed fitting the prior trends of 4-DMAP-Au and DIPP-Au complexes (Figure 33), with variance from both the starting material and **T-B28**. With a shift downfield in all the aromatic peaks, no return of the more acid proton for the NHC-H precursor, and complete loss of -249 ppm peak in ^{19}F NMR observed (**T-B5**). An attempt with one equivalent was reacted and led to no discernible product in the reaction mixture after a week, and eventually decomposed to purple sediment.

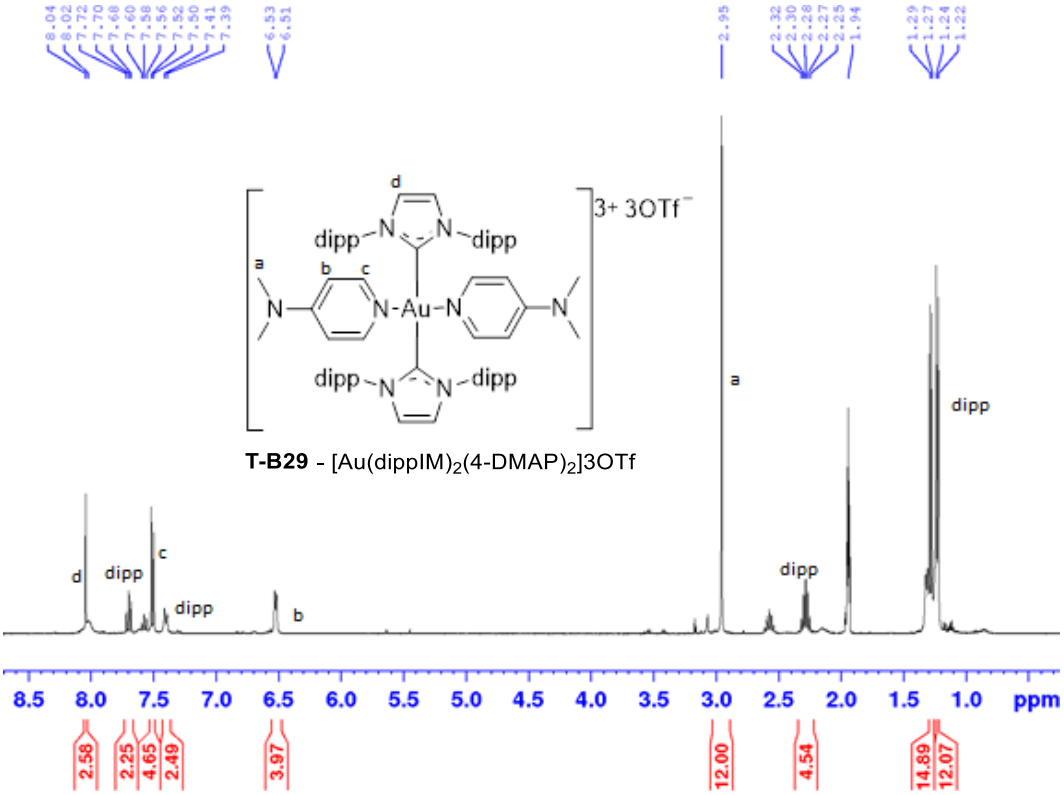

Figure 33 ^1H NMR of T-B29

This observation when a single equivalent of **T-B28** was used supports what has been witnessed throughout. Mono-substitution is not favourable with Au^{III}-*trans*-difluorides, the effect on the *trans*-F bond, increases the labilisation of the fluoride, and consumption of a single F^- by TMS only encourages the decomposition.

To show the TMS exchange is not just limited to **T-B5**, two equivalents of **T-B27** were reacted with **T-B6** (in the synthesis of **T-B30**). Proving to be a more efficient reaction and proceeding at a visibly faster rate with the NMR spectra observed showed a difference in the proton chemical shift for all the species involved from the precursors (Figure 34). The faster rate at which this reaction proceeds further encourages the argument for the reaction mechanism to follow a pentacoordinate complexing state, as the increased electron rich environment observed in the fluorides of the MeIM ligated Au complexes would result in larger activity. Yet, if they were to follow the tri-coordinate decomposition pathway, it would be both unfavourable to either release F^+ (based off oxidation potentials) or to increase in reaction time with a decrease in reactivity.

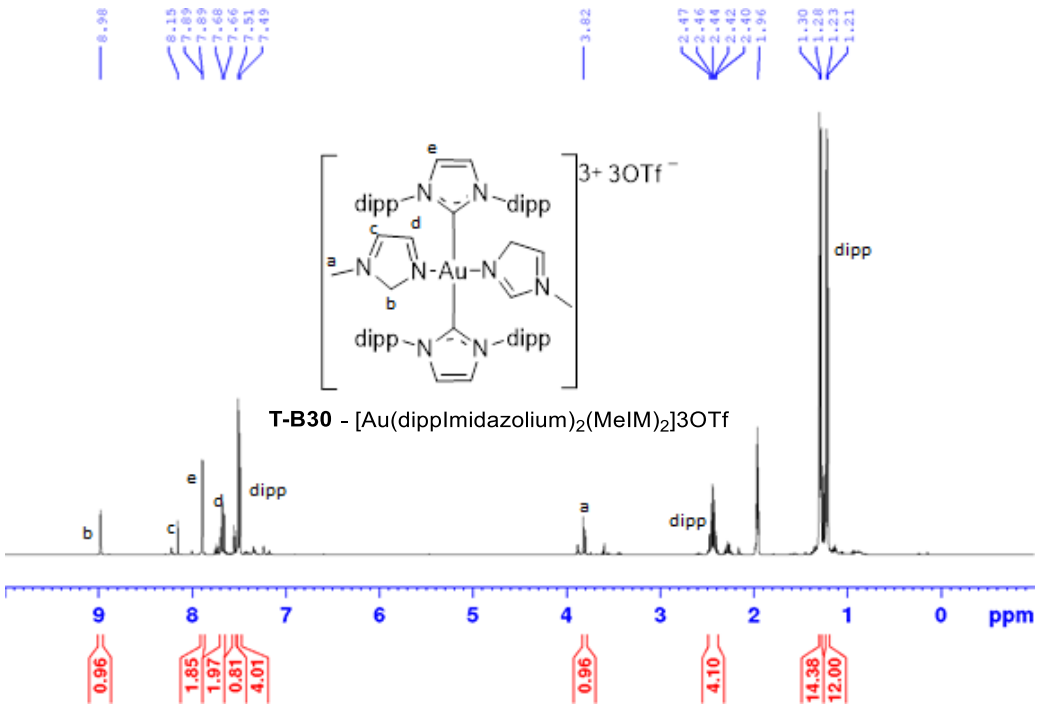

Figure 34. ^{1}H NMR of the formation of T-B30

Synthesis of **T-B30** (Figure 34) was confirmed by the same means as **T-B29** (Figure 33), notably the near 1 ppm shift of the methylene protons of the MeIM groups (3.82 ppm). The near-complete consumption of the peak observable in the ^{19}F NMR would suggest the reason for much of the scattering in figure 34 around the bases of the peaks labelled a, d and the dipp

multiplet in the aromatic region as unreacted starting material. The clean isolation of these complexes shows that the use of TMS-L can efficiently and cleanly deliver C-ligands to the initial N-ligated complexes that $TMSCF_3$ never did and with a good deal of efficiency under mild reaction conditions.

While the Au^{III}-F_2 complexes synthesised and experimented with throughout this work demonstrated a high level of reactivity, taking advantage of thermodynamic favourability of Si-F appeared insufficient for the delivery of CF_3 to Au^{III}. With the observations of the 4-DMAP and MeIM complexes showing an array of results depending on the solvent in use, it could be assumed their trifluoromethylation could be hindered by the transient coordination and interactions of the bulk solvent when using a coordinating solvent such as MeCN, as multiple NMR environments was observed yet reaction in THF did not proceed. All the while the use of a substoichiometric amounts would just encourage decomposition.

This indiscriminate nature towards these Au^{III}- *trans*-F_2 with CF_3, while appearing to exchange with ease when other substituents were used, highlights the importance of the *trans* effect in the stability of high oxidation state Au complexes. As discussed earlier, F^- and CF_3^- represent different ends of the *trans* effecting spectrum. Reverse engineering a complex to have the same resonance observed by ^{19}F NMR inadvertently showed the instability of the intended complexes and inability to synthesise by our intended Si-F bond-forming method. Yet the CF_3 moiety rests on the stronger end of the *trans* effecting spectrum which should suggest the formation of stronger bonds to the Au centre when they are *trans* to one another, and can tend towards shorter distances than the N-bound complexes that are known to be stable as a *trans* difluoride.[28, 29] As this should present a stabler complex than the Au^{III}-F_2, the observations of the Au^{III}-F_2 complex stability suggests the electronic pull of the F^- to the metal centre to be of key importance to stabilising Au^{III}.

The proposition that fluorides weak trans-effect diminishes the exchange at the *trans*-position; coupled with the CF_3 encouragement of *trans*-lability,[23] seemingly could be summarised as a stand-off of F^- hindering the rate at which the Si-F bond form, but once it has this results in the CF_3 lengthening the Au-F bond leading to dissociation and without a secondary species to form a stronger bond with, the Au complex decomposes. Alluding to the idea that the moiety that bonds *trans* to the F^- would have to be of similar σ-donating ability and possess occupied p-orbitals to be inaccessible to the metals d-orbitals.

This idea was incidentally looked at further while testing to see if the methodology would work at all, the path of synthesising a series of TMS analogues showed remarkable reactivity with the L_2Au^{III}-F_2 complexes.

Much like the previous observation, the modified TMS compounds that contained moieties that were capable of back bonding appeared to be the only compounds that were observed to cleanly deliver, implying a necessity for accepting some of the electron density from the metal d orbitals to sustain the complex long enough for the secondary metathesis reaction to take place, provided the moiety's electron affinity cannot overcome the $Au^{III/I}$ reduction potential.

Using these compounds with this TMS delivery method, known complexes of Au^{III} were easily recreated. and the addition of one equivalent TMS-L in all cases would exacerbate decomposition of the Au-complexes, further enforcing the domineering *trans* effect.

Using these ligands and starting with *trans* complexes saw no confirmed isomerised or reductive elimination products. Yet there is further application of this TMS-L delivery system to be explored with $L_2Au^{III}F_2$ species, as other metals have shown that *cis* fluorine conformations are still strong enough to support high oxidation state metals yet experience a slightly heightened degree of lability.[42]

2.5 **Computational look at Au-F bonds.**

From the observations within this work it is seen that the Au-F bond shows a remarkable level of reactivity. While the scale at which the F^- resonance moves in ^{19}F NMR should be tantamount to this, in lieu of lab access and time a computational approach towards understanding the reactivity and possible tunability of the Au-F bond was approached by members of my team, and some of their data will discussed.

Table 1. Output from computational data produced by another member within our team. The table shows the Au-F bond length and BDE for Au^{III}-F species when ligated by neutral and negative ligands

Ligand Charge	Complexes	*Trans*-Ligand	Au-F Bond Length	(%$_{diff}$)	Au-F BDE (kJ/mol)	(%$_{diff}$)
Neutral	$Au(Py)_3F$	Pyridine	1.977	0.000	-1485	0.000
	$Au(Py)_2$(n,n`-dimethylimdazole)F	n,n`-dimethylimidazole	2.006	1.456	-1433	3.564
	$Au(Py)_2(PMe_3)F$	Trimethylphosphine	2.017	2.003	-1376	7.620
	$Au(Py)_2(PPh_3)F$	Triphenylphosphine	2.048	3.528	--	--
Negative	Au(Py)2(Cl)F	Chlorine	2.012	1.755	-1193	21.81
	$Au(Py)_2F_2$	Fluorine	1.986	0.454	-1319	11.84
	$Au(Py)_2(CCH)F$	Acetylene	2.028	2.547	-1158	24.74
	$Au(Py)_2(Ph)F$	Phenyl	2.085	5.318	-1030	36.18

Table 2. Computational output showing Au-Cl bond length and Au-Cl BDE for Au^{III} chlorides. Calculated by another member of the authors group

Ligand Charge	Complexes	*Trans*-Ligand	Au-F Bond Length	(%$_{diff}$)	Au-F BDE (kJ/mol)	(%$_{diff}$)
Neutral	$Au(Py)_3Cl$	Pyridine	2.388	0.000	-1345	0.000
	$Au(Py)_2$(n,n`-dimethylimdazole)Cl	n,n`-dimethylimidazole	2.418	1.248	-1272	5.579
	$Au(Py)_2(PMe_3)Cl$	Trimethylphosphine	2.433	1.867	-1248	7.482
	$Au(Py)_2(PPh_3)Cl$	Triphenylphosphine	2.462	3.052	--	--
Negative	$Au(Py)2(Cl)_2$	Chlorine	2.426	1.579	-1050	24.63
	$Au(Py)_2(F)(Cl)$	Fluorine	2.401	0.543	-1158	14.94
	$Au(Py)_2(CCH)Cl$	Acetylene	2.439	2.113	-993	30.11
	$Au(Py)_2(Ph)Cl$	Phenyl	2.793	4.302	-866	43.33

Across the 4 tables above and below, the output generated a curious comparison into the strengths of the Au-X and Pt-X bonds, in respect to F^- and Cl^-. Under this method the most stable complexes calculated were to be supported by three neutral Py ligand, for both sets of metals with either Cl^- or F^- *trans* ligands. Amongst the Au subsets with F^- and Cl^-, the general stability trend observed in the previous sections is further supported by the increasing trend amongst bond dissociation energy, with the decrease in the degree of back bonding capability of the ligands. The Ph ligand expressing the strongest *trans* effect towards the Au-F bond, increasing the bond length by 5.318% (Table 1) compared to the 4.302% (Table 2) calculated for the Au-Cl bond length, and increasing the Au-F BDE by upwards of 36.18% (Table 1) compared to the three Py ligands.[57]

Though the Py ligand has a structural similarity towards phenyl, in general the calculations show that the use of anionic ligands shows a more drastic alteration of both the bond length and BDE for Au and Pt complexes compared to the neutral ligands. All of which were calculated to change the Au-X bond length by less than 10%. Comparatively the Pt^{II} neighbour shares vast similarity with the increased stabilisation trends for Pt-F bonds while generally the values suggest the Pt^{II}-F species to exhibit more favourable fluoride dissociation (Table 3), which implies Au^{III}-F complexes could be more versatile in terms of modification, storage, and possible turnover of catalytic activity.[58] A notable exception to this appears with $Pt(Py)_2(Ph)Cl$, where there is a drastic decrease in bond length and smaller increase in BDE.

Table 3. Computational output showing Pt-F bond length and Pt-F BDE for Pt^{II} fluorides. Calculated by another member of the authors group

Ligand Charge	Complexes	*Trans*-Ligand	Au-F Bond Length	(%$_{diff}$)	Au-F BDE (kJ/mol)	(%$_{diff}$)
Neutral	$Pt(Py)_3F$	Pyridine	1.999	0.000	-1075	0.000
	$Pt(Py)_2$(n,n`-dimethylimdazole)F	n,n`-dimethylimidazole	2.041	2.079	-1020	5.251
	$Pt(Py)_2(PMe_3)F$	Trimethylphosphine	2.021	1.095	-1005	6.731
	$Pt(Py)_2(PPh_3)F$	Triphenylphosphine	2.028	1.440	--	--
Negative	Pt(Py)2(Cl)F	Chlorine	2.037	1.883	-766	33.57
	$Pt(Py)_2F_2$	Fluorine	2.029	1.490	-800	29.33
	$Pt(Py)_2(CCH)F$	Acetylene	2.085	4.212	-721	39.42
	$Pt(Py)_2(Ph)F$	Phenyl	2.128	6.252	-654	48.70

Table 4. Computational output showing Pt-Cl bond length and Pt-Cl BDE for Pt^{II} chlorides. Calculated by another member of the authors group

Ligand Charge	Complexes	*Trans*-Ligand	Au-F Bond Length	(‰diff)	Au-F BDE (kJ/mol)	(‰diff)
Neutral	$Pt(Py)_3Cl$	Pyridine	2.397	0.000	-918	0.000
	$Pt(Py)_2$(n,n`-dimethylimdazole)Cl	n,n`-dimethylimidazole	2.773	1.901	-852	7.458
	$Pt(Py)_2(PMe_3)Cl$	Trimethylphosphine	2.424	1.120	-870	5.369
	$Pt(Py)_2(PPh_3)Cl$	Triphenylphosphine	2.431	1.408	--812	12.25
Negative	$Pt(Py)2(Cl)_2$	Chlorine	2.438	1.696	-615	35.69
	$Pt(Py)_2(F)(Cl)$	Fluorine	2.439	1.737	-640	39.53
	$Pt(Py)_2(CCH)Cl$	Acetylene	2.492	3.886	-557	48.95
	$Pt(Py)_2(Ph)Cl$	Phenyl	2.535	5.60	-498	62.71

This computational data looked at partly supports this notion by showing that the stability of the higher oxidation metal complexes increases proportionally with the increase of d-electron acceptance by the supporting ligands and suggests the use of heavily backbonding bidentate neutral ligands could aid in achieving mono fluorinated products. Though this necessity for the ligand to be able to accept the metals d-electrons in order to stabilise the *trans* bond (opposed to donating the bulk of electronic density) hinders the possibility of modification but does open a window into the realm of possible modifications to achieving novel Au complexes.

As this data also shows the subtle yet grand changes the *trans*-effect has on the Au-X bond, a curious note within the computation data (while missing for Au), the Pt-F BDE from the calculations of PPh_3 and PMe_3 shows the slight change in the electronic density of the p orbitals of the ligands results in the increase in BDE of the *trans*-x species. This trend while not calculated for Au, can be assumed based of the trends of the complexes calculated and helps elucidates the effect the occupation of the ligands p-orbitals has on the *trans* moiety that has been suggested throughout this work.

Aside from the comparisons between the Au and Pt complexes calculated, it's shown across table 1 & 2 the direct *trans* effect of the ligands on many of the Cl^- and F^- Au complexes, and shows a greater change in terms of bond length and dissociation energy between the switch from a Cl to F for both anionic and neutral ligands, though more profound for F^-. For example

the calculations showed between Cl-Au-Cl to F-Au-Cl there is nearly a doubling of the % change of the bond, while there is still a large general increase for the Pt complexes, it is suggested within this data to be more exemplified for that of Au species, showing the drastic effects *trans* ligands bring to Au species. This lengthening of the Au-X bond, which has been observed experimentally, has been suggested to be in-part responsible for the unique level of reactivity these Au complexes exhibit.[26]

Along with this, the favourable substitution for the heavier halides could be suggested through the tendency towards lower energy and less reactive states is driven by the increased lability of the F^-, compared to the Cl^-. In contradiction to the observed behaviour however, the calculations suggest that the Au-Cl dissociation should be more favourable over Au-F despite the calculated (comparative) lengthening of the Au-F bond, yet experimentally researchers have shown the tendency for heavier halogens to displace F^- from Au to be very favourable.[37] A delicate interplay between effective bond type and electronegativity is suggested to be at play here, while the more electronegative F^- has a stronger electronic affinity than Cl^-, the lesser tendency of the Cl^- and slightly increased ability to not draw away electronic density seems to provide an adequate support for sustaining a monosubstituted Au^{III} complex. As the increase in stability was calculated to follow a trend of increase of back bonding and the Py and NHC support ligands appeared to offer the most support as a scaffold for the metal centres reactivity. While this apparently grander effect caused by anionic ligands on the *trans* F^-, highlights many issues around modification of a mono fluorinated Au^{III} complex. Though coupling the calculated data showing little change between the Au-F and Au-Cl bonds with the experimental observations where the NHC ligands had drastic changes in the F^- electronic environment in NMR, adds to the idea of the 'tuneability' of asymmetrical complexes, while not only offering a large level of support, but large promise in creating a viable stable catalyst. The comparative values show a larger tendency for stabilisation for Au^{III}-F to Pt^{II}-F, suggesting that while less reactive than the Pt counterparts, the large degree of reactivity towards Si-F formation in the presence of organosilicon compounds still presents favourable modification of the Au^{III} complexes to be possible.

2.6 Electro-oxidation of Au^{I}.

As an endeavour of this work is to create a system that can be easily synthesised, and as mentioned earlier the current methods for obtaining Au in its III state are often expensive, or not very pleasant to handle. An alternative initial oxidative method was explored using electrochemical techniques to eliminate the need for the synthesis and use of expensive oxidants such as hypervalent iodine or XeF_2 in reaching these homoleptic n-bound Au^{III} complexes that are susceptible to attack from the more economical nucleophilic fluoride sources.

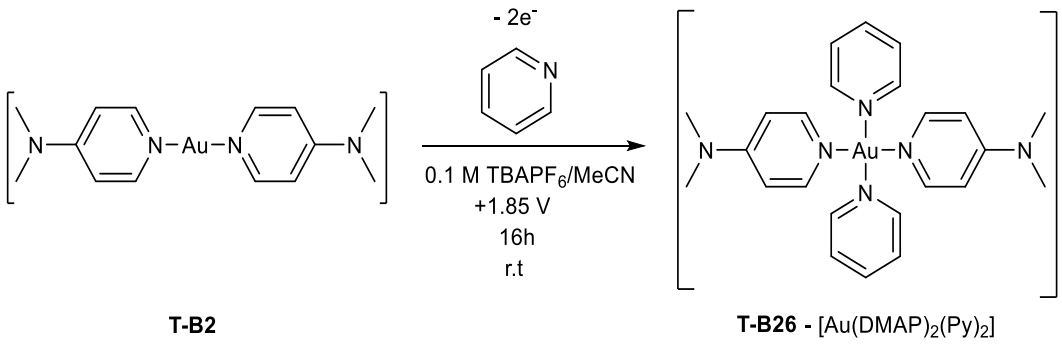

*Scheme 18 Intentional electrochemical synthesis of **T-B29***

Attempts at synthesising a tetrakis Au^{III} complexes from the linear Au^{I} precursors were performed making use of the Ika® Electrasyn 2.0, to use electricity as a cheaper and safer alternative to the previously used oxidants. This device was chosen for its ease of use and standardisation of components to both industrial synthesis and small-scale bench top research. Allowing for all the work below to be performed with a Ika® branded and designed glassy carbon working electrode for cyclic voltammetry, as well as standardised graphite blocks for both the auxiliary and working electrodes for synthesis.

To facilitate the displacement step of the pyridine for nucleophilic F^-, compound **T-B26** was chosen as the target compound, considering **T-B2** demonstrates the most stability out of the Au^{I} species experimented with here in, while the secondary Py ligands could be introduced to **T-B2** as the solution itself.

Preliminary studies were undertaken to determine the optimal electrochemical conditions required. The supporting electrolyte chosen was 0.1 M $TBAPF_6$ and the following solvent mixtures were investigated: pure pyridine or 5:1, 1:1, 1:5, and 1:10 mixtures of pyridine and MeCN. These studies showed the ideal conditions to minimise the amount of Py used to be 1:10 Py/MeCN as excess pyridine appeared to increase the amount of current flowing, which obscured potentially necessary electrochemical information. Working with a pseudo-

reference electrode of Ag/Ag^+ these conditions appeared to not effect the solvent within the potential window expected to be able to observe the $Au^{I/III}$ redox couple (Figure 35). This expected window was assumed to be between -1 V and +1 V vs Fc/Fc^+ and as seen in figure 36, the observation of oxidation of $Au^{I/III}$ would not be hidden by a signal from Py nor would Py be oxidised over the Au.

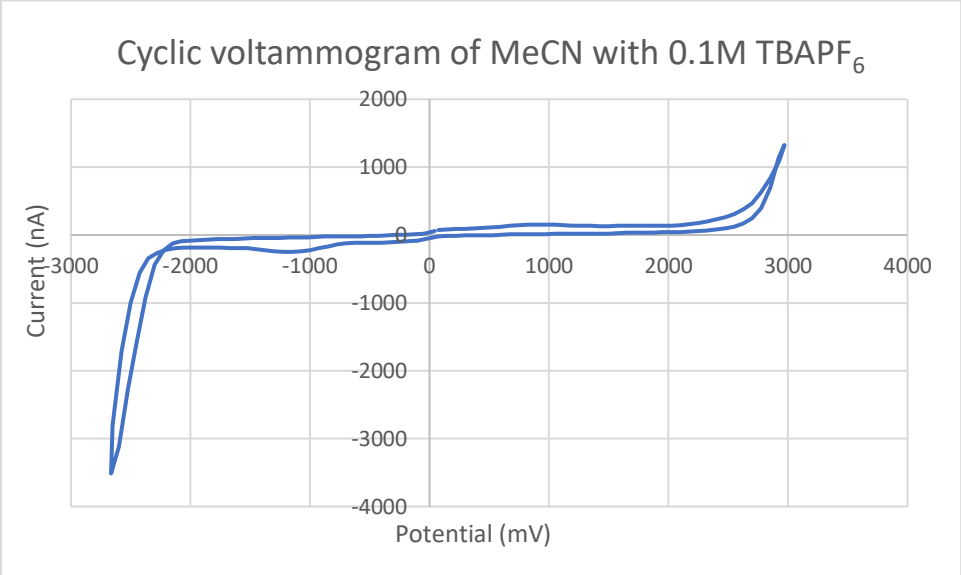

Figure 35. Cyclic Voltammogram of MeCN in $TBAPF_6$ showing oxidative and reductive window for the solvent against Ag/Ag^+

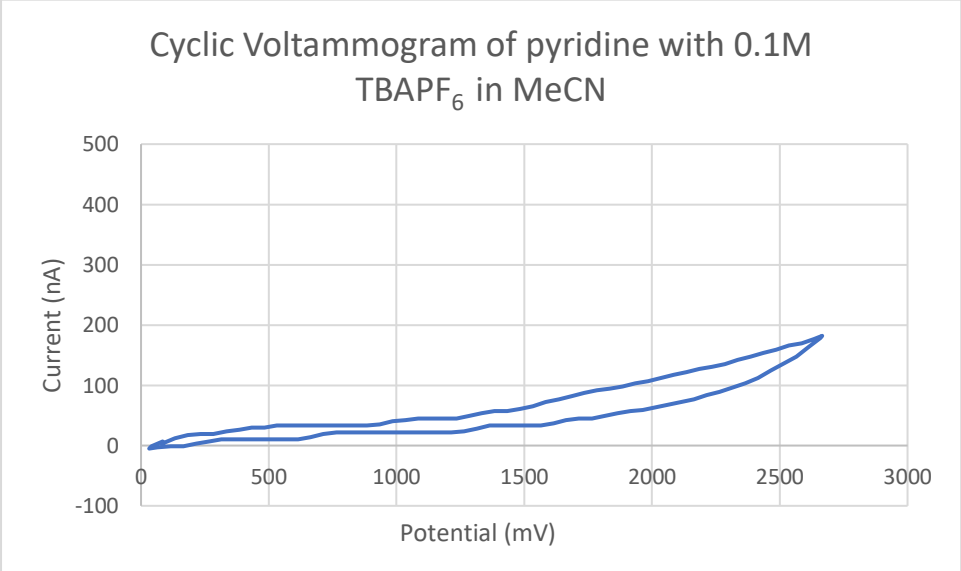

Figure 36. Cyclic voltammogram of pyridine showing oxidative window fitting the known data for T-B5

As the devices ability to run and record data was not as sensitive as equipment previously used, or as well resolved as previous data analysed by our group on the same specimens,[8]

along with the use of a single pseudo reference electrode required a scan rate/current dependence study to be performed.

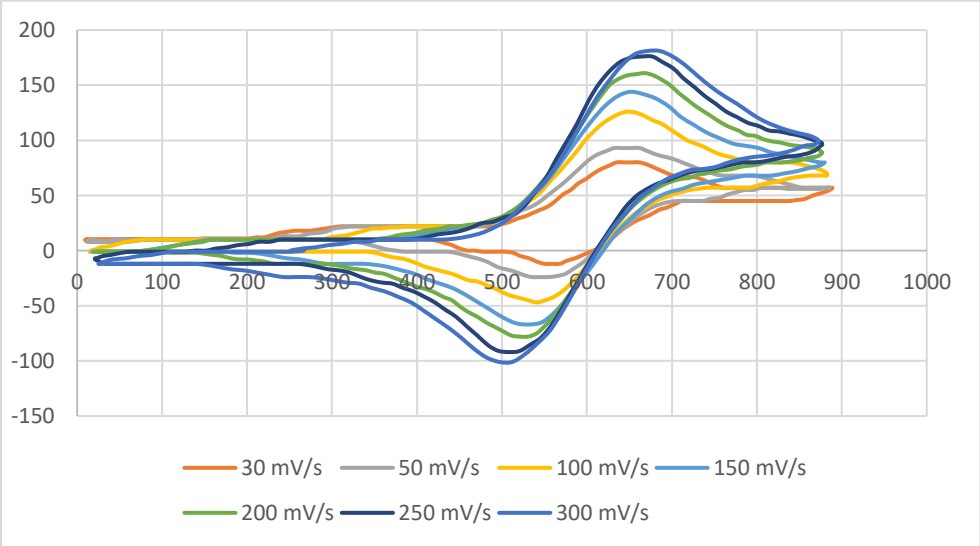

Figure 37. Multiple CVs of Fc/Fc⁺ in MeCN/0.1 M TBAPF6 vs. Ag/Ag+ at different scan rates

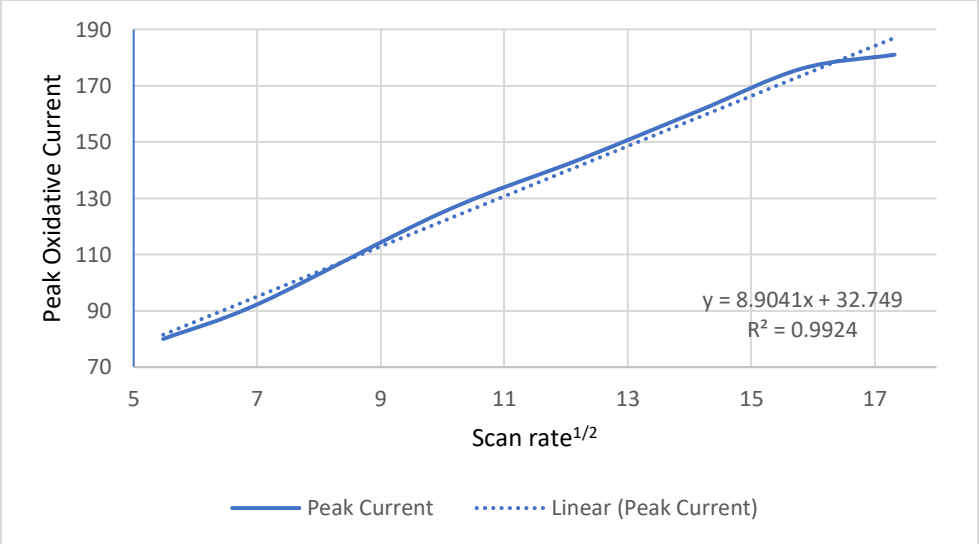

Figure 38. Plot of peak oxidative current vs the square root of the scan rate

Using ferrocene at a range of lower scan rates to ensure the returned values were consistent with the current-scan rate dependence model, as well as consistency in the quality of the data acquisition at the rates used in the reference literature. In determining the optimal scan rate for the Electrasyn 2.0s degree of sensitivity (Figure 37), the plotting of the peak oxidation current against the square root of the scan rate (Figure 38) shares a linear relationship at over the standard scan rate used in the known data, fitting the model proposed in the Randles-sevcik equation below.

$$i_p = 0.4463nFAC\left(\frac{nF\nu D}{RT}\right)^{\frac{1}{2}}$$

As this consistency at a standardised scan rate by the Electrasyn appears acceptable and the optimal reaction conditions determined to be of the lower ratio of Py to MeCN, exposing **T-B2** to these conditions and scanning over the oxidation potential window to +2 V vs Ag/Ag^+ shows an oxidation in the expected window (Figure 39) not observed under the blank conditions in figures 35 and 36. The only issue that arose amongst these tests was the observation of a large discrepancy between measured and set potential for the Electrasyn 2.0, bringing unreliability to the measurements of the negative potentials, however as the positive windows shared linearity between set and measured potential the curve fitting observed in figure 38 should stand true for the oxidative current.

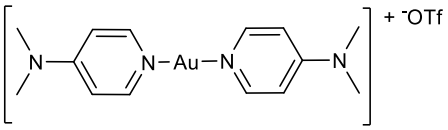

T-B2 $[Au(4\text{-}DMAP)_2]OTf$

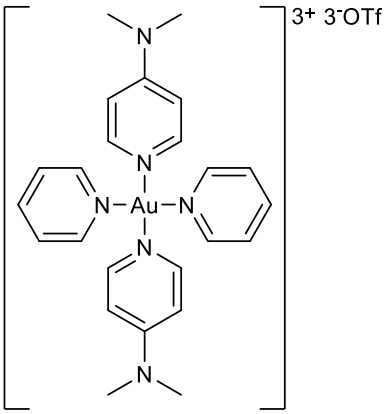

T-B26 - $[Au(4\text{-}DMAP)_2(Py)_2]3OTf$

Under the chosen conditions the disappearance of the oxidation peak was observed (Figure 39) and immediate lack of returning reduction current indicates the analyte undergoes an irreversible oxidation at this potential from the I to III state, yet while in the presence of excess Py would suggest possible formation of **T-B26**. Coupling with the reduction of III/I seen in both figures 39 & 40, and rising current at more negative potentials assumed to be I/0 reduction the author attempted to not have occur to prevent fouling onto the working electrode, however due to the nature of the Electrasyn 2.0® and Ag/Ag^+ reference electrode knowing the exact potentials of the electron transfer events are hindered by lack of sensitivity and potentially large potential drifts.

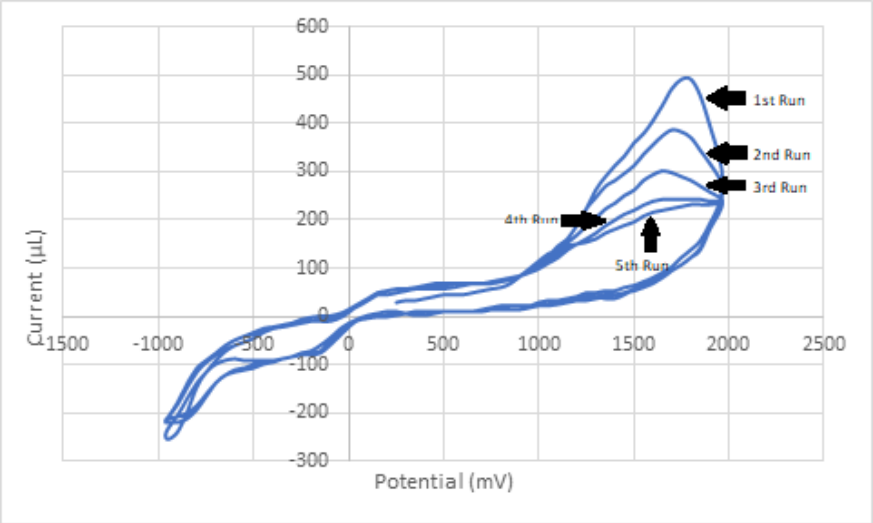

Figure 39. cyclic voltammogram of $[Au(DMAP)_2]OTf$ in the presence of Py vs Ag/Ag^+ with a forward scan rage of 200 mV/s

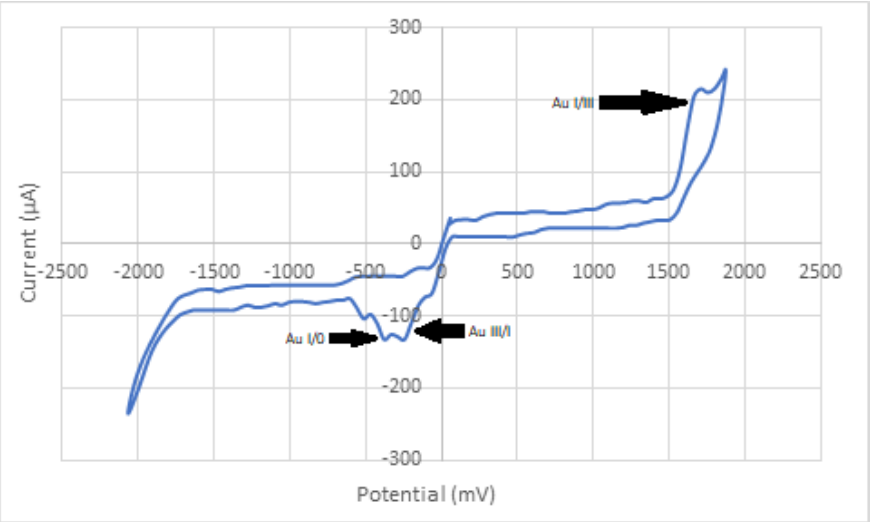

*Figure 40. CV of **T-B2** in 0.1 M $TBAPF_6$/MeCN, no pyridine, at 300 mV/s vs Ag/Ag^+*

Comparatively in figure 40, the same oxidation peak of I/III is observed, however there is a lack of increase in current as the potential approaches -1 V, suggesting that a ligand is required for the stabilisation of these complexes at potentials lower than Ag/Ag^+ redox potential.

Attempts at electrosynthesis and isolation of **T-B26** proceeded by holding a constant oxidative potential of +1.85 V for 60 minutes using the same electrolyte and concentration. A yellow colour slowly formed from the anode, similar-to the colour anecdotally observed from solutions of low concentrations of the tetrakis pyridyl Au^{III} complexes.

Due to the colour change and observation of the diminishing peak in figure 39, the concentration of reactant was further increased to hopefully obtain an isolatable product, and the use of a split cell was employed to separate the oxidative and reductive compartments with sacrificial electrodes to prevent stray reduction and fouling of the Au species, as well as sacrificial graphite electrodes produced by Ika®. However due to the use of a pseudo reference electrode, the potential drift caused by the Ag/Ag^+ coupling saw the observed oxidation of the **T-B2** sample had shifted slightly (appearing at +1.4 V, figure 42 shows CV adjusted to vs Fc/Fc^+), yet the reaction was held under a constant +1.85 V for 16 hours to be keep the reaction conditions the same to the prior observation.

In expectation of the formation of **T-B26**, a reference sample was synthetically produced using the same method shown in scheme 8 on page 20 by the oxidation of **T-B2** with $[PhI(Py)_2]OTf$ showing target signals in ^1H NMR and CV.

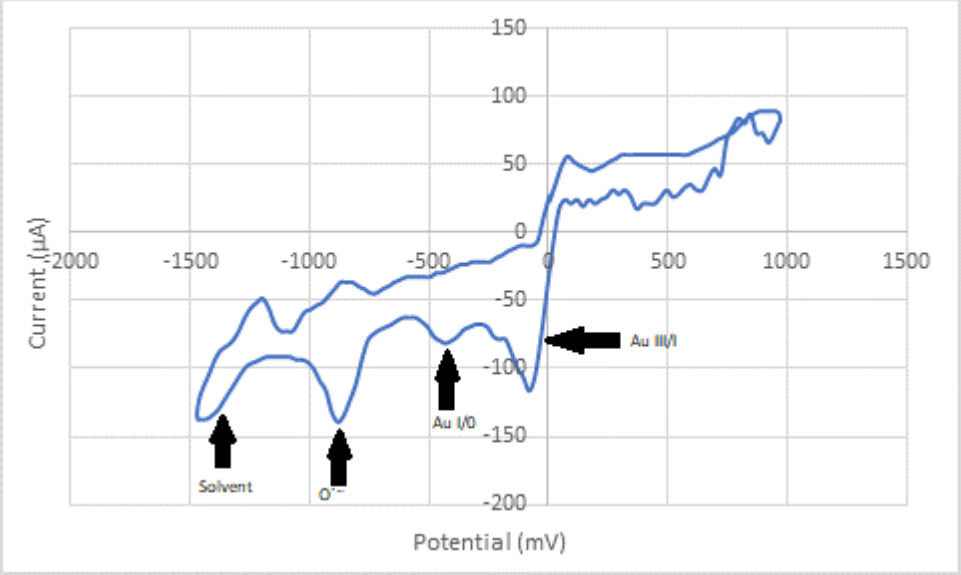

*Figure 41. CV of 0.1 mmol **T-B26** in 0.1M $TBAPF_6$ with a forward scan rate of 1000mV/s vs Fc/Fc^+*

Figure 41 above of the synthetically produced reference sample shows a slight reduction peak at -80 mV, the beginning of another reduction at -430 mV before it another at -880 mV, and finally one at -1452 mV vs Ag/Ag^+. The first two of the peaks and the last mentioned are the ones of interests as the peak at -880 mV could be indicative of the reduction of oxygen to the O_2^- radical. Though typically this is very reversible reaction, the author suspects the generation of an electron rich oxygen species in the presence of electron deficient Au species results in an electron transfer to the Au complex. With this transfer event happening chemically and not at the electrode interface it is not detected, and results in the lack of a return oxidation peak in the CV. Importantly to note the addition of Fc to create a baseline for

the potential would often destroy the returned signal and while the potentials seen above are different to many of the potentials observed for the same suggested electron transfer events, all happen within the same boundaries and similar potentials if a generalised 400 mV (the typical Fc/Fc^+ potential when vs Ag/Ag^+) is subtracted. With this taken into account the peak at -1452 mV should be considered the edge of the solvent window.[59] An important observation to note is the appearance of the noise in the oxidative sweeps in figure 41 (0 → + potentials) the author suggests to be caused by the devise itself as it struggles when starting with a falling sweep and crossing over to the oxidative potentials from reductive, coupled with the fouling (and subsequent deformation) of the Au to the electrode interface from the initial reductions.

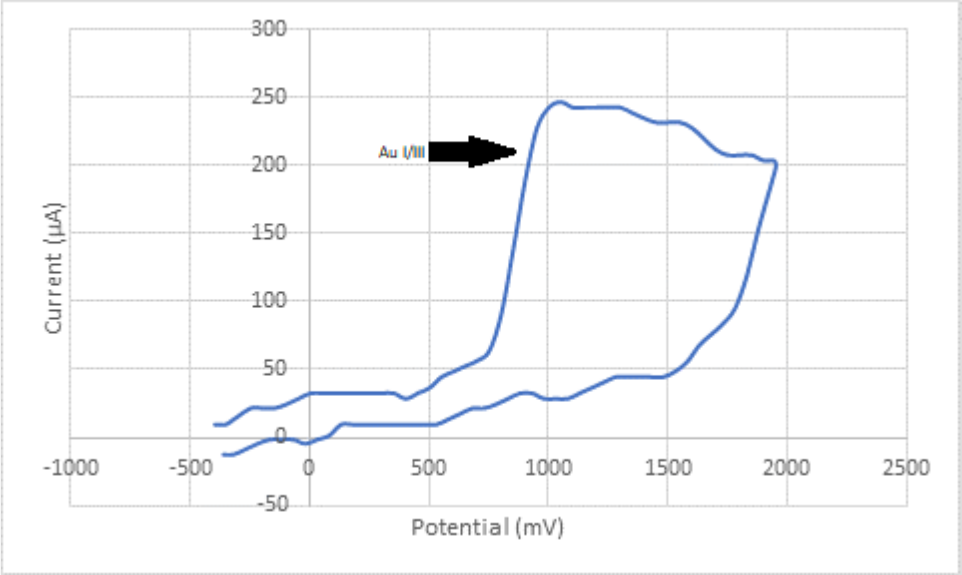

Figure 42. Cyclic Voltammogram of [Au(DMAP)2]OTf with an excess of Py vs Fc/Fc^+ with a forward scan rate of 1 V/s

After the reaction was completed through multiple plagued attempts between fumehood and general power outages, a CV (Figure 43) was run on the cell once the current had returned to the baseline. The CV above showing the oxidation peak previously observed in the preparatory CV near +1 V in figure 42 had disappeared and multiple reduction peaks had appeared at -367mV, -694 mV, and -1380 mV. Aside from the loss of the oxidation at +1 V, the appearance of the peak at -367mV represents a very significant change from figure 42 as a species that can undergo electroreduction at that potential was not present initially. Due to previously mentioned power supply issues, the reaction frequently stalled and was performed over multiple attempts and the total charge applied to determine the overall reaction turn over could not be determined, the reaction was halted and inspected after the measured current

returned the same value of 0.1 mA measured by a dummy cell with the same solvent/electrolyte system.

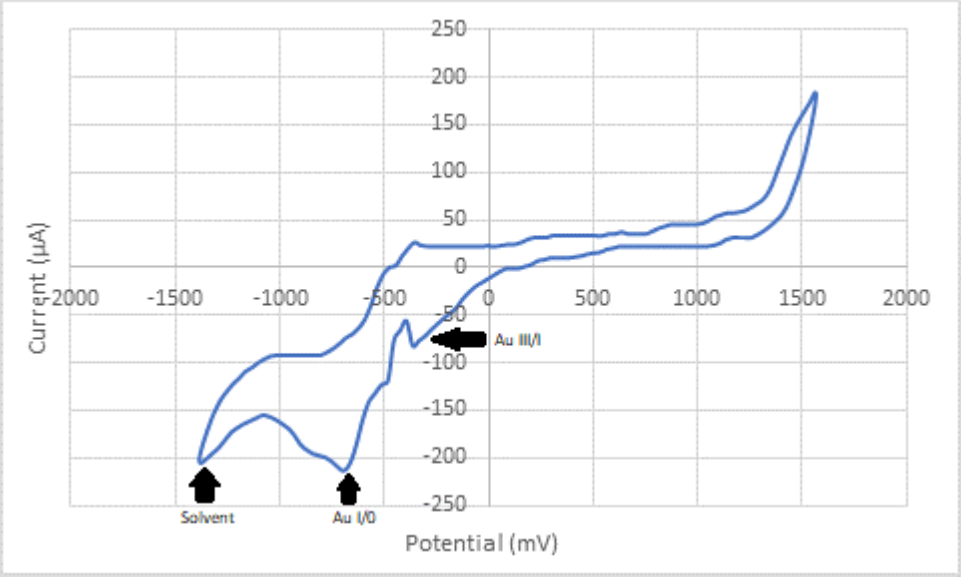

Figure 43. Cyclic Voltammogram of electrosynthetic Product vs Fc/Fc^{+} with a forward scan rate of 200mV/s

The observed reductions in figure 43 confirm the alignment of the data to know observations of the same class of complexes.[8] The reduction at -367 mV fits the stability trend witnessed with these species as the III/I reduction happens at a more negative potential compared to the homoleptic pyridine and cyanopyridine, yet more positive than the 4-DMAP species. The I/0 reduction observed at -694 mV deviates from this trend, appearing more positive than any of the known homoleptic species. This reduced reduction potential shows the drastic response Au complexes display due to adjustments of their supporting ligands, while the homoleptic species all tend to have a similar I/0 reduction, and the III/I is observed to move more drastically across the species, the displacement of I/0 above from the general trend suggests uneven displacement of electron donation/withdrawal leads to complexes more favourable towards the complete reduction of Au to its elemental state.

While the suspected ligand reduction peak (-1380 mV, figure 43) appears at much high potentials previously reported, there is a possibility that this peak is indicative of the $Au^{I/0}$ reduction. Though the sheer increase in potential from the observations of the similar class of compounds would suggest that the complex **T-B26** exists at a remarkably stable state compared to the other knowns. However, as the excessive amounts of Py in solution would have resulted in the observed signal at more negative potentials from the area of interest to drown out the analytes signal if scanned lower to confirm these suspicions. The probability that this peak is not directly related to the Au centre can also be inferred through the

observation of the lack of this peak appearing in figure 40 of the Au^{I} starting product in the absence of Py.

An Isolation method was developed to allow isolation of the formed Au complex from the large excess of $TBAPF_6$ supporting electrolyte. Here THF was used as the solvent because its low dielectric constant allowed for the dissolution of $TBAPF_6$, while the Au complexes were insoluble and could be collected by centrifugation. However, further confirmation of the formation of the **T-B26** species was hindered by stability issues. As the predominate anion in the reaction mixture was PF_6, known to not counter cationic gold species strongly due to relatively weaker coulombic interactions,[60] and the overall discrepancy in stoichiometry in the charge balance resulted in an inability to isolate the product from the electrolyte solution.

Acquiring an electrolyte with a more Au^{+} suitable counterion to try to increase the chance of isolation was hindered by time constraints coupled with pandemic restriction responses.

An extension to the reaction was conceived but unable to be implemented due to pandemic restrictions. As the general idea was to use electrochemical oxidation to achieve the Au^{III} state in a complex susceptible to fluorination by nucleophilic fluorides. Upon its oxidation it is conceivably possible to use the method outlaid in figure 44, with the addition of KF and 18-crown-6, to displace the pyridine and form **T-B5**. The displacement by the nucleophilic fluorides should provide the addition 2 units of negative charge required to balance the chemical equation, this general scheme is outlaid below.

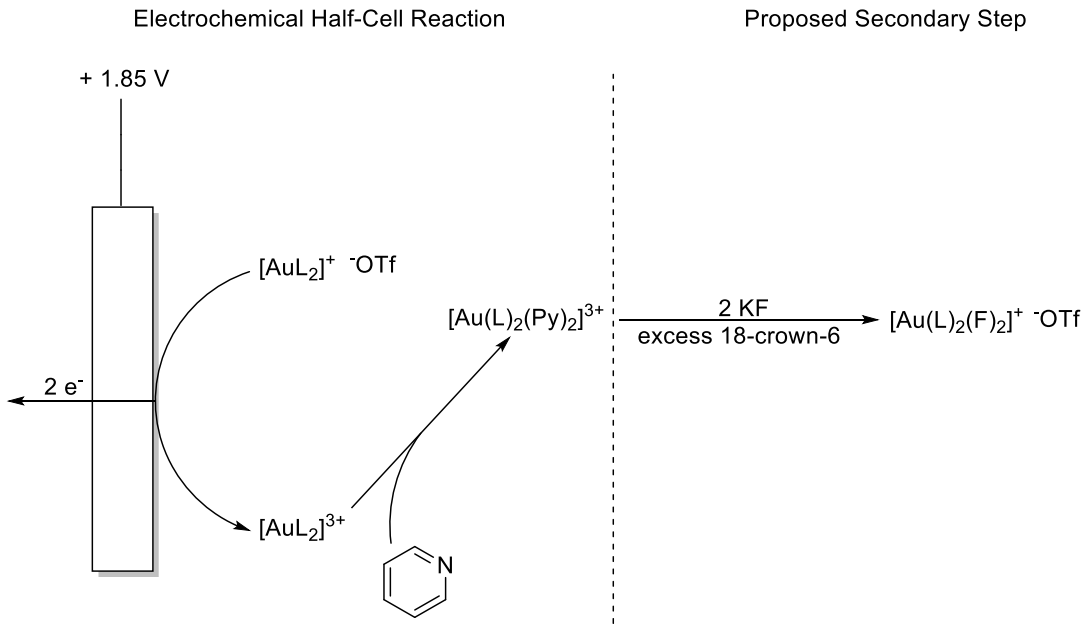

Figure 44. Half-Cell reaction and scheme for proposed secondary step to isolate a stable Au^{III}-F_2

This electrochemical oxidation pathway shows evidence towards a cheaper alternative synthesis of higher oxidation Au complexes yet due to the insensitive nature of the Electrasyn 2.0 no reliable information that could be used to determine rates or mechanistic processes was able to be extrapolated. The author still expresses mild concern for the precision of the values acquired through this device as no measures were taken to assess this aspect of the Electrasyn 2.0, and as it is not an analytical device with the current measuring resolution as advertised at 0.1 mA. These data rest as nothing more but a promising opening for new means of accessing these rare Au^{III} complexes until a compound can be physically isolated and analysed by other means.

Complimentary studies with an analytical set-up for a potentiostat could yield more information on the nature of the peaks observed by CV. As the particular connector for the reference electrode for the Electrasyn 2.0 does not appear easily replaceable and though coating of the electrode with AgCl would severely limit the potential drifting and aid in giving more precise comparative values for the electron transfer events observed between figures 39 and 41. This approach was not deemed feasible within the time periods caused by the pandemic. Though, fundamentally the peak allocation of the CVs could only be achieved through an analytical approach, the peak heights observed in figures 40 and 42 at -300 to -400 mV as suggested above are to be of a two electron transfer, while the peak slightly more negative to be of a single electron transfer. While typically the opposite trend is observed this could be explained through the Electrasyn 2.0s tendency to scan to the more negative potentials at a faster rate than positive potentials. While a slight diffusion layer does build up at the electrode interface as observed in both figures, by the time the potential differential is enough to reduce from I/0, a difference of 2.5 seconds in figure 42, any Au^{III} still in solution will continue to reduce to the Au^{0} state along with the Au^{I}, adding to the full increase in peak current.

Further elucidation as to whether the formation of the Au^{III} species was successfully formed by NMR was hindered by relative scale of electrolyte to analyte and its' isolation remains a conundrum. A method previously developed by our team for displacement of the pyridyl species presents a viable step to bypass the counterion discrepancy and theoretically could yield an isolatable solid. As at the moment the disbalance in stoichiometry of the electrochemical cell after the oxidation event drastically hinders isolation as the Au complexes seem to willingly exist in the electrolyte solution yet upon work up, when the excess electrolyte and

solvating solutions begins to be removed, it results in the Au complexes not being balanced and auto-reduction takes place. This was observed once with the recovery of **T-B2** after no III/I oxidation was observed by CV, and another time where a compound was observed by M.S to have a mass equal to a suspected coupling between two 4-DMAP molecules however this mass of 242 is shared by TBA^+, though the possible formation of coupled 4-DMAP would be a direct sign of reductive elimination of Au, confirmation of either species by NMR was inconclusive due to minimal amounts of the compound recovered. Data for neither of these examples have been included herein.

2.7 Conclusion and Future Possibilities

Throughout this work Si-$C_{carbene}$ and Si-N activation was witnessed by our L_2AuF_2 with the use of $TMSCF_3$ to drive the thermodynamically favourable Si-F bond. However, all attempts at using this method to synthesise a mono-substituted $(L_2)X\text{-}Au^{III}\text{-}F$ from these *trans* complexes were too unstable and resulted in decomposition. Since TMSF formation and simultaneous ligand delivery was shown to be possible when 2 equivalents of TMS-L were added, a small variety of known and unknown complexes had been recreated and synthesised by this method and while experimentation offered little aside from this novel metathesis fruit. The computational research suggests increased modification of the Au scaffold could yield promising results provided the unability for the metal centre to donate towards the F^- can be compensated for through varying the degree of d-electron backbonding.

Alternatively the preliminary use of electricity as an oxidant provided a large amount of hope for the future of accessing Au-F chemistry, the theoretical method for bypassing the charge discrepancy offers a vastly safer and cheaper option for accessing this class of compound. Although no catalytic activity was observed amongst these *trans*-difluorides, potential experimentation with *cis* difluoride complexes could lead towards catalytic activity. With these two method present here, there is new potential for synthesis and modification in the unexplored world of $L_2Au^{III}F_2$, along with the potential for forming many novel compounds such as $[L_2Au(PPh_3)_2]^+$ and $[L_2Au(cAAC)_2]^+$, neither of which have been successfully synthesised by current methods in Au chemistry.

3 Experimental

3.1 General procedure

Unless otherwise noted all reactions were performed under a N_2 environment, by either shlenk or glovebox techniques. All reaction sequences involving XeF_2 were performed in plastic vessels. All ^{1}H NMR are referenced to the chemical shift of $Si(CH_3)_4$ and ^{19}F NMR are referenced to $CFCl_3$. The procedures below were all performed under a range of different concentrations and relative amounts of reactants, as the results made no difference when 0.01 to 0.1 mmol of the Au substrates were used, all reactions mentioned below are capable of undergoing the reaction scheme when adhering to the stoichiometric ratios and the general mass of the amounts used seemed irrelevant, unless otherwise noted. However, due to the similarity of many reactions and attempts at forming either mono- or di- substituted complexes, these reaction protocols have been combined due to insufficient evidence of a successful reaction.

3.2 Synthetic methods

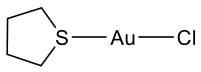

T-B1 THTAuCl

3.2.1 **T-B1** Tetrahydrothiophene Gold Chloride **THTAuCl**

In a round bottom flask, gold powder (200 mg, 1 mmol) was dissolved in aqua regia (20 ml) and left for 12 hours in the dark. The solvent was removed via vacuum with gentle heating to 85 °C, the resulting precipitate was washed with HCl and vacuumed to dryness. The collected red solid was redissolved in EtOH/Water (1:1) and THT (257 μl, 3 mmol) was added dropwise, precipitating a white solid, which was washed with DCM. Yield 64%.

3.2.2 **T-B2** bis(n,n`-dimethyl-4-aminopyridine) gold trifluoromethanesulfonate **[Au(4-DMAP)$_2$]OTf**

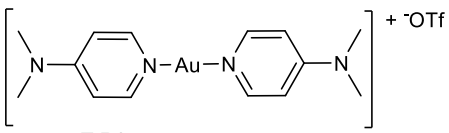

T-B2 [Au(4-DMAP)$_2$]OTf

To **T-B1** (100 mg, 3.12 mmol), KOTf (58 mg, 3.12 mmol) and 4-DMAP (76 mg 6.24 mmol) was added and left to stir in a 1:1 mixture of DCM/EtOH for 12 hours, in the absence of light. The resulting mixture was filtered through celite and the filtrate was vacuumed to dryness, redissolved in DCM and a white solid was crashed out with the addition of Et_2O.

Yield 70%, ^{1}H NMR (400 MHz, D_3ACN) δ (ppm) = 2.52 (s, 12H), 6.25 (d, 4H), 7.64 (d, 4H) ESI-MS = 441 m/z (+) $[Au(4\text{-}DMAP)_2]^+$

3.2.3 **T-B3** bis(n-methylimidazole) gold trifluoromethanesulfonate **$[Au(MeIM)_2]OTf$**

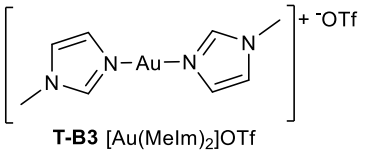

T-B3 $[Au(MeIm)_2]OTf$

Compound **T-B3** was synthesised by the same procedure as **T-B2** with MeIM in place of 4-DMAP. Yielding a white solid.

Yield 62%, ^{1}H NMR (400 MHz, $CDCl_3$) δ (ppm) = 3.85 (s, 3H), 7.08 (d, 2H), 8.36 (s, 1H)

3.2.5 **T-B4** bispyridine gold tetrafluoroborane **$[Au(Py)_2]BF_4$**.[61]

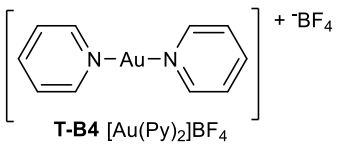

T-B4 $[Au(Py)_2]BF_4$

Gold powder (140 mg, 0.70 mmol) was dissolved in MeCN (4 ml), $NOBF_4$ (82 mg, 0.71) was added dropwise and left to stir for 4 hours. The resulting solution was filtered through a kim-wipe to collect unreacted gold powder. To the isolated filtrate, pyridine (114 μL, 1.46 mmol) was added dropwise forming a yellow solution. The solution was reduced under vacuum and addition of Et_2O crashed out a yellow solid which turned beige after drying under vacuum.

Yield 41%, ^{1}H NMR (400 MHz, D_3ACN) δ (ppm) =7.64 (m, 2H), 8.04 (d, 1H), 8.85 (t, 2H), ESI-MS = 355.1 m/z(+) $[Au(Py)_2]^+$

3.3 Oxidation reactions

3.3.1 **T-B5** bis(n,n`-dimethyl-4-aminopyridine) difluoro gold trifluoromethanesulfonate **$[Au(4\text{-}DMAP)_2F_2]OTf$**

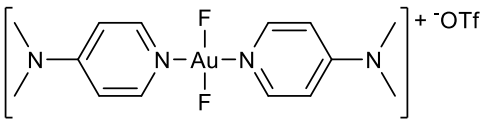

T-B5 - $[Au(4\text{-}DMAP)_2F_2]OTf$

To a solution of **T-B2** (100 mg, 0.17 mmol) in DCM (5 ml), XeF_2 (29 mg, 0.17 mmol) was added and left to stir for 4 hours. The reaction mixture was reduced under vacuum recovering a yellow solid, which was washed with DCM.

Yield 70%, ^{1}H NMR (400 MHz, D_3ACN) δ (ppm) = 3.17 (s, 6H), 6.80 (d, 2H), 7.97 (d, 2H), ^{19}F NMR (400 MHz, D_3ACN) δ (ppm) = -249.23 (s, F), ESI-MS = 479.1 m/z(+) $[Au(4\text{-}DMAP)_2F_2]^+$

3.3.2 **T-B6** bis(n-methylimidazole) difluoro gold trifluoromethanesulfonate **$[Au(MeIM)_2F_2]OTf$**

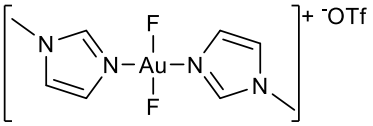

T-B6 - $[Au(MeIm)_2F_2]OTf$

Reaction **T-B6** was performed under the same procedure as **3.3.1**, with **T-B3**, the reaction was left for 6 hours. A white solid was recovered.

Yield 67%, ^{1}H NMR (400 MHz, $CDCl_3$) δ (ppm) = 4.01 (s, 3H), 7.02 (s, 4H), 7.54 (s, 4H), 8.44 (s, 2H), ^{19}F NMR (400 MHz, $CDCl_3$) δ (ppm) = -277.57 (s, F)

3.3.3 **T-B7** bis(pyridine) difluoro gold trifluoromethanesulfonate **$[Au(Py)_2F_2]OTf$**

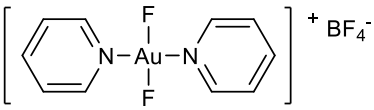

T-B7 - $[Au(Py)_2F_2]BF4$

Reaction **T-B7** was performed under the same procedure as **T-B5**. The reaction mixture was left for 6 hours, recovering a yellow solid.

Yield 40%, ^{1}H NMR (400 MHz, D_3ACN) δ (ppm) = 7.73 (m, 2H), 8.20 (t, 1H), 8.60 (d, 2H), ^{19}F NMR (400 MHz, $CDCl_3$) δ (ppm) = -237.71

3.4 N-ligand trifluoromethylation

3.4.1 **T-B8** bis(n-dimethyl-4-aminopyridine) bis(trifluoromethane) gold trifluoromethanesulfonate **$[Au(4\text{-}DMAP)_2(CF_3)_2]OTf$**

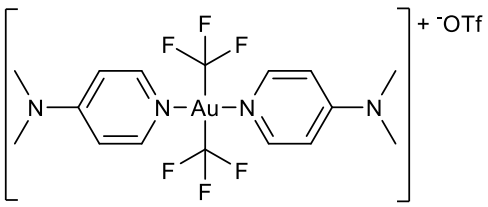

T-B8 - $[Au(4\text{-}DMAP)_2(CF_3)_2]OTf$

An aliquot of **T-B6** (20 mg, 0.032 mmol) was dissolved in MeCN (2 ml) with $TMSCF_3$ added (5 μL, 0.045 mmol – 50 μL, 0.045 mmol), the resulting solution was left to stir for 2 hours to 2 weeks. The reaction mixture was reduced under vacuum and Et_2O was added to isolate a beige powder.

Yield n.d, ^{1}H NMR (400 MHz, D_3ACN) δ (ppm) = 3.11 (s, 12H), 6.69 (d, 4H), 7.84 (d, 4H), ^{19}F NMR (400 MHz, $CDCl_3$) δ (ppm) = -33.26 (s, CF_3), -34.05 (s, CF_3), -35.30 (s, CF_3)

3.4.1.1

To an allotment of **T-B4** (5 mg, 0.012 mmol), **PhI(4-DMAP)$_2$]OTF** (4.9 mg, 0.012 mmol) was added and left to stir for 4 hours in DCM. The reaction mixture was reduced under vacuum and ether was added, the resulting yellow/orange solid. Working up the reaction was not needed as ^{19}F NMR chemical shift was sufficient for these purposes.

Yield n.d, ^{1}H NMR (500 MHz, D_3ACN) δ (ppm) = 3.13 (s, 6H), 6.81 (d, 2H), 8.18 (d, 2H), ^{19}F NMR (500 MHz, D_3ACN) δ (ppm) = 41.15 (s, CF_3), ESI-MS = 457 m/z(+) $[Au(4\text{-}DMAP)(CF_3)_2]^+$

3.4.2 **T-B9** bis(n-methylimidazole) bis(trifluoromethane) gold trifluoromethanesulfonate **[Au(MeIM)$_2$(CF$_3$)$_2$]OTf**

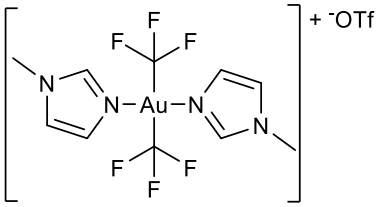

T-B9 - $[Au(MeIM)_2(CF_3)_2]OTf$

The reaction sequence followed the procedure of **3.4.1**

Yield n.d., ^{1}H NMR (400 MHz, D_3ACN) spectrum scattered, multiple sets of products, spectrum integrated to highlight potential relative amounts, ^{19}F NMR (400 MHz, $CDCl_3$) δ (ppm) = -26.11 (s, CF_3), -27.50 (s, CF_3), -31.79 (s, CF_3), -30 (s, CF_3) ESI-MS (**T-B10.2**) = 499 m/z (+) $[Au(MeIm)_2F_2]^+$

3.4.3 **T-B10** bis(pyridine) bis(trifluoromethane) gold trifluoromethanesulfonate **[Au(Py)(CF$_3$)$_2$]OTf**

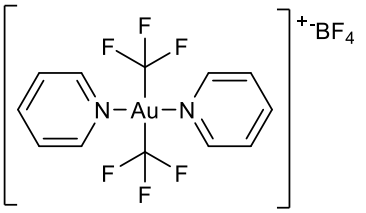

T-B10 - $[Au(Py)_2(CF_3)]BF_4$

The reaction sequence followed the procedure of **3.4.1**

Yield n.d., NMR and MS not acquired due to complex instability.

The secondary reaction sequence followed the protocol for **3.4.1.1**

Yield n.d., ^{19}F NMR (500 MHz, D_3ACN) δ (ppm) = 41.83 (s, CF_3), 31.95 (s, CF_3) ESI MS = 493 m/z(+) $[Au(Py)_2(CF_3)_2]^+$ (see discussion, 2.2.2)

3.2.4 **T-B11** bis(trifluoromethane) gold tetraphenylphosphene **[Au(CF$_3$)$_2$]PPh$_4$**.[28]

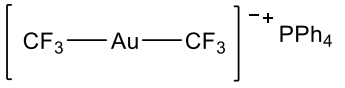

T-B11 - $[Au(CF_3)_2]PPh_4$

To an aliquot of **T-B1** (100 mg, 3.12 mmol) and $[PPh_4]Br$ (106 mg, 3.12 mmol) were dissolved in THF (15 ml). In a second flask and $TMSCF_3$ (462 μL, 31.2 mmol) and CsF (471 mg, 3.12 mmol) were dissolved in THF and cooled to -78 °C for 2 hours. The **T-B1**/$[PPh_4]Br$ solution was transferred over in a dropwise manner, the reaction mixture was removed from the -78 °C bath and allowed to warm to room temperature over-night, and left stirring for three days.

The brown reaction mixture was reduced under vacuum, yielding a black tar-like substance. Once dissolved in DCM/Et_2O (1:1), addition of hexane yielded a white solid.

Yield 20%, ^{19}F NMR (500 MHz, DCM) δ (ppm) = -28.19 (s, CF_3), ESI-MS = 334.1 m/z(-) $[Au(CF_3)]^-$

3.5 Reactions of $[Au(CF_3)_2]^-$ and PhI(L)

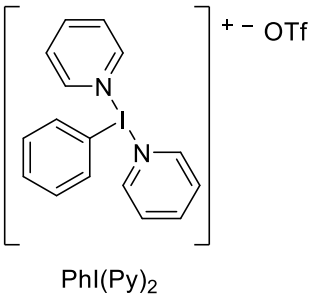

$PhI(Py)_2$

3.5.1 dipyridine phenyliodide trifluoromethanesulfonate [**PhI(Py)2]OTf**

An allotment of $PhI(OAc)_2$ (312 mg, 0.97 mmol) was dissolved in DCM (20 ml), and Py (156 μL, 0.194 mmol) was added with one equivalent of TMSOTf (365 μL, 0.97 mmol). The reaction mixture was left to stir for 2 hours before a white solid precipitated out. The white solid was washed with DCM twice and Et_2O once before being dried under vacuum.

Yield 83%, ^1H NMR (400 MHz, D_3ACN) δ (ppm) = 7.67 (t, 2H), 7.82 (d, 5H), 8.39 (t, 2H), 8.62 (t, 1H), 8.94 (d, 2H)

3.5.2 bisdimethyl-4-aminopyridine phenyliodide trifluoromethanesulfonate

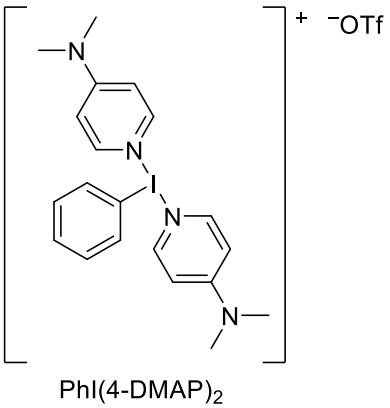

$PhI(4\text{-}DMAP)_2$

This reaction followed the same protocol as **3.5.1**, using 4-DMAP in place of Py.

3.6 Synthesis of Au-NHC Complexes

3.6.1 **T-B12** n,n`-dimethylbenzyimidazole gold chloride **DMBI-AuCl**

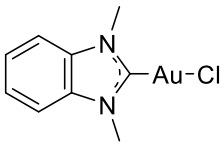

T-B12 - (DMBI)AuCl

Under standard atmosphere and in the dark, Ag_2O (180 mg, 0.78 mmol) was suspended in EtOH/DCM (1:1), n,n'-dimethylimidazolium iodide (427 mg, 1.56 mmol) was added and left to stir over night. The grey milky substance collected was filtered through celite. The resulting yellow filtrate was reduced under vacuum and a white solid was isolated by the addition of hexane.

Yield 37% ^{1}H NMR (400 MHz, D_3ACN) δ (ppm) = 4.01 (s, 6H), 7.48 (m, 2H), 7.60 (m, 2H)

3.6.2 **T-B13** dipp-imidazolium gold chloride **dippIM-AuCl**

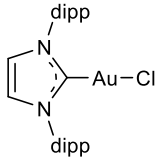

T-B13 - (DIPP-imidazolium)AuCl

The reaction sequence followed the protocol for **3.6.1**

Yield 62% ^{1}H NMR (400 MHz, D_3ACN) δ (ppm) = 1.34 (d, 12H), 1.43 (d, 12H), 2.65 (sept, 4H), 7.26 (s, 2H), 7.35 (t, 4H), 7.58 (q, 2H)

3.6.3 **T-B14** n,n`-dimethylbenzyimidazole gold pyridine trifluoromethanesulfonate **[Au(DMBI)Py]OTf**

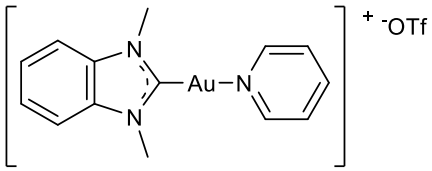

T-B14 - [Au(DMBI)Py]OTf

To an allotment of **T-B12** (103 mg, 0.27 mmol) dissolved in DCM (20 mL), pyridine (215 μL, 027 mmol) was added with AgOTf (69 mg, 0.27 mmol) and left to stir overnight. The murky grey liquid was filtered over celite yielding a yellow filtrate. Dropwise addition of hexane precipitated a white solid.

Yield 52%, ^{1}H NMR (400 MHz, D_3ACN) δ (ppm) = 4.15 (s, 6H), 7.56 (q, 2H), 7.71 (q, 2H), 7.81 (s, 2H), 8.21 (s, 1H), 8.73 (s, 1H)

3.6.4 **T-B15** n,n`-dimethylbenzyimidazole trifluoromethane gold **[Au(DMBI)(CF_3)]OTf**

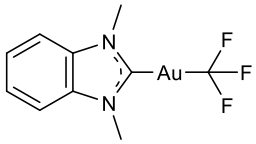

T-B15 - Au(DMBI)CF3

To **T-B12** (100 mg, 0.26 mmol) in minimal DCM, an equivalent of AgF (32.25 mg, 0.26 mmol) and $TMSCF_3$ (195 μL, 0.26 mmol) were added and left to stir in the dark for 4 hours. The reaction mixture was reduced under vacuum and placed in the freezer overnight. The beige precipitate that crashed out was isolated by centrifugation and washed with Et_2O.

Yield 40%, ^{1}H NMR (400 MHz, D_3ACN) δ (ppm) = 4.00 (s, 6H), 7.47 (s, 2H), 7.60 (s, 2H), ^{19}F NMR (400 MHz, D_3ACN) δ (ppm) = -28.83 (s, CF_3)

3.6.5 **T-B16** n,n`-dimethylbenzyimidazole n-methylimidazole gold trifluoromethanesulfonate **[Au(DMBI)(MeIM)]OTf**

The reaction sequence followed the same protocol as **3.6.3**.

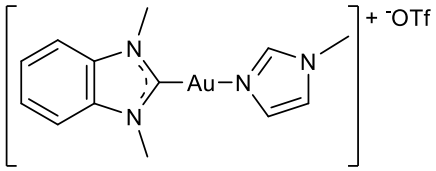

T-B16 - [Au(DMBI)MeIM]OTf

Yield 95%, ^{1}H NMR (400MHz, D_3ACN) δ (ppm) = 4.09 (s, 6H), 7.23 (s, 1H), 7.53 (s, 1H), 7.53 (t, 2H), 7.66 (t, 2H), 8.03 (s, 1H) ESI-MS = 425 m/z (+) $[Au(DBMI)(MeIm)]^+$

3.6.6 **T-B17** n,n`-dimethylbenzyimidazole pyridine difluoro gold trifluoromethanesulfonate **[Au(DMBI)PyF_2]OTf**

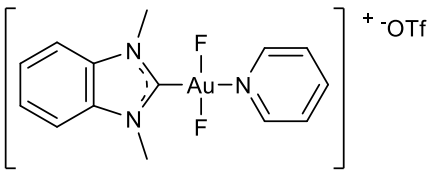

T-B17 - [Au(DMBI)PyF_2]OTf

To an allotment of **T-B14** (67 mg, 0.11 mmol), an equivalent of XeF_2 (20 mg, 0.12 mmol) was added and left to stir for 3 hours. The reaction mixture was reduced under vacuum, addition of hexane yielded a white solid.

Yield 52% ^{1}H NMR (400 MHz, D_3ACN) δ (ppm) = 4.15 (s, 6H), 7.56 (m, 2H), 7.70 (m, 2H), 7.72 (m, 1H), 8.21 (s, 1H), 8.73 (s, 1H) ^{19}F NMR (400 MHz, D_3ACN) δ (ppm) = -287.51 (s, F)

3.6.7 **T-B18** n,n`-dimethylbenzyimidazole trifluoromethane difluoro gold **[Au(DMBI)(CF_3)F_2]**

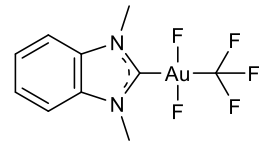

T-B18 - Au(DMBI)(CF_3)F_2)

The reaction sequence followed the same protocol as **3.6.6**.

Yield n.d., ^{1}H NMR (400 MHz, $CDCl_3$) δ (ppm) = 3.43 (s, 6H), 6.98 (m, 2H), 7.11 (m, 2H), ^{19}F NMR (400 MHz, $CDCl_3$) δ (ppm) = -32.21 (s, CF_3), 38.83, (s, CF_3), -214.95 (d, F), -224.62 (s, F), -227.80 (d, F)

3.6.8 **T-B19** n,n`-dimethylbenzyimidazole n-methylimidazole difluoro gold trifluoromethanesulfonate **[Au(DMBI)(MeIM)F_2]OTf**

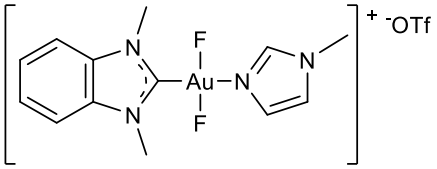

T-B19 - [Au(DMBI)MeIMF_2]OTf

The reaction sequence followed the same protocol as **3.6.6**

Yield n.d., compound decomposed under vacuum. ^{1}H NMR (400 MHz, $CDCl_3$) δ (ppm) = 3.90 (s, 3H), 4.14 (s, 6H), 7.09 (s, 1H), 7.13 (s, 1H), 7.50 (d, 2H), 7.51 (d, 2H), 8.69 (s, 1H) ^{19}F NMR (400 MHz, $CDCl_3$) δ (ppm) = 305.88 (s, F), ESI-MS = 463.1 m/z (+)

3.6.9 **T-B20** n,n`-dimethylbenzyimidazole pyridine bistrifluromethane gold trifluoromethanesulfonate **[Au(DMBI)(Py)(CF_3)$_2$]OTf**

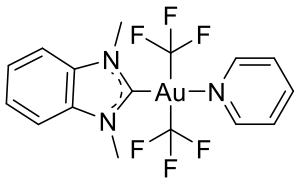

T-B20 - Au(Py)(CF_3)$_2$

The reaction sequence followed the same protocol as **3.4.1**

Yield n.d. ^{19}F NMR (400 MHz, D_3ACN) δ (ppm) = -24.01 (s, CF_3), -32.44 (s, CF_3)

3.7 **Trimethylsilyl compounds**

3.7.1 **T-B21** n,n`-dimethyl-4-aminopyridine trimethylsilyl trifluoromethanesulfonate **[TMS(4-DMAP)]OTf**

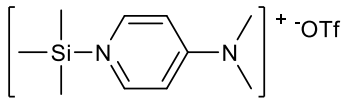

T-B21 - [TMS(4-DMAP)]OTf

An allotment of 4-DMAP (36 mg, 0.30 mmol) was dissolved in MeCN (2 ml), TMSOTf (52 μL, 0.30 mmol)and left to stir for 1.5 hours. The solvent was reduced under vacuum and Et_2O was added precipitating out a white solid. Washed with Et_2O.

Yield 90%. ^{1}H NMR (400 MHz, D_3ACN) δ (ppm) = 0.06 (s, 9H), 3.18 (s, 6H), 6.83 (d, 2H), 7.97 (d, 2H)

3.7.2 **T-B22** pyridine trimethylsilyl trifluoromethanesulfonate **[TMS(Py)]OTf**

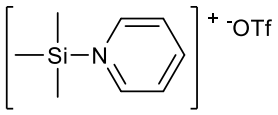

T-B22 - [TMS(Py)]OTf

The reaction sequence followed the same procedure as **3.7.1**, with Py in place of 4-DMAP.

Yield 77% ^{1}H NMR (400 MHz, D_3ACN) δ (ppm) = 0.06 (s, 9H), 8.04 (t, 2H), 8.60 (m, 1H), 8.70 (d, 2H)

3.7.3 **T-B23** n-methylimidazole trimethylsilyl trifluoromethanesulfonate **[TMS(MeIM)]OTf**

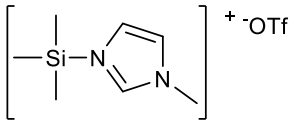

T-B23 - [TMS(MeIM)]OTf

The reaction sequence followed the same procedure as **3.7.1**, with MeIM in place of 4-DMAP.

Yield 69%, ^{1}H NMR (400 MHz, $CDCl_3$) δ (ppm) = 0.56 (s, 6H), 3.84 (s, 3H), 7.16 (s, 1H), 7.24 (s, 1H), 8.37 (s, 1H)

3.7.4 **T-B24** cyanopyridine trimethylsilyl trifluoromethanesulfonate **[TMS(CyPy)]OTf**

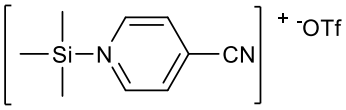

T-B24 - [TMS(CyPy)]OTf

The reaction sequence followed the same procedure as 3**.7.1**, with CyPy in place of 4-DMAP.

Yield n.d., as compound would steadily decompose when dry. ^{1}H NMR (400 MHz, $CDCl_3$) δ (ppm) = 0.57 (s, 3H), 8.02 (s, 2H), 8.87 (s, 2H)

3.7.5 **T-B25** tetrakis(n,n`-dimethyl-4-aminopyridine) gold trifluoromethanesulfonate **[Au(4-DMAP)$_4$]3OTf**

To **T-B5** (10 mg, 0.016 mmol), **T-B21** (11 mg, 0.032 mmol) was added and left to stir in CD_3CN over 3 days, producing a red solution. The reaction mixture was reduced under vacuum yielding a red solid.

Yield 82%, ^{1}H NMR (400 MHz, D_3ACN) δ (ppm) = 3.12 (s, 12H), 6.73 (d, 4H), 7.98 (d, 4H)

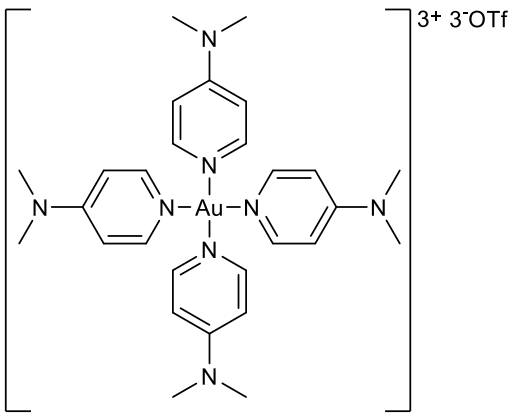

T-B25 - [Au(4-DMAP)$_4$]3OTf

3.7.6 **T-B26** bis(n,n`-dimethyl-4-aminopyridine) bis(pyridine) gold trifluoromethanesulfonate **[Au(4-DMAP)$_2$(Py)$_2$]OTf**

To **T-B5** (10 mg, 1.60*10^{-2} mmo), **T-B22** (9.5 mg, 3.20*10^{-2} mmol) was added and left to stir in CD_3CN for 3 days. The red/orange solution was reduced under vacuum yielding a red solid.

Yield 84%, ^{1}H NMR (400 MHz, D_3ACN) δ (ppm) = 3.09 (s, 12H), 6.67 (d, 4H), 7.87 (t, 4H), 7.99 (d, 4H), 8.36 (t, 2H), 8.79 (t, 4H)

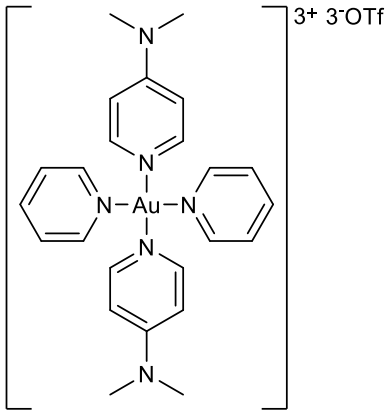

T-B26 - [Au(4-DMAP)$_2$(Py)$_2$]3OTf

3.7.8 (no code as compound did not make it into an experimentation, nor an important target) triphenylphosphine trimethylsilyl trifluoromethanesulfonate **[TMS(PPh$_3$)]OTf**

An allotment of PPh_3 (100mg, 0.38 mmol) was dissolved in MeCN (5 ml) and one equivalent of TMSOTf (69 μL, 0.38 mmol) was added. The mixture was left to stir for 2 hours to 2 days. The solution was removed by vacuum.

Reaction was unsuccessful.

^{31}P NMR (400 MHz, D_3ACN) δ (ppm) = 5.76 (s, P), this peak matched stock sample of PPh_3

3.7.9 **T-B27** n-n`-dimethylbenzylimidazolium trimethylsilyl trifluoromethanesulfonate **[TMS(DMBI)]OTf**

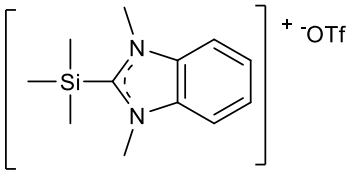

T-B27 - [Trimethylsilyl(DMBI)]OTf

An allotment of n,n'-dimethylbenzylimidazolium iodide (97 mg, 0.35 mmol) was dissolved in THF (10 ml), K*t*BuO (44 mg, 0.39 mmol) was added and left to stir for 4 hours. The solution was centrifuged and the solid was discarded. The filtrate was left in the freezer for 2 hours and TMSOTf (52 μL 0.35 mmol) was added in a dropwise manner crashing out a white solid (~10-20% yield due to formation of oil)

True yield n.d, compound formation hindered by formation of other products.

3.7.10 **T-B28** 1,3-bis(2,6-diisopropylphenyl)imidazolium trimethylsilyl trifluoromethanesulfonate **[TMS(dipp-imidazole)]OTf.**[56]

The reaction sequence followed the same procedure as 3**.7.9**, with DippIM-NHC in place of DMBI-NHC.

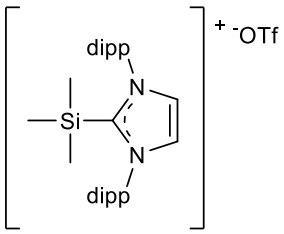

T-B28 - [Trimethylsilyl(dippIm)]OTf

Yield 86%, ^{1}H NMR (400 MHz, $CDCl_3$) δ (ppm) = -0.18 (s, 9H), 1.27 (d, 12H), 1.33 (d, 12H), 2.37 (sept, 4H), 7.38 (d, 4H), 7.62 (t, 2H), 8.42 (s, 2H)

3.7.11 **T-B29** bis(1,3-bis(2,6-diisopropylphenyl)imidazolium) bis(n,n`-dimethyl-4-aminopyridine) gold trifluoromethanesulfonate **[Au(dipp-imidazole)$_2$(4-DMAP)$_2$]3OTf**

To an allotment of **T-B5** (22 mg, 0.037 mmol) in MeCN (2 ml), **T-B28** (10 mg, 0.075 mmol) was added in a dropwise manner and left to stir for 30 minutes. The resulting red solution was vacuumed off leaving a solid of the same colour. ^{1}H NMR (400 MHz, $CDCl_3$) δ (ppm) = 1.23 (d, 12H), 1.28 (d, 12H), 2.28 (sept, 4H), 2.95 (s, 12H), 6.52 (d, 4H), 7.40 (d, 2H), 7.51 (m, 4H), 7.70 (t, 2H), 8.03 (d, 2H)

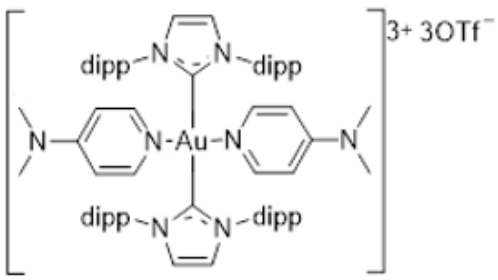

T-B29 - [Au(dIppIM)$_2$(4-DMAP)$_2$]3OTf

3.7.12 **T-B30** bis1,3-bis(2,6-diisopropylphenyl)imidazolium) bis(n-methylimidazole) gold trifluoromethanesulfonate **[Au(dipp-imidazole)$_2$(MeIM)$_2$]3OTf**

To an allotment of **T-B6** (22 mg, 0.040 mmol) in CD_3CN (2 ml), two equivalents of **T-B28** (10 mg, 0.080 mmol) was added in a dropwise manner, instantly changing the solution red, after 2 hours of stirring Et_2O and hexane (3:1) was added crashing out a white solid, the red filtrate was vacuumed to dryness yielding a red solid.

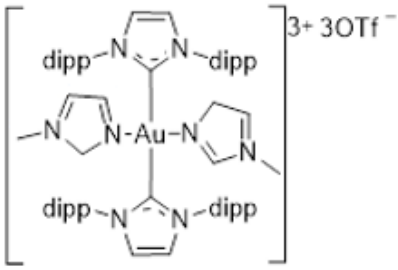

T-B30 - [Au(dippImidazollum)$_2$(MeIM)$_2$]3OTf

Yield n.d., ^{1}H NMR (400 MHz, $CDCl_3$) δ (ppm) = 1.22 (d, 12H), 1.39 (d, 12H), 2.24 (sept, 4H), 7.50 (d, 4H), 7.67 (d, 2H), 8.15 (s, 2H), 8.92 (s, 1H)

3.7.13 Electrochemical Procedure

The potentiostat employed for electrosynthesis was the Ika® Electrasyn 2.0, sacrificial graphite electrodes, Ag/Ag^+ pseudo reference electrode, and glassy carbon working electrode.

The electrodes were cleaned by 0.1 M HCl, before washing and sonication in ultrapure water, the working electrode was polished in-between data acquisition on a polishing pad with 0.3 µm ultrapure water/alumina slurry.

The split cell used was designed and build by Ika® for the exclusive purpose of working with the Electrasyn 2.0. As the Electrasyn was designed for the purpose of standardisation of equipment, all the complimentary technical data for both the Electrasyn 2.0 and accompanying electrodes can reached through the Ika® website: https://www.ika.com.

The chosen electrolyte was 0.1 M $TBAPF_6$ in MeCN, for CV of synthetic samples, 0.1 mM concentrations were used.

For the split cell oxidations. **T-B2** (58 mg, 0.1 mmol) was used and held at a constant voltage of +1.85 V, power supply issues to the fume hood resulted in multiple stalls in the reactions, and the total oxidative turn-over in terms of F/mol could not be determined as on occasions to a where a power outage had occurred, all data recorded by the device during the run would be deleted, and severely reduced access to the labs prevented any long-term monitoring throughout the day.

REFERENCES

1. T. W. Lyons and M. S. Sanford, *Chem. Rev.* 2010**,** *110*, 1147-1169.
2. S. R. Neufeldt and M. S. Sanford, *Acc. Chem. Res.* 2012**,** *45* (**6**), 936-946.
3. A. S. K. Hashmi, C. Lothschütz, R. Döpp, M. Ackermann, J. D. B. Becker, M. Rudolph, C. Scholz and F. Rominger, *Adv. Synth. Catal.* 2012**,** *354*, 133-147.
4. B. H. Lipshutz and S. Sengupta, *Org. React. (Hoboken, NJ, U. S.)* 2004.
5. B. Hammer and J. K. Nørskov, *Nature* 1995**,** *376* (**6537**), 238.
6. P. Gualco, S. Ladeira, K. Miqueu, A. Amgoune and D. Bourissou, *Organometallics* 2012**,** *31*, 6001-6004.
7. N. P. Mankad and F. D. Toste, *Chem. Sci.* 2012**,** *3*, 72-76.
8. R. Corbo, T. P. Pell, B. D. Stringer, C. F. Hogan, D. J. D. Wilson, P. J. Barnard and J. L. Dutton, *J. Am. Chem. Soc.* 2014**,** *136*, 12415-12421.
9. H. J. Teles, S. Brode and M. Chabanas, *Angew. Chem. Int. Ed.* 1998**,** *37* (**10**).
10. N. P. Mankad and F. D. Toste, *J. Am. Chem. Soc.* 2010**,** *132*, 12859-12861.
11. A. Tamaki and J. K. Kochi, *J. Organomet. Chem.* 1972**,** *40* (**1**).
12. L. T. Ball, G. C. Lloyd-Jones and C. A. Russell, *Science* 2012**,** *337* (**6102**), 1644-1648.
13. H. Gilman and L. A. Woods, *J. Am. Chem. Soc.* 1948**,** *70* (**2**), 550-552.
14. G. E. Coates and C. Parkin, *J. Chem. Soc.* 1963, 421-429.
15. S. Komiya and A. Shibue, *Organometallics* 1985**,** *4* (**4**), 684-687.
16. P. Gualco, S. Ladeira, K. Miqueu, A. Amgoune and D. Bourissou, *Gold Chem.* 2011**,** *50*, 8320-8324.
17. N. Lassauque, P. Gualco, S. Mallet-Ladeira, K. Miqueu, A. Amgoune and D. Bourissou, *J. Am. Chem. Soc.* 2013**,** *135*, 13827-13834.
18. J. Guenther, S. Mallet-Ladeira, L. Estevez, K. Miqueu, A. Amgoune and D. Bourissou, *J. Am. Chem. Soc.* 2014**,** *136*, 1778-1781.
19. M. Aresta and G. Vasapollo, *J. Organomet. Chem.* 1973**,** *50*, C51-C53.
20. S. Komiya, T. A. Albright, R. Hoffman and J. K. Kochi, *J. Am. Chem. Soc.* 1976**,** *98* (**23**), 7255-7265.
21. A. Tamaki, S. A. Magennis and J. K. Kochi, *J. Am. Chem. Soc.* 1974**,** *96* (**19**), 6140-6148.
22. P. L. Kuch and R. S. Tobias, *J. Organomet. Chem.* 1976**,** *122*, 429-446.
23. R. H. Crabtree, *The Organometallic Chemistry of the Transition Metals*. 6 ed.; John Wiley & Sons, Inc., Hoboken, New Jersey: New Jersey, 2014; p 9-10; 248-249.
24. V. J. Scott, J. A. Labinger and J. E. Bercaw, *Organometallics* 2010**,** *29*, 4090-4096.
25. D. S. Laitar, P. Müller, T. G. Gray and J. P. Sadighi, *Organometallics* 2005**,** *24*, 4503-4505.
26. R. Kumar, A. Linden and C. Nevado, *J. Am. Chem. Soc.* 2016**,** *138*, 13790-13763.
27. M. Joost, A. Amgoune and D. Bourissou, *Angew. Chem. Int. Ed.* 2015**,** (**54**), 15022-15045.
28. S. Martínez-Salvador, L. R. Falvello, A. Martín and B. Menjón, *Chem-Eur. J.* 2013**,** *43* (**19**), 14540-14552.
29. M. Albayer, R. Corbo and J. L. Dutton, *Chem. Comm.* 2018**,** *54*, 6832-6834.
30. A. Tlahuext-Aca, M. N. Hopkinson, C. G. Danilius and F. Glorius, *Chem-Eur. J. Comm.* 2016**,** *22*, 11587-11592.
31. R. Kumar, A. Linden and C. Nevado, *Angew. Chem. Int. Ed.* 2015**,** *54*, 14287-14290.
32. J. R. L. Brandt, Eunsung., G. Boursalian and T. Ritter, *Chem. Sci.* 2014**,** *5* (**1**).
33. S. Purser, P. R. Moore, S. Swallow and V. Gouverneur, *Chem. Soc. Rev.* 2008**,** *37* (**2**), 320-330.
34. M. G. Campbell and T. Ritter, *Chem. Rev.* 2015**,** *115* (**2**), 612-633.
35. C. P. Johnston, T. H. West, R. E. Dooley, M. Reid, A. B. Jones, E. J. King, A. G. Leach and G. C. Lloyd-Jones, *J. Am, Chem, Soc.* 2018**,** *140* (**35**), 11112-11124.
36. T. A. Engesser, C. Friedmann, A. Martens, D. Kratzert, P. J. Malinowski and I. Krossing, Chem. Euro. J. 2016**,** *22* (**42**), 15085-15094.

37. A. Pérez-Bitrián, M. Baya, J. M. Casas, A. Martín, B. Menjón and J. Orduna, *Angew.* 2018**,** *57*, 6517-6521.
38. J. H. Clark, J. E. Denness, M. A. McClinton and A. J. Wynd, *J. Fluorine. Chem.* 1990**,** *50* (**3**), 411-426.
39. H. P. A. Mercier, M. D. Moran, G. J. Schrobilgen, C. Steinberg and R. J. Suontamo, *J. Am. Chem. Soc.* 2004**,** *126* (**17**), 5533-5548.
40. N. P. Chmel, S. E. Howson, L. E. N. Allan, J. Barker, G. J. Clarkson, S. S. Turner and P. Scott, *Dalton Trans.* 2010, 11.
41. D. K. Zopes, S. Scherer, H. Belkoura, L. Pantenburg, I. Tyrra, W. Mathur, S., *Eur. J. Inorg. Chem.* 210**,** (**2**), 273-280.
42. N. D. Ball, J. W. Kampf and M. S. Sanford, *Dalton Trans.* 2011**,** (**2**), 632-640.
43. H. M. J. Wang, C. S. Vasam, T. Y. R. Tsai, S. Chen, A. H. H. Chang and I. J. B. Lin, *Organometallics* 2005**,** *24*.
44. M. Albayer and J. L. Dutton, *Journal of Coordination Chemistry* 2019**,** *72*.
45. D. Benitez, N. D. Shapiro, E. Tkatchouk, Y. Wang, W. A. Goddard III and F. D. Toste, *Nat. Chem.* 2009**,** *1*, 482-486.
46. D. V. Partyka, T. J. Robilotto, J. B. Updegraff, M. Zeller, A. D. Hunter and T. G. Gray, *Organometallics* 2009**,** *28* (**3**), 795-801.
47. C. Dash, M. Yousufuddin, T. R. Cundari and H. V. R. Dias, *J. Am. Chem. Soc.* 2013**,** *135* (**41**), 15479-15488.
48. T. Knauber, F. Arikan, G.-V. Röschenthaler and L. J. Gooßen, Chem. Eur. J. 2011**,** *17* (**9**), 2689-2697.
49. M. Tobisu, Y. Kita, Y. Ano and N. Chatani, *J. Am. Chem. Soc.* 2008**,** *130* (**47**), 15982-15989.
50. A. Bartoszewicz, M. Kalek and J. Stawinski, *Tetrahedron* 2008**,** *64* (**37**), 8843-8850.
51. A. P. M. Robertson, S. S. Chitnis, S. Chhina, H. J, C. S, B. O. Patrick, H. A. Jenkins and N. Burford, *Can. J. Chem.* 2016**,** *94*, 424+.
52. J. Possart, A. Martens, M. Schleep, A. Ripp, H. Scherer, D. Kratzert and I. Krossing, *Chem. Eur. J.* 2017**,** *50* (**23**).
53. https://sdbs.db.aist.go.jp (National Institute of Advanced Industrial Science and Technology
54. B. Langer Erikson and P. M. Vedsø, S. Begtrup, M., *J. of Org. Chem.* 1998**,** *63* (**1**), 12-16.
55. K. Nagata, T. Itoh, M. Okada and A. Ohsawa, *Tetrahedron* 1996**,** *52* (**19**), 6569-6580.
56. D. Mendoza-Espinosa, B. Donnadieu and G. Bertrand, *J. Am. Chem. Soc.* 2010**,** *132* (**21**), 7264-7265.
57. R. D. and J. D., *Dalton Trans.* 2008**,** *47*, 6724-6731.
58. E. Y. Ko, E. D. Park, H. C. Lee, D. Lee and S. Kim, *Angew. Chem. Int. Ed. 46* (**5**), 734-737.
59. N. Elgishi, K. J. Rountree, B. D. McCarthy, E. S. Rountree, T. T. Eisenhart and J. L. Dempsey, *J. Chem. Educ.* 2018**,** *95*, 197-206.
60. J. F. Ayme, J. E. Beves, C. J. Campbell, G. Gil-Ramirez, D. A. Leigh and A. J. Stephens, *J. Am. Chem. Soc. 137*, 9812-9815.
61. R. Corbo, G. F. Ryan, M. A. Haghighatbin, C. F. Hogan, D. J. D. Wilson, M. D. Hulett, P. J. Barnard and J. L. Dutton, *Inorg. Chem.* 2016**,** *55* (**6**), 2830-2839.